NTNU

Norwegian University of
Science and Technology

Superconductivity in Dirac Materials

Severin Bøyesen Sjømark

Master of Science in Physics and Mathematics
Submission date: June 2016
Supervisor: Asle Sudbø, IFY

Norwegian University of Science and Technology
Department of Physics

Summary

In this Master's thesis we consider superconductivity in Bravais and bipartite lattice fermion models with nearest neighbour hopping and Rashba-type spin-orbit coupling. The superconductivity is modelled from a negative-U Hubbard model, leading to a general interaction Hamiltonian we simplify by mean field theory. We investigate inter- and intraband superconducting pairing mechanisms with no momentum-transfer in the helicity band basis, and the consequent structure in the spin basis. The goal of this thesis is to find some general requirements on the pairing mechanisms in order to achieve Majorana edge states. We do this by considering the symmetry properties of our systems, and look at the requirements on the superconducting pairing to achieve non-trivial topological phases. Particular focus is put on the proposed venue of chiral p-wave pairing, well known to lead to a relativistic energy dispersion, and Majorana fermions. Because of spin-momentum locking as a result of spin-orbit coupling, a chiral p-wave pairing in the diagonalized band basis is required for a relativistic dispersion. By transforming the chiral p-wave superconducting terms back to the spin basis, it is observed that the form of the superconducting gap functions in this basis need not be chiral. This is a consequence of the momentum-dependent transformation between the band and spin basis.

Sammendrag

I denne Masteroppgaven ser vi på superledning i Bravais og undergitter fermion-modeller med nærmeste nabo hopping og Rashba spinn-bane kobling. Superledningen er modellert fra en negativ-U Hubbard modell, som leder til en generell vekselvirkning i Hamilton-funksjonen vi reduserer ved hjelp av middelfeltsteori. Vi undersøker forskjellige superledende vekselvirkningsmekanismer i båndbasisen, og ser på den resulterende strukturen i spinn-basisen. Målet med denne oppgaven er å finne generelle vilkår for vekselvirkningsmekanismene som fører til Majorana kanttilstander. Vi gjør dette ved å undersøke symmetriegenskapene til de superledende modellene, og ser på krav på de superledende parametrene som kan føre til ikke-trivielle topologiske tilstander. Spesielt fokus blir satt på kiral p-bølge parring av elektroner, en mekanisme som er kjent for å lede til en relativistisk dispersjonsrelasjon og Majorana fermioner. På grunn av spinn-impuls locking som et resultat av spinn-bane koblingen, kreves en kiral p-bølge parring i den diagonaliserte båndbasisen for å oppnå en relativistisk dispersjon. Ved å transformere de kirale p-bølge superledningsleddene tilbake til spinn-basisen finner vi at formen på de superledende gap-funksjonene ikke trenger være kirale p-bølger i denne basisen. Dette er en konsekvens av at transformasjonen som knytter spinn-basisen til bånd-basisen er avhengig av impuls.

Preface

This Master's thesis is the final submission of a five-year Master's degree programme in Mathematics and Physics at the Norwegian University of Science and Technology. The project falls under theoretical condensed matter physics, and was supervised by professor Asle Sudbø. I would like to thank my supervisor for the guidance and insights provided to me throughout the work on this thesis.

Severin Sjømark
Trondheim, Norway
June, 2016

Contents

Chapter 1

Introduction

1.1 Motivation and Background

Condensed matter physics has in the last decades seen an explosion in experimental detection and research on new phenomena. Among these, novel quantum phenomena play a major role, perhaps most prominently the field of superconductivity. In 1911 H. K. Onnes discovered an abrupt disappearance of resistance upon cooling mercury down to 4.2 K[1]. In the years to follow, several other materials was found to display the same property at similar near-zero temperatures. In 1933 W. Meissner and R. Ochsenfeld discovered that in this regime of zero resistance, the materials also expelled magnetic fields[2], an effect named after Meissner. Two years later F. and H. London provided the first theoretical explanation of the peculiar Meissner effect in superconductors[3]. In 1950 a phenomenological theory of superconductivity was put forth by V. L. Ginzburg and L. D. Landau[4], providing a model of superconductivity as a second-order phase transition. The most important theoretical step came in 1957, with the first microscopic theory of superconductivity by J. Bardeen, L. Cooper and J. R. Schriffer[5]. The BCS-theory describes an attractive, phonon-mediated interaction between electrons, resulting in Cooper pairs that support superconductivity. The fact that the interaction is mediated by phonons is in agreement with observations that the critical temperature of a superconducting material, the temperature at which it transitions from a normal to a superconducting state, depends on the isotope mass of the material. Phonons, being vibrational excitations of the positive ions of a material, are thus expected to enter in the microscopic mechanism of superconductivity, see figure 1.1. In the late 1970s and early 1980s heavy fermion compounds were found that exhibited a superconducting phase transition at $T_c \lesssim 1$ K[6]. One might be tempted to think of these as low-T_c, but relative to the Fermi energy, inversely proportional to effective mass, this critical temperature is relatively high as compared to those of conventional superconductors, with a larger Fermi energy. It is unlikely that BCS-theory is capable of explaining superconductivity in these heavy fermion compounds, hinting at a different mechanism. Additionally, phonon-mediated superconductivity should break down at temperatures exceeding ~ 30 K, due to thermal fluctuations. However, in 1986 a cuprate material was found with a higher critical temperature[7], providing more evidence for other possible mechanisms of superconductivity than in the BCS-theory. In the last three decades several more of these high-temperature cuprate superconductors, in addition to others, have been discovered. The microscopic mechanism of these is still very much an open question in condensed matter physics, although there has been some recent

research shedding light on various aspects of it[8].

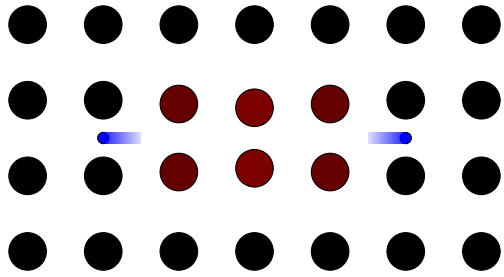

FIGURE 1.1: A qualitative picture of Cooper pairs. As an electron (blue) travel past ions there is a Couloumbic attraction exerted on them, leaving a positive concentration in its wake. Another electron is attracted by this concentration of charge. Movements in the lattice are called phonons, and the Cooper pair is formed by an attractive, phonon-mediated interaction.

Another class of materials that have spurred a lot of interest and research in the last decades are Dirac materials. Dirac materials, whose low-energy fermionic excitations behave as massless Dirac particles, satisfy the relativistic Dirac equation, rather than the non-relativistic Schrödinger equation. In essence, this group of materials display novel electronic properties that are of great interest within computation and electronics[9–17]. Graphene, the perhaps most known Dirac material, was first theorized in 1947 by P.R. Wallace [18] and for the first time fabricated in 2004 by Nobel Prize winners A. Geim and K. Novoselov[19]. The Dirac properties of graphene were theorized in 1984 by D. P. DiVincenzo and E. J. Mele [20]. Graphene is a two-dimensional lattice of carbon atoms, and due to its bipartite honeycomb lattice structure, gapless edge states arise, even though the bulk is insulating. See figure 1.2 for the well-known energy dispersion of graphene. The gapless edge states in graphene are protected by both inversion and time-reversal symmetry[21]. In 1987 edge states protected by time-reversal symmetry were predicted in HgTe quantum wells[22]. This prediction started the field of *topological insulators*, materials that are insulators in the bulk, but due to non-trivial topological bulk properties, possess gapless, and thus conducting edge states. The HgTe quantum well was experimentally realized in 2007[10], and since its prediction several other 2D and 3D materials have been discovered with topologically protected states. Grand efforts has also been undertaken in constructing the theoretical framework for this class of materials, and microscopic models, field theories and classification schemes have been developed[9, 23–26].

The fusion of the two fields superconductivity and topological insulators has brought forth the rather young research area of *topological superconductivity*. Topological phases in superconductors had been explored prior to the classification and theoretical framework of topological insulators[27], but the revelations arising from the latter has brought about increased focus on topological superconductors.

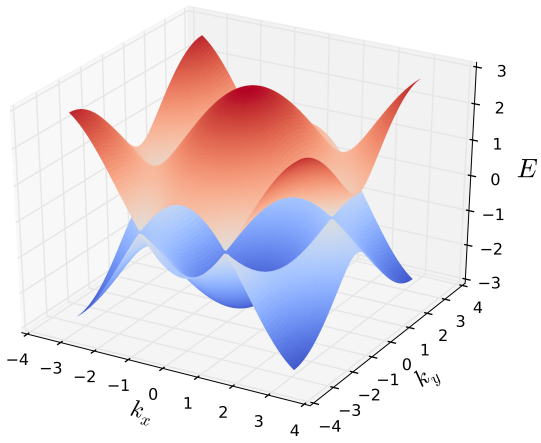

FIGURE 1.2: The energy dispersion of graphene. At six special points in the Brillouin zone the two bands touch and make Dirac cones, linear in momentum.

This class of systems display topologically protected superconducting edge states in the form of Majorana fermions[9, 28, 29]. Majorana fermions, first hypothesized by E. Majorana in 1937[30], are particles that are their own antiparticles, as opposed to Dirac fermions. Majorana fermions in topological superconductors exist as quasiparticles, and have been shown to obey non-Abelian statistics, and they may consequently lead the way to topological quantum computation[31]. The most prominently proposed mechanism for topological superconductivity is through a chiral p-wave superconductive pairing[9, 21, 29]. The chiral p-wave pairing ensures a relativistic quasiparticle dispersion, providing the grounding for Majorana fermions. Recently, the first experimental detection of Majorana fermions were made in a topological quantum spin liquid[32].

As is evident, a lot of interesting physics lies at the intersection of superconductivity and topological materials. The motivation for this thesis lies in the study of superconductivity in spin-orbit coupled systems. Spin-orbit coupling in general is a vastly rich field in that the effect is central to topological insulators, heterostructures, and other novel electronic phenomena[25, 33]. Spin-orbit coupling leads to spin-momentum locking and a splitting of spin-degenerate energy bands, effects that have interesting physical consequnces. In this thesis, we will focus on nearest neighbor hopping and Rashba-type spin-orbit coupling in two-dimensional Bravais- and bipartite lattices. The Hamiltonian for these two types of lattices is somewhat different, caused by the sublattice structure of the bipartite lattice. Diagonalizing these one-particle problems we will further the analysis to general

two-particle interaction terms in the Hamiltonian, bringing superconductivity into the picture through a mean field theory approach. The next step is to go into some detail on different pairing mechanisms in the diagonalized band basis, and investigate the resulting spin structure. We will investigate general requirements in these lattice models on the pairing interaction to achieve topologically non-trivial superconductivity, in particular through chiral p-wave pairing. In doing so the stage is opened up for Majorana edge states.

1.2 Structure of Thesis

This thesis starts off by going through some very basic preliminaries in terms of mathematical notation and physical theory in chapter 2. Chapter 3 will serve as a short introduction to aspects pertaining to symmetry and topology relevant to subsequent chapters. In chapter 4 we delve further into the underlying concepts and theory from physics that we build upon later in this thesis, among which are spin-orbit coupling, superconductivity and topological materials. We investigate the two-dimensional Bravais lattices in detail in chapter 5, and expand to bipartite lattices in chapter 6. Appendix A provides a simplified `Python`-code used for plotting energybands.

Chapter 2

Preliminaries

2.1 Mathematical Conventions

We will follow common notation in physics. Vectors and matrices are written boldfaced as in $\mathbf{A}$, while real and complex numbers are not, as in A. The cartesian unit vectors are written as $\hat{x}$, $\hat{y}$ and $\hat{z}$. Complex conjugation is noted by an asterisk z^*, Hermitian conjugation is denoted by a dagger $\mathbf{A}^\dagger$ and transposition is written with a T, as in $\mathbf{A}^T$. The commutator relationship of two matrices or operators is written with square brackets $[\mathbf{A}, \mathbf{B}] \equiv \mathbf{AB} - \mathbf{BA}$, while the anti-commutator is written with curly brackets $\{\mathbf{A}, \mathbf{B}\} \equiv \mathbf{AB} + \mathbf{BA}$. We will denote the derivative with respect to a varieble i as ∂_i. All instances of $\mathbf{r}$ and $\mathbf{x}$ refer to a spatial coordinate, $\mathbf{p}$ refer to a momentum coordinate, $\mathbf{k}$ refer to momentum space, σ refer to spin and E or ϵ to an energy. The Pauli spin matrices are

$$\sigma_x = \begin{pmatrix} 0 & 1 \\ 1 & 0 \end{pmatrix} \qquad \sigma_y = \begin{pmatrix} 0 & -i \\ i & 0 \end{pmatrix} \qquad \sigma_z = \begin{pmatrix} 1 & 0 \\ 0 & -1 \end{pmatrix}. \tag{2.1}$$

The tensor product of two matrices $\mathbf{A}$ and $\mathbf{B}$ is denoted $\mathbf{A} \otimes \mathbf{B}$. The tensor product is non-commutative and obey the following rule, for the example of 2x2 matrices $\mathbf{A}$ and $\mathbf{B}$

$$\begin{aligned} \mathbf{A} \otimes \mathbf{B} &= \begin{pmatrix} A_{11} & A_{12} \\ A_{21} & A_{22} \end{pmatrix} \otimes \begin{pmatrix} B_{11} & B_{12} \\ B_{21} & B_{22} \end{pmatrix} \\ &= \begin{pmatrix} A_{11}\begin{pmatrix} B_{11} & B_{12} \\ B_{21} & B_{22} \end{pmatrix} & A_{12}\begin{pmatrix} B_{11} & B_{12} \\ B_{21} & B_{22} \end{pmatrix} \\ A_{21}\begin{pmatrix} B_{11} & B_{12} \\ B_{21} & B_{22} \end{pmatrix} & A_{22}\begin{pmatrix} B_{11} & B_{12} \\ B_{21} & B_{22} \end{pmatrix} \end{pmatrix}. \end{aligned} \tag{2.2}$$

2.2 Quantum Theory

Some quick remarks regarding notation from quantum theory. For a more thorough treatment, see e.g. [34]. The most interesting quantum mechanical operator, and the one that describes the dynamics of a quantum system, is the Hamiltonian operator

$$\mathcal{H} = \frac{\mathbf{p}^2}{2m} + V(\mathbf{x}, t). \tag{2.3}$$

We will assume a time-independent potential. Together with a wavefunction, $\psi(\mathbf{x}, t)$, describing the state of our system, the Hamiltonian satisfies Schrödingers

equation

$$i\partial_t \psi(\mathbf{x},t) = \mathcal{H}\psi(\mathbf{x},t) = E\psi(\mathbf{x},t), \tag{2.4}$$

where E are the energy eigenvalues (or the spectrum of the Hamiltonian) of our system, i.e. the possible energies it can have. The Hamiltonian is hermitian, meaning that it is self adjoint

$$\mathcal{H}^\dagger \equiv \mathcal{H}^{*T} = \mathcal{H}. \tag{2.5}$$

A consequence of this is that the operator $\mathcal{H}$ has only real eigenvalues, as the energy must be real. The spectrum of a system will often be denoted by E_i or ϵ_i, where i denote the quantum numbers of the system, e.g. linear momentum, $\mathbf{p}$, crystal momentum, $\mathbf{k}$, or spin, σ.

We will make use of the second quantization formalism from Quantum Field Theory[a]. Particles are in second quantization understood as excitations of fields, and employ creation and annihilation operators, which will be reviewed presently. A state $|n_k\rangle$ can be created (excited) from the vacuum, $|0\rangle$, via a creation operator

$$\mathbf{c}_k^\dagger |0\rangle = |n_k\rangle. \tag{2.6}$$

Similarly a state may be destroyed via an annihilation operator

$$\mathbf{c}_k |n_k\rangle = |0\rangle. \tag{2.7}$$

Electrons are fermions (half-integer spin), and owing to the Pauli principle the creation and annihiliation operators for electrons must obey the following anti-commutator relations

$$\{\mathbf{c}_k^\dagger, \mathbf{c}_k^\dagger\} = 0 \tag{2.8}$$

$$\{\mathbf{c}_k, \mathbf{c}_k\} = 0 \tag{2.9}$$

$$\{\mathbf{c}_{k_i}^\dagger, \mathbf{c}_{k_j}\} = \delta_{ij}. \tag{2.10}$$

Given that the first-quantized form of a single-particle Hamiltonian is known, $\mathcal{H}_1 |\phi_k\rangle = \epsilon_k |\phi_k\rangle$, the single-particle operator is in second-quantized language written as

$$\mathcal{H}_1 = \sum_{k_i k_j} \langle k_i | \mathcal{H}_1 | k_j \rangle \mathbf{c}_{k_i}^\dagger \mathbf{c}_{k_j}, \tag{2.11}$$

where the matrix elements are $\langle k_i | \mathcal{H}_1 | k_j \rangle = \int \phi_{k_i}^*(\mathbf{x}_1) \mathcal{H}_1 \phi_{k_j}(\mathbf{x}_2) d\mathbf{x}_1 d\mathbf{x}_2$. For a non-interacting system there is only on-site overlap, and we write

$$\mathcal{H}_1 = \sum_k \epsilon_k \mathbf{c}_k^\dagger \mathbf{c}_k. \tag{2.12}$$

[a] See e.g. [35] for a more thorough treatment of many-body quantum theory.

A two-particle operator is in second-quantized language written as

$$\mathcal{H}_2 = \sum_{k_i k_j k_n k_m} \langle k_i k_j | \mathcal{H}_2 | k_n k_m \rangle \mathbf{c}^\dagger_{k_i} \mathbf{c}^\dagger_{k_j} \mathbf{c}_{k_n} \mathbf{c}_{k_m}, \tag{2.13}$$

with $\langle k_i k_j | \mathcal{H}_2 | k_n k_m \rangle = \int \phi^*_{k_i}(\mathbf{x}_1) \phi^*_{k_j}(\mathbf{x}_2) \mathcal{H}_2 \phi_{k_n}(\mathbf{x}_2) \phi_{k_m}(\mathbf{x}_1) d\mathbf{x}_1 d\mathbf{x}_2$. These matrix elements describe two ingoing particles $\phi_{k_m}(\mathbf{x}_1)$ and $\phi_{k_n}(\mathbf{x}_2)$ interacting through the mechanism $\mathcal{H}_2$ resulting in the two outgoing particles $\phi_{k_i}(\mathbf{x}_1)$ and $\phi_{k_j}(\mathbf{x}_2)$.

Starting out with creation and annihilation operators working in a discretized, periodic position space, $\mathbf{c}^\dagger_{\mathbf{x}_i}$ and $\mathbf{c}_{\mathbf{x}_i}$, we may in second quantization language write the Fourier transform to continuous momentum space and vice versa by

$$\mathbf{c}_{\mathbf{k}} = \frac{1}{\sqrt{N}} \sum_{\mathbf{x}_i} \mathbf{c}_{\mathbf{x}_i} e^{-i\mathbf{k}\cdot\mathbf{x}_i} \tag{2.14}$$

$$\mathbf{c}^\dagger_{\mathbf{k}} = \frac{1}{\sqrt{N}} \sum_{\mathbf{x}_i} \mathbf{c}_{\mathbf{x}_i} e^{i\mathbf{k}\cdot\mathbf{x}_i} \tag{2.15}$$

$$\mathbf{c}_{\mathbf{x}_i} = \frac{1}{\sqrt{N}} \sum_{\mathbf{k}} \mathbf{c}_{\mathbf{k}} e^{i\mathbf{k}\cdot\mathbf{x}_i} \tag{2.16}$$

$$\mathbf{c}^\dagger_{\mathbf{x}_i} = \frac{1}{\sqrt{N}} \sum_{\mathbf{k}} \mathbf{c}_{\mathbf{k}} e^{-i\mathbf{k}\cdot\mathbf{x}_i}, \tag{2.17}$$

N being the number of discrete lattice points in our system. These will be extensively used, in addition to the relations

$$\frac{1}{N} \sum_{\mathbf{k}} e^{i\mathbf{k}\cdot(\mathbf{x}_i - \mathbf{x}_j)} = \delta_{ij} \tag{2.18}$$

$$\frac{1}{N} \sum_{\mathbf{x}_i} e^{i\mathbf{x}_i\cdot(\mathbf{k} - \mathbf{k}')} = \delta(\mathbf{k} - \mathbf{k}'). \tag{2.19}$$

Chapter 3

Topology and Symmetry

In mathematics, topology is the study of geometrical properties and spatial relations unaffected by the continuous change of shape or size of figures. What lies at the heart of applied topology is the distinction between different topologies, which in physics translates to the distinction of different topological phases. We say that a physical system, call it A, is topologically distinct from system B, if by the underlying theorems of topology, we cannot continuosly change system A to B. As a result, the two systems are in different topological phases, and will display different physics. Topology is a vast field, even when applied to physics, so this chapter will aim to give a brief and conscice introduction to the aspects of relevance to this thesis, namely topological insulators and superconductors. For more thorough treatments applied to physics, see for instance [9, 23, 25].

3.1 The Berry Phase and The Chern Number

In 1984 M. V. Berry derived[36] a topological invariant for quantum systems, described through a geometric quantum phase. When going around a closed loop $\mathcal{C}$ in $\mathbf{k}$-space, the eigenstates of a quantum system acquire a non-trivial geometrical phase factor, $e^{i\gamma(\mathcal{C})}$, where $\gamma(\mathcal{C})$ is referred to as the Berry phase. The Berry phase for a given eigenstate $|u_m(\mathbf{k})\rangle$ is given by the line integral along $\mathcal{C}$ of the Berry connection

$$\gamma_m(\mathcal{C}) = \oint_{\mathcal{C}} \mathcal{A}_m(\mathbf{k}) d\mathbf{k}, \tag{3.1}$$

where the Berry connection $\mathcal{A}_m(\mathbf{k})$ is a vector potential given by

$$\mathcal{A}_m = i \langle u_m(\mathbf{k}) | \nabla_{\mathbf{k}} | u_m(\mathbf{k}) \rangle. \tag{3.2}$$

This result assumes an adiabatic evolution of the quantum system, i.e. that we go around the closed loop slowly. It is observed that the Berry connection is not gauge invariant. Applying a $U(1)$ gauge transformation to an eigenstate

$$|u_m(\mathbf{k})\rangle \to e^{i\phi(\mathbf{k})} |u_m(\mathbf{k})\rangle, \tag{3.3}$$

will transform the vector potential by

$$\mathcal{A}_m(\mathbf{k}) \to \mathcal{A}_m(\mathbf{k}) + i\nabla_{\mathbf{k}}\phi(\mathbf{k}). \tag{3.4}$$

This again will transform the Berry phase as

$$\gamma_m(\mathcal{C}) \to \gamma_m(\mathcal{C}) + 2\pi N, \tag{3.5}$$

with the integer $N = \oint \nabla_{\mathbf{k}} \phi(\mathbf{k}) d\mathbf{k}$. It is then obvious that the actual phase factor an eigenstate acquires, $e^{i\gamma(\mathcal{C})}$, is gauge-invariant, and has the properties of a U(1) gauge field. Via Stokes theorem[37] the line integral of the Berry connection can also be found from the surface integral of the curl of the Berry connection

$$\gamma_m(\mathcal{C}) = \int \mathcal{F}_m d^2\mathbf{k}. \tag{3.6}$$

The curl of the Berry connection, $\mathcal{F}_m = \nabla \times \mathcal{A}_m$ is called the Berry curvature[38], or the Berry flux[23], and resembles a magnetic field mathematically. The integral is over the two-dimensional sphere S^2 in $\mathbf{k}$-space. $\mathcal{F}_m$ is found from[21]

$$\mathcal{F}_m = \mathcal{I}m \sum_{n \neq m} \frac{\langle u_m(\mathbf{k}) | \nabla_{\mathbf{k}} \mathcal{H}(\mathbf{k}) | u_n(\mathbf{k}) \rangle \times \langle u_n(\mathbf{k}) | \nabla_{\mathbf{k}} \mathcal{H}(\mathbf{k}) | u_m(\mathbf{k}) \rangle}{(E_n(\mathbf{k}) - E_m(\mathbf{k}))^2}, \tag{3.7}$$

where $E_n(\mathbf{k})$ is the energy dispersion relation for the eigenstate $|u_n(\mathbf{k})\rangle$. As can be easily seen from the denominator, a degenerate energy value causes a singularity in the Berry curvature. As such, degeneracies in the energy dispersion are the contributors to $\gamma_m(\mathcal{C})$. One can now define a topological invariant, called the first Chern number[a]

$$\mathrm{Ch}_1 = \frac{\gamma_m(\mathcal{C})}{2\pi}. \tag{3.8}$$

The Chern number is an integer[40], $\mathbb{Z}$, and an invariant even if the loop $\mathcal{C}$ encloses a degeneracy of the Hamiltonian $\mathcal{H}(\mathbf{k})$. In essence, the Chern number is a measure of the flux of the vector potential $\mathcal{A}_m$ through the $\mathbf{k}$-space, meaning that the Chern number is non-trivial only when $\mathcal{A}_m$ has a singularity. The Chern number carries with it some important consequences. The textbook example is that of the inteqer quantum Hall effect[41]. Exerting a two-dimensional electron gas to a perpendicular magnetic field will restrict the motion of the electrons to quantized circular orbits. This will again lead to quantized energy levels, and in turn to quantized conductivity. The integer quantum Hall conductivity may be written[40, 42]

$$\sigma_H = \frac{e^2}{h} \mathrm{Ch}_1, \tag{3.9}$$

i.e. the Hall conductivity is quantized by the Chern number. Halperin[43] and Hatsugai[44] showed that the Hall conductivity can also be written as

$$\sigma_H = \frac{e^2}{h} n_{\mathrm{edge}}, \tag{3.10}$$

where n_{edge} is the number of gapless edge states in the system. *This means that if a two-dimensional system has a bulk with a non-trivial Chern number, there will exist gapless states at the edge/boundary of the system*. This relation between a topological quantity of the bulk and edge states is called the bulk-edge correspondence, and is

[a] The topological invariant also goes by the names the Chern invariant[23, 39], or the Thouless-Kohmoto-den Njis-Nightingale (TKNN) number[29]

our first encounter with what many argue prerequisites a topological material.

The Chern number is more generally defined as a winding number. The winding number, in its simplest form, is the number of times a closed curve travels around a given point in some space, without going through the point. The winding number is also called the degree of a continuous mapping. The energy dispersion is described by a mapping from the momenta $\mathbf{k}$ to the Hamiltonian $\mathcal{H}(\mathbf{k})$. We say that two target spaces, $\mathcal{H}(\mathbf{k})$, can be continuosly deformed into each other if the deformation keeps all gaps in the energy dispersion open. Hamiltonians that satisfy this condition belong to the same equivalence class, and have the same winding number. The Chern number discussed above is just an example of such a winding number. This means that if a Hamiltonian is deformed into another, and this deformation closes the energy gap, the two Hamiltonians belong to different topological phases, characterized by different winding numbers. As such, a change in the winding number constitutes a topological phase transition.

3.2 Symmetries and the $\mathbb{Z}_2$ Invariant

The Chern number classifies systems that break time-reversal symmetry[23]. For the case of the quantum Hall effect this is true because time-reversal combined with the magnetic field flips the direction of motion of the electrons. Time-reversal invariant systems can however be topologically classified by another topological number, if spin-orbit coupling is added to the system. In 2005 Kane and Mele[25] defined the $\mathbb{Z}_2$ invariant of time-reversal invariant topological insulators ν via the quantities

$$\delta_a = \frac{\sqrt{\det[w(\Gamma_a)]}}{\mathrm{Pf}[w(\Gamma_a)]}. \tag{3.11}$$

$w(\Gamma_a)_{nm}$ is the matrix connecting an eigenstate $|u_n(\mathbf{k})\rangle$ with the other time-reversed eigenstates $|u_m(-\mathbf{k})\rangle$

$$w(\Gamma_a)_{nm} = \langle u_m(-\mathbf{k})|\,\Theta\,|u_n(\mathbf{k})\rangle. \tag{3.12}$$

Γ_a are the time-reversal invariant momenta, which can be generally written

$$\Gamma_a = \frac{n_1\mathbf{b}_1 + n_2\mathbf{b}_2}{2}, \tag{3.13}$$

where $\mathbf{b}_i$ is a reciprocal lattice vector. The spin-orbit coupling lifts the spin-degeneracy of the energy dispersion, except at these time-reversal invariant momenta. Pf denotes the Pfaffian of the matrix, with the property $\mathrm{Pf}(A) = \det(A)^2$. With the quantities δ_a, the topological invariant, ν, may be written

$$(-1)^\nu = \prod_{n=0,1} \delta_{a=(n_1,n_2)}. \tag{3.14}$$

δ_a satisfy the following conditions:

- The quantity is only defined at time-reversal invariant momenta.

- The quantity takes on only the values $\delta_a = \pm 1$.
- The quantity can only change when the gap of the system closes, given a fixed gauge.

Let us now relate these quantities to properties of the system. [45] considers systems with an additional inversion symmetry, which could be for instance the honeycomb lattice. The system then satisfies $\hat{P}\mathcal{H}(\mathbf{k})\hat{P}^{-1} = \mathcal{H}(-\mathbf{k})$, i.e. the Hamiltonian of the system is invariant under $\hat{P}\mathbf{k} \to -\mathbf{k}$. The eigenvalues of $\hat{P}$, P, evaluated at the time-reversal invariant momenta, $P(\Gamma_a)$, are found to satisfy the same properties as δ_a, such that the topological invariant for these systems with inversion symmetry may be written

$$(-1)^{\nu} = \prod_m P_m(\Gamma_a). \tag{3.15}$$

This means that one can easily distinguish topological insulators from trivial insulators with the help of parity and eigenstate considerations.

In [46] the same scheme as above is followed for a triplet superconductor. A general Hamiltonian for this system is[b]

$$\mathcal{H} = \sum_{\mathbf{k}} \psi^{\dagger}_{\mathbf{k}} \mathcal{H}(\mathbf{k}) \psi_{\mathbf{k}} \tag{3.16}$$

$$\mathcal{H}(\mathbf{k}) = \begin{pmatrix} \epsilon(\mathbf{k})\mathcal{I}_{2\times 2} & \Delta(\mathbf{k}) \\ \Delta(\mathbf{k})^{\dagger} & -\epsilon(\mathbf{k})\mathcal{I}_{2\times 2} \end{pmatrix}, \tag{3.17}$$

with the Nambu spinor $\psi^{\dagger}_{\mathbf{k}} = (\mathbf{c}^{\dagger}_{\mathbf{k},\sigma}\ \mathbf{c}_{-\mathbf{k},\sigma})$. We assume that the normal state of this system, described by $\epsilon(\mathbf{k})$, satisfies inversion symmetry ($\hat{P}$) and time-reversal symmetry ($\hat{\Theta}$), such that $\epsilon(-\mathbf{k}) = \epsilon(\mathbf{k})$. Time-reversal invariancy demands

$$\hat{\Theta}\mathcal{H}(\mathbf{k})\hat{\Theta}^{-1} = \mathcal{H}(-\mathbf{k})^*, \tag{3.18}$$

with the time-reversal operator

$$\hat{\Theta} = i\sigma_y \otimes \mathcal{I}_{2\times 2}. \tag{3.19}$$

A spin-triplet pairing is characterized by

$$\Delta(-\mathbf{k}) = -\Delta(\mathbf{k}). \tag{3.20}$$

This allows us to define a new symmetry for $\mathcal{H}(\mathbf{k})$

$$\Pi\mathcal{H}(\mathbf{k})\Pi^{-1} = \mathcal{H}(-\mathbf{k}), \tag{3.21}$$

with $\Pi = \mathcal{I}_{2\times 2} \otimes \sigma_z$. The eigenvalues of Π are given by the sign of the normal state dispersion evaluated at the time-reversal invariant momenta

$$\pi_a = -\text{sgn}\ \epsilon(\Gamma_a). \tag{3.22}$$

[b] We will look more closely at how this Hamiltonian comes about later in the thesis. It is written explicitly here to make it more clear what we are talking about.

Remarkably, these eigenvalues satisfy the same properties as the δ_a. It is then suggested that one may write the $\mathbb{Z}_2$ topological invariant as

$$(-1)^{\nu} = \prod_{n_j=0,1} \operatorname{sgn} \epsilon(\Gamma_{a=(n_1,n_2)}). \tag{3.23}$$

The quantity $\prod_{n_j=0,1} \operatorname{sgn} \epsilon(\Gamma_{a=(n_1,n_2)})$ may again be related to the number of different connected components in the normal state $\epsilon(\mathbf{k})$, which is denoted $\rho_0(S_F)$, such that

$$(-1)^{\nu} = (-1)^{\rho_0(S_F)}. \tag{3.24}$$

In other words, the topological invariant is directly connected to the number of distinct Fermi surfaces the system has, see figure 3.1. In addition, the bulk-edge correspondence may be written[46]

$$(-1)^{\nu} = (-1)^{N}, \tag{3.25}$$

where N is the number of edge states. Based on this, an odd number of Fermi surfaces ensures an odd, non-trivial topological invariant of the system, and thus an odd number of edge states. On the other hand, given that the topological invariant of our system is $\mathbb{Z}_2$, an even number of Fermi surfaces is equivalent to $\nu = 0$. The system is in the topologically trivial phase, and there cannot be any edge states. The important point is that if we have a system with a topologically non-trivial bulk, we are ensured to have topologically protected edge states

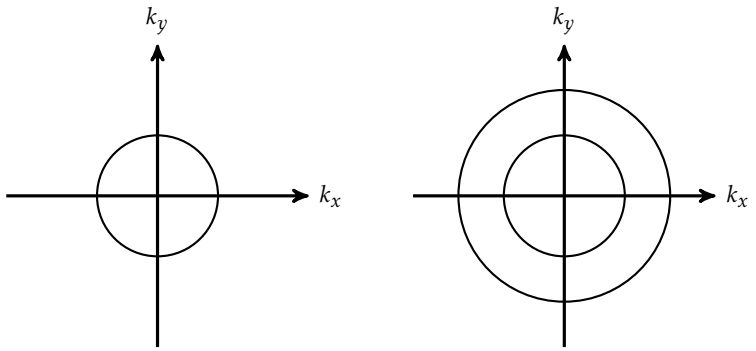

Figure 3.1: Left: An odd number of Fermi surfaces, resulting in edge states. Right: An even number of Fermi surfaces, resulting in no edge states.

So far we have seen a sampling of systems with parity, time-reversal symmetry and others. There are countless other combinations of symmetries that could be considered, and all of these can be structured to make "the periodic table" of topological insulators and superconductors[47], see Table 3.1. The labeling AZ refers to the 10 symmetry classes in the notation of [48]. TRS refers to time-reversal symmetry, PHS to particle-hole symmetry and CS to chiral symmetry. Chiral symmetry is the

Table 3.1: The periodic table of topological insulators and superconducors. The labeling AZ refers to the 10 symmetry classes in the notation of [48]. TRS refers to time-reversal symmetry, PHS to particle-hole symmetry and CS to chiral symmetry. The value zero in the symmetry columns reflects that the symmetry is broken, while ±1 denotes the eigenvalue if the symmetry is unbroken. The three rightmost columns are labelled by their dimension, d. The value zero in these columns denote that there is no topological invariant in the given dimension, and hence that the corresponding system is trivial in terms of topology. Based on Table I of [23].

	Symmetry			d		
AZ	TRS	PHS	CS	1	2	3
A	0	0	0	0	$\mathbb{Z}$	0
AIII	0	0	1	$\mathbb{Z}$	0	$\mathbb{Z}$
AI	1	0	0	0	0	0
BDI	1	1	1	$\mathbb{Z}$	0	0
D	0	1	0	$\mathbb{Z}_2$	$\mathbb{Z}$	0
DIII	-1	1	1	$\mathbb{Z}_2$	$\mathbb{Z}_2$	$\mathbb{Z}$
AII	-1	0	0	0	$\mathbb{Z}_2$	$\mathbb{Z}_2$
CII	-1	-1	1	$\mathbb{Z}$	0	$\mathbb{Z}_2$
C	0	-1	0	0	$\mathbb{Z}$	0
CI	1	-1	1	0	0	$\mathbb{Z}$

combined effect of time-reversal symmetry and particle-hole symmetry, $\hat{\Theta}\hat{T}$. The value zero in the symmetry column reflects that the symmetry is broken, while ±1 denotes the eigenvalue of the symmetry operator squared if the symmetry is unbroken, e.g. $\hat{T}^2$. The three rightmost columns are labelled by their dimension, d. The value zero in these columns denote that there is no topological invariant in the given dimension. The quantum Hall state falls into class A in two dimensions, the time-reversal invariant topological insulators in AII and the triplet superconductor falls into class DIII.

Chapter 4

Underlying Concepts and Theory

This chapter will review and rederive physical theories and results of importance to this thesis, in particular nearest neighbour hopping and Rashba spin-orbit coupling, the BCS approach to superconductivity, and topological insulators and superconductivity.

4.1 The One-Particle Problem

The Hamiltonian of a collection of identical, non-interacting particles in an ion lattice can be written

$$\mathcal{H} = \sum_i \frac{\mathbf{p}_i^2}{2m} + U(\mathbf{r}_i), \tag{4.1}$$

where $\frac{\mathbf{p}_i^2}{2m}$ is the standard intrinsic kinetic energy of particle i, and $U(\mathbf{r}_i)$ is the external potential from the ion lattice experienced by a particle at position $\mathbf{r}_i$. Since we are working on a lattice, it is natural to assume that a particle will spend most of its time at a given lattice point, so the external potential can be split into two parts

$$U(\mathbf{r}_i) = U(\mathbf{r}_i, \mathbf{R}_i) + \sum_{i \neq j} U(\mathbf{r}_i, \mathbf{R}_j). \tag{4.2}$$

$\mathbf{R}_i$ denotes the coordinate of lattice point i, such that the first term accounts for the potential contribution from a particles "mother" ion, while the second term accounts for the contribution from every other ion in the lattice. With these definitions it is logical to work with basis functions, $\psi_{i,\sigma}(\mathbf{r}_i)$, that are eigenfunctions of electrons around these isolated ions

$$\left(\frac{\mathbf{p}_i^2}{2m} + U(\mathbf{r}_i, \mathbf{R}_i)\right)\psi_{i,\sigma}(\mathbf{r}_i) = \epsilon_{i,\sigma}\psi_{i,\sigma}(\mathbf{r}_i). \tag{4.3}$$

The quantum numbers we are concerned with are position, i, and spin, σ. One could additionally take e.g. orbitals into account, but we will restrict ourselves to a single orbital at each ion. The second-quantization form of this Hamiltonian is

$$\mathcal{H} = \sum_{i,\sigma} \epsilon_{i,\sigma} \mathbf{c}_{i,\sigma}^\dagger \mathbf{c}_{i,\sigma}. \tag{4.4}$$

It is natural to assume a site- and spin-independent ϵ such that

$$\mathcal{H} = \epsilon \sum_{i,\sigma} \mathbf{c}^{\dagger}_{i,\sigma} \mathbf{c}_{i,\sigma}. \tag{4.5}$$

$\mathbf{c}^{\dagger}_{i,\sigma} \mathbf{c}_{i,\sigma}$ defines the number operator, $\mathbf{n}_{i,\sigma}$, which count the number of particles in a given state i, σ. As such the expression (4.5) is the number of particles multiplied by the energy of a single particle. Introducing the second external potential term will now lead to scattering of particles from one lattice point to another, since we are considering contributions from other positions $\mathbf{R}_j$. In second-quantization this potential-term is

$$\sum_{i} \sum_{i \neq j} U(\mathbf{r}_i, \mathbf{R}_j) \rightarrow \sum_{i,j,\sigma} t_{i,j} \mathbf{c}^{\dagger}_{i,\sigma} \mathbf{c}_{j,\sigma}, \tag{4.6}$$

where the matrix element $t_{i,j}$ is the scattering amplitude from ion lattice site j to i, i.e. a hopping amplitude. It is independent of spin because the external potential is spin-independent. This hopping from one site to another is inherently the kinetic energy of the particle in the lattice, while the intrinsic kinetic energy ϵ now takes the form of an on-site energy in the lattice; the energy required to excite the state in the first place. To simplify matters, it is assumed that the hopping amplitude is symmetric, $t_{i,j} = t_{j,i}$, and that the largest contributions to the term are from lattice points that are nearest neighbours. The hopping amplitude is then set to $t_{i,j} \equiv t_{\mathrm{NN}}$ such that

$$\mathcal{H} = \epsilon \sum_{i,\sigma} \mathbf{c}^{\dagger}_{i,\sigma} \mathbf{c}_{i,\sigma} + \sum_{\langle i,j \rangle \sigma} t_{\mathrm{NN}} \mathbf{c}^{\dagger}_{i,\sigma} \mathbf{c}_{j,\sigma}. \tag{4.7}$$

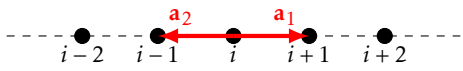

Figure 4.1: The one-dimensional unit chain with the nearest neighbor vectors $\mathbf{a_1}$ and $\mathbf{a_2}$.

To look at a specific example, consider the one-dimensional unit chain of lattice points, such that $\mathbf{k} = k$. Each point has two nearest neighbours, given by nearest neighbour vectors $\mathbf{a}_1 = 1$ and $\mathbf{a}_2 = -1$, see figure 4.1. Fourier transforming the Hamiltonian to momentum space yields

$$\begin{aligned} \mathcal{H} &= \epsilon \sum_{k,\sigma} \mathbf{c}^{\dagger}_{k,\sigma} \mathbf{c}_{k,\sigma} + \sum_{k,\sigma} t_{\mathrm{NN}} \mathbf{c}^{\dagger}_{k,\sigma} \mathbf{c}_{k,\sigma} (e^{ik} + e^{-ik}) \\ &= \sum_{k,\sigma} \tilde{\epsilon}_{k,\sigma} \mathbf{c}^{\dagger}_{k,\sigma} \mathbf{c}_{k,\sigma}, \end{aligned} \tag{4.8}$$

with the one-particle energy

$$\tilde{\epsilon}_{k,\sigma} = \epsilon + 2 t_{\mathrm{NN}} \cos(k). \tag{4.9}$$

The on-site energy ϵ defines a reference level for the momentum-dependent energy dispersion.

4.1.1 The Dirac Equation and Spin-Orbit Coupling

Spin-orbit coupling is a quantum effect stemming from the interaction between a particle's motion, described by its momentum, and its spin. The effect of spin-orbit coupling is to lock the spin of a particle to its linear momentum, and to split the spin-degeneracy of energy bands[33]. The spin-orbit interaction is a relativistic correction to Schrödingers equation and can be found from the Dirac equation. The Dirac equation[49] in its original form is

$$\Big(\beta mc^2 + c\sum_{\mu=1}^{3}\alpha_\mu p_\mu\Big) = i\hbar\partial_t\psi(x,t). \tag{4.10}$$

Here β and α_μ are 4-matrices that satisfy the following relations

$$\alpha_\mu^2 = \beta^2 = 1 \tag{4.11}$$

$$\alpha_\mu\alpha_\nu + \alpha_\nu\alpha_\mu = 0 \tag{4.12}$$

$$\alpha_\mu\beta + \beta\alpha_\mu = 0, \tag{4.13}$$

i.e their squares are equal to the identity matrix, and for μ, ν distinct they mutually anticommute. Let us look at an electron with charge e and mass m_e. Assuming a vector-potential $\mathbf{A}$, scalar potential ϕ and kinetic and potential energies much less than $m_e c^2$, it can be shown[50] that the Dirac equation reads

$$\Big(\frac{1}{2m_e}(\mathbf{p} - \frac{e}{c}\mathbf{A})^2 + e\phi - \frac{e\hbar}{2m_e c}\sigma\cdot\mathbf{B} + i\frac{e\hbar}{4m_e^2c^2}\mathbf{E}\cdot\mathbf{p} - \frac{e\hbar}{4m_e^2c^2}\sigma\cdot(\mathbf{E}\times\mathbf{p})\Big)\psi = W\psi, \tag{4.14}$$

with $E_{tot} = W + mc^2$. The first and second term is here equivalent to Schrödingers equation for external fields $\mathbf{A}$ and ϕ. The third term is the interaction between the magnetic moment of the electron, caused by its spin $-\mu = \frac{e\hbar}{2m_e}\sigma$, and a magnetic field, $\mathbf{B}$. The fourth and the fifth term are the leading relativistic corrections to the energy, the fourth being a zero-point fluctuation energy, and the fifth is the spin-orbit coupling. Assuming a centrally symmetric $\mathbf{E}$, like the case for orbital motion of an electron around an atom, the electric field may be written[51]

$$\mathbf{E} = -\frac{1}{e}\frac{\mathbf{r}}{r}\frac{dV}{dr}. \tag{4.15}$$

The spin-orbit coupling term of the Dirac equation can then be rewritten as

$$\mathcal{H}_{\text{SOC}} = -\frac{e\hbar}{4m_e^2c^2}\sigma\cdot(\mathbf{E}\times\mathbf{p}) \tag{4.16}$$

$$= \frac{e}{2m_e^2c^2}\mathbf{S}\cdot\Big(-\frac{1}{e}\frac{\mathbf{r}}{r}\frac{dV}{dr}\times\mathbf{p}\Big) \tag{4.17}$$

$$= \frac{1}{2m_e^2c^2}\frac{1}{r}\frac{dV}{dr}(\mathbf{S}\cdot\mathbf{L}) \tag{4.18}$$

$$\equiv \lambda_{SO}\mathbf{S}\cdot\mathbf{L}, \tag{4.19}$$

where $\mathbf{S} = \frac{\hbar}{2}\boldsymbol{\sigma}$ and $\mathbf{L} = \mathbf{r} \times \mathbf{p}$. The spin-orbit coupling Hamiltonian is now cast in a familiar form, and the interaction between spin and orbital motion is clear. Looking at the spin-orbit coupling term in (4.14) let us assume an electric field perpendicular to our two-dimensional lattice, i.e. $\mathbf{E} = E\hat{z}$. The spin-orbit coupling Hamiltonian is then

$$\mathcal{H}_{\text{SOC}} = -\frac{e\hbar}{4m_e^2c^2} E\boldsymbol{\sigma} \cdot (\hat{z} \times \mathbf{p}) \tag{4.20}$$

$$= i\frac{e\hbar^2}{4m_e^2c^2} E\Big(\sigma_y \frac{\partial}{\partial x} - \sigma_x \frac{\partial}{\partial y}\Big) \tag{4.21}$$

$$= \frac{e\hbar^2 E}{4m_e^2c^2}(\sigma_x k_y - \sigma_y k_x). \tag{4.22}$$

This type of spin-orbit coupling is named Rashba-type spin-orbit coupling[52], and with $\lambda_R = \frac{e\hbar^2 E}{4m_e^2c^2}$, the expression is

$$\mathcal{H}_{\text{SOC}} = \lambda_R(\sigma_x k_y - \sigma_y k_x). \tag{4.23}$$

It is apparent from the expression that $\mathcal{H}_{\text{SOC}}(-\mathbf{k}) = -\mathcal{H}_{\text{SOC}}(\mathbf{k})$, i.e. odd in momentum. The pauli matrices σ_i act on the spin-part of the operators

$$\sigma_x \uparrow = \downarrow \tag{4.24}$$

$$\sigma_x \downarrow = \uparrow \tag{4.25}$$

$$\sigma_y \uparrow = i \downarrow \tag{4.26}$$

$$\sigma_y \downarrow = -i \uparrow, \tag{4.27}$$

and $k_i = -i\partial_i$. Consider again the one-dimensional unit chain of lattice points, with nearest neighbors $\mathbf{a}_1 = 1$ and $\mathbf{a}_2 = -1$, figure 4.1. In one dimension, along the x-direction, we only need to consider the term $\sigma_y k_x$, and on the chain k_x may be discretized as

$$k_x = -i(\mathbf{c}_i^\dagger \mathbf{c}_{i+1} - \mathbf{c}_i^\dagger \mathbf{c}_{i-1}). \tag{4.28}$$

Taking spin into account, the product $\sigma_y k_x$ is then

$$\begin{aligned}\sigma_y(-i(\mathbf{c}_i^\dagger \mathbf{c}_{i+1} - \mathbf{c}_i^\dagger \mathbf{c}_{i-1})) &= -i\begin{pmatrix}\mathbf{c}_{i,\uparrow}^\dagger & \mathbf{c}_{i,\downarrow}^\dagger\end{pmatrix}\begin{pmatrix}0 & -i\\ i & 0\end{pmatrix}\begin{pmatrix}\mathbf{c}_{i+1\uparrow}\\ \mathbf{c}_{i+1\downarrow}\end{pmatrix} + i\begin{pmatrix}\mathbf{c}_{i,\uparrow}^\dagger & \mathbf{c}_{i,\downarrow}^\dagger\end{pmatrix}\begin{pmatrix}0 & -i\\ i & 0\end{pmatrix}\begin{pmatrix}\mathbf{c}_{i-1\uparrow}\\ \mathbf{c}_{i-1\downarrow}\end{pmatrix}\\ &= -\mathbf{c}_{i,\uparrow}^\dagger \mathbf{c}_{i+1,\downarrow} + \mathbf{c}_{i,\downarrow}^\dagger \mathbf{c}_{i+1,\uparrow} + \mathbf{c}_{i,\uparrow}^\dagger \mathbf{c}_{i-1,\downarrow} - \mathbf{c}_{i,\downarrow}^\dagger \mathbf{c}_{i-1,\uparrow}.\end{aligned} \tag{4.29}$$

The total Rashba Hamiltonian may now be written

$$\mathcal{H}_{\text{SOC}} = \lambda_R \sum_i \Big(-\mathbf{c}_{i,\uparrow}^\dagger \mathbf{c}_{i+1,\downarrow} + \mathbf{c}_{i,\downarrow}^\dagger \mathbf{c}_{i+1,\uparrow} + \mathbf{c}_{i,\uparrow}^\dagger \mathbf{c}_{i-1,\downarrow} - \mathbf{c}_{i,\downarrow}^\dagger \mathbf{c}_{i-1,\uparrow} \Big). \tag{4.30}$$

Fourier transforming to momentum space results in

$$\mathcal{H}_{\text{SOC}} = \lambda_R \sum_k \Big(\mathbf{c}_{k,\uparrow}^\dagger \mathbf{c}_{k,\downarrow}(e^{-ik} - e^{ik}) + \mathbf{c}_{k,\downarrow}^\dagger \mathbf{c}_{k,\uparrow}(e^{ik} - e^{-ik}) \Big) \tag{4.31}$$

$$= \sum_k \Big(s_k^* \mathbf{c}_{k,\uparrow}^\dagger \mathbf{c}_{k,\downarrow} + s_k \mathbf{c}_{k,\downarrow}^\dagger \mathbf{c}_{k,\uparrow} \Big), \tag{4.32}$$

with $s_k = 2i\lambda_R \sin(k)$. The Rashba Hamiltonian thus describes a hopping process in which the spin flips, with matrix element s_k. Another, more illuminating and general way to write the Rashba Hamiltonian for an arbitrary lattice is

$$\mathcal{H}_{\text{SOC}} = \lambda_R \sum_{\mathbf{r}_i, \mathbf{a}_j, \alpha, \beta} \mathbf{c}^\dagger_{\mathbf{r}_i,\alpha} \Big[-\sigma_x^{\alpha\beta}(i\mathbf{a}_j \cdot \hat{y}) + \sigma_y^{\alpha\beta}(i\mathbf{a}_j \cdot \hat{x}) \Big] \mathbf{c}_{\mathbf{r}_i + \mathbf{a}_j, \beta}. \tag{4.33}$$

$\mathbf{a}_j$ are the nearest neighbour vectors, and α and β here refer to the spin-indices on the operators. We have used that $k_i = -i\partial_i$, and that acting on $e^{i\mathbf{k}} \cdot \mathbf{a}_j$ with ∂_i picks out $i\mathbf{a}_j \cdot \hat{i}$. From this form it is straightforward to calculate the Rashba spin-orbit coupling term for any lattice.

4.2 Two-Particle Interaction Term

We next look at a two-particle interaction term, starting from a Hubbard model, and going from there to a general model. The Hubbard model reads

$$\mathcal{H} = \sum_{\langle i,j \rangle \sigma} t \mathbf{c}^\dagger_{i,\sigma} \mathbf{c}_{j,\sigma} + U \sum_i \mathbf{n}_{i,\uparrow} \mathbf{n}_{j,\downarrow}. \tag{4.34}$$

The first term is recognized as a hopping term, while the second term is an on-site repulsion caused by having more than one electron at a site. This is of course allowed by the Fermi principle if their spins are opposite, as is clear from the expression. Focusing on the second term only, and writing out the number operators leads to

$$\mathcal{H}_U = U \sum_i \mathbf{c}^\dagger_{i,\uparrow} \mathbf{c}_{i,\uparrow} \mathbf{c}^\dagger_{i,\downarrow} \mathbf{c}_{i,\downarrow}. \tag{4.35}$$

Fourier transforming to momentum space yields

$$\mathcal{H}_U = \frac{U}{N^2} \sum_i \sum_{\mathbf{k}_1, \mathbf{k}_2, \mathbf{k}_3, \mathbf{k}_4} \mathbf{c}^\dagger_{\mathbf{k}_1,\uparrow} \mathbf{c}_{\mathbf{k}_2,\uparrow} \mathbf{c}^\dagger_{\mathbf{k}_3,\downarrow} \mathbf{c}_{\mathbf{k}_4,\downarrow} e^{i\mathbf{r}_i \cdot (\mathbf{k}_2 + \mathbf{k}_4 - \mathbf{k}_1 - \mathbf{k}_3)}, \tag{4.36}$$

and using

$$\frac{1}{N} \sum_{\mathbf{r}_i} e^{i\mathbf{r}_i \cdot (\mathbf{k} - \mathbf{k}')} = \delta(\mathbf{k} - \mathbf{k}'), \tag{4.37}$$

leads to

$$\mathcal{H}_U = \frac{U}{N} \sum_{\mathbf{k}_1, \mathbf{k}_2, \mathbf{k}_3} \mathbf{c}^\dagger_{\mathbf{k}_1,\uparrow} \mathbf{c}_{\mathbf{k}_2,\uparrow} \mathbf{c}^\dagger_{\mathbf{k}_3,\downarrow} \mathbf{c}_{\mathbf{k}_1 + \mathbf{k}_3 - \mathbf{k}_2,\downarrow}. \tag{4.38}$$

Applying the anticommutation relations for fermion operators twice results in

$$\mathcal{H}_U = \frac{U}{N} \sum_{\mathbf{k}_1, \mathbf{k}_2, \mathbf{k}_3} \mathbf{c}^\dagger_{\mathbf{k}_1,\uparrow} \mathbf{c}^\dagger_{\mathbf{k}_3,\downarrow} \mathbf{c}_{\mathbf{k}_1 + \mathbf{k}_3 - \mathbf{k}_2,\downarrow} \mathbf{c}_{\mathbf{k}_2,\uparrow}. \tag{4.39}$$

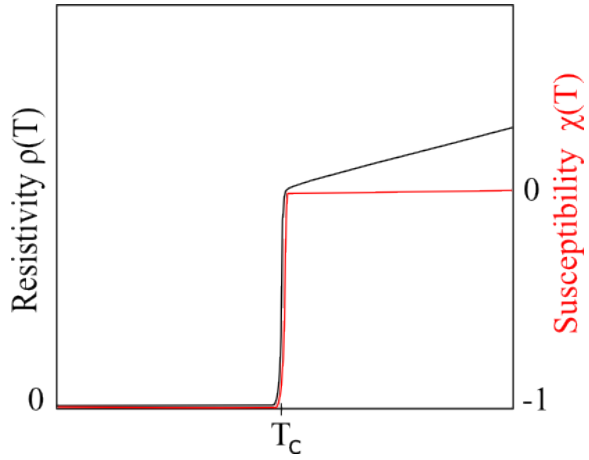

FIGURE 4.2: Resistivity $\rho(T)$ and magnetic susceptibility $\chi(T)$ for a conventional superconductor. At the critical temperature T_c the resistivity rapidly drops to zero, and the superconductor expels applied magnetic fields, i.e. perfect diamagnetism $\chi(T < T_C) = -1$.

Introducing $\mathbf{q} \equiv \mathbf{k}_1 + \mathbf{k}_3$, $\mathbf{k}_1 \equiv \mathbf{k}$ and $\mathbf{k}_2 \equiv \mathbf{k}'$, the Hamiltonian may be written as

$$\mathcal{H}_U = \frac{U}{N} \sum_{\mathbf{k},\mathbf{k}',\mathbf{q}} \mathbf{c}^\dagger_{\mathbf{k},\uparrow} \mathbf{c}^\dagger_{-\mathbf{k}+\mathbf{q},\downarrow} \mathbf{c}_{-\mathbf{k}'+\mathbf{q},\downarrow} \mathbf{c}_{\mathbf{k}',\uparrow}. \tag{4.40}$$

It is obvious that this expression can be generalized to have a momentum-dependent potential $\frac{U}{N} \to V_{\mathbf{k},\mathbf{k}',\mathbf{q}}$, which results in a general two-particle interaction Hamiltonian

$$\mathcal{H}_I = \sum_{\mathbf{k},\mathbf{k}',\mathbf{q}} V_{\mathbf{k},\mathbf{k}',\mathbf{q}} \mathbf{c}^\dagger_{\mathbf{k},\uparrow} \mathbf{c}^\dagger_{-\mathbf{k}+\mathbf{q},\downarrow} \mathbf{c}_{-\mathbf{k}'+\mathbf{q},\downarrow} \mathbf{c}_{\mathbf{k}',\uparrow}. \tag{4.41}$$

This is a two-particle scattering term, where two electrons in the states $\mathbf{k}', \uparrow$ and $-\mathbf{k}' + \mathbf{q}, \downarrow$ are scattered to the two new states $\mathbf{k}, \uparrow$ and $-\mathbf{k} + \mathbf{q}, \uparrow$. The momentum-dependent magnitude of this scattering process is described by $V_{\mathbf{k},\mathbf{k}',\mathbf{q}}$.

4.3 Superconductivity

A superconductor is a material that below the transition temperature T_c exhibit zero resistance and an expulsion of external magnetic fields, i.e. perfect diamagnetism, see fig. 4.2. We will be concerned with the nature of the superconducting gap, or order parameter, as it describes the pairing mechanism in any given superconducting system. In order to get familiar with the order parameter, the BCS theory for conventional superconductors is reviewed.

4.3.1 BCS theory

The first microscopic theory of superconductors came in 1957 with the BCS theory[5]. Going through the steps of the BCS theory will prove fruitful for later sections. The theory lies grounded in the BCS reduced Hamiltonian[53]

$$\mathcal{H}_{BCS} = \sum_{\mathbf{k},\sigma} \epsilon_{\mathbf{k}} c^{\dagger}_{\mathbf{k},\sigma} c_{\mathbf{k},\sigma} + \sum_{\mathbf{k},\mathbf{k}',\sigma} V_{\mathbf{k},\mathbf{k}'} c^{\dagger}_{\mathbf{k},\sigma} c^{\dagger}_{-\mathbf{k},-\sigma} c_{-\mathbf{k}',-\sigma} c_{\mathbf{k}',\sigma}. \tag{4.42}$$

The first term is the diagonal one-particle kinetic term. The second term captures the assumptions made on the interaction, and describes the Cooper pairs. First of all they have opposite momentum, $\mathbf{k}$ and $-\mathbf{k}$. In addition they have opposite spins, σ and $-\sigma$. We note that it has the form of the general interaction Hamiltonian in (4.41), with $\mathbf{q} = 0$. These restrictions are mounted in the assumption of a pairing mechanism of two electrons both very close to the Fermi level. The goal is to diagonalize the BCS reduced Hamiltonian, but as it stands now this can not be done. First of all, by writing out the sum over the spin degrees of freedom, $\sigma = \uparrow, \downarrow$, and rewriting results in

$$\mathcal{H}_{BCS} = \sum_{\mathbf{k},\sigma} \epsilon_{\mathbf{k}} c^{\dagger}_{\mathbf{k},\sigma} c_{\mathbf{k},\sigma} + \sum_{\mathbf{k},\mathbf{k}'} V_{\mathbf{k},\mathbf{k}'} c^{\dagger}_{\mathbf{k},\uparrow} c^{\dagger}_{-\mathbf{k},\downarrow} c_{-\mathbf{k}',\downarrow} c_{\mathbf{k}',\uparrow}. \tag{4.43}$$

The next step is to apply a mean field assumption on the operators

$$\begin{aligned} c_{-\mathbf{k},\downarrow} c_{\mathbf{k},\uparrow} &= \langle c_{-\mathbf{k},\downarrow} c_{\mathbf{k},\uparrow} \rangle + c_{-\mathbf{k},\downarrow} c_{\mathbf{k},\uparrow} - \langle c_{-\mathbf{k},\downarrow} c_{\mathbf{k},\uparrow} \rangle \\ &= b_{\mathbf{k}} + \delta_{b_{\mathbf{k}}}, \end{aligned} \tag{4.44}$$

where $b_{\mathbf{k}} = \langle c_{-\mathbf{k},\downarrow} c_{\mathbf{k},\uparrow} \rangle$ is the mean value (not an operator), while $\delta_{b_{\mathbf{k}}} = c_{-\mathbf{k},\downarrow} c_{\mathbf{k},\uparrow} - \langle c_{-\mathbf{k},\downarrow} c_{\mathbf{k},\uparrow} \rangle$ is the assumed small deviation from the mean value. Inserting this back into the reduced BCS Hamiltonian, and neglecting terms of $\mathcal{O}(\delta^2_{b_{\mathbf{k}}})$ yields

$$\mathcal{H}_{BCS} = \sum_{\mathbf{k},\sigma} \epsilon_{\mathbf{k}} c^{\dagger}_{\mathbf{k},\sigma} c_{\mathbf{k},\sigma} + \sum_{\mathbf{k},\mathbf{k}'} V_{\mathbf{k},\mathbf{k}'} \Big\{ b^{\dagger}_{\mathbf{k}} c_{-\mathbf{k}',\downarrow} c_{\mathbf{k}',\uparrow} + b_{\mathbf{k}'} c^{\dagger}_{\mathbf{k},\uparrow} c^{\dagger}_{-\mathbf{k},\downarrow} - b^{\dagger}_{\mathbf{k}} b_{\mathbf{k}'} \Big\}. \tag{4.45}$$

Let us now define the following functions

$$\Delta^{\dagger}_{\mathbf{k}'} = -\sum_{\mathbf{k}} V_{\mathbf{k},\mathbf{k}'} b^{\dagger}_{\mathbf{k}} \tag{4.46}$$

$$\Delta^{\dagger}_{\mathbf{k}} = -\sum_{\mathbf{k}'} V_{\mathbf{k},\mathbf{k}'} b^{\dagger}_{\mathbf{k}'}. \tag{4.47}$$

Writing the chemical potential explicitly, μ, and slightly rewriting the first term in the BCS reduced Hamiltonian leads to

$$\begin{aligned} \mathcal{H}_{BCS} = &\sum_{\mathbf{k}} \Big\{ (\epsilon_{\mathbf{k}} - \mu) c^{\dagger}_{\mathbf{k},\uparrow} c_{\mathbf{k},\uparrow} + (\epsilon_{\mathbf{k}} - \mu)(1 - c^{\dagger}_{-\mathbf{k},\downarrow} c_{-\mathbf{k},\downarrow}) \Big\} \\ &- \sum_{\mathbf{k},\mathbf{k}'} \Big(\Delta^{\dagger}_{\mathbf{k}} c_{-\mathbf{k}',\downarrow} c_{\mathbf{k}',\uparrow} + \Delta_{\mathbf{k}'} c^{\dagger}_{\mathbf{k},\uparrow} c^{\dagger}_{-\mathbf{k},\downarrow} \Big) + \sum_{\mathbf{k}} \Delta_{\mathbf{k}} b^{\dagger}_{\mathbf{k}}. \end{aligned} \tag{4.48}$$

The one-particle part is split in two halves, positive and negative $\mathbf{k}$. The Hamiltonian may now be written on matrix form

$$\begin{aligned}\mathcal{H}_{BCS} = &\sum_{\mathbf{k}} (\epsilon_{\mathbf{k}} - \mu + \Delta_{\mathbf{k}} b_{\mathbf{k}}^{\dagger}) \\ &+ \sum_{\mathbf{k}} \psi_{\mathbf{k}}^{\dagger} \begin{pmatrix} \epsilon_{\mathbf{k}} - \mu & -\Delta_{\mathbf{k}} \\ -\Delta_{\mathbf{k}}^{\dagger} & -(\epsilon_{\mathbf{k}} - \mu) \end{pmatrix} \psi_{\mathbf{k}}, \end{aligned} \tag{4.49}$$

with the Nambu spinor $\psi_{\mathbf{k}}^{\dagger} = (c_{\mathbf{k},\uparrow}^{\dagger} \; c_{-\mathbf{k},\downarrow})$. The matrix in the second term can now be easily diagonalized by rewriting

$$\begin{aligned}\sum_{\mathbf{k}} \psi_{\mathbf{k}}^{\dagger} \mathcal{H}_{\mathbf{k}} \psi_{\mathbf{k}} &= \sum_{\mathbf{k}} \psi_{\mathbf{k}}^{\dagger} \mathbf{U}^{-1} \mathbf{U} \mathcal{H}_{\mathbf{k}} \mathbf{U}^{-1} \mathbf{U} \psi_{\mathbf{k}} \\ &= \sum_{\mathbf{k}} \tilde{\psi}_{\mathbf{k}}^{\dagger} \begin{pmatrix} \lambda_{+} & 0 \\ 0 & \lambda_{-} \end{pmatrix} \tilde{\psi}_{\mathbf{k}} \end{aligned} \tag{4.50}$$

with the eigenvalues

$$\lambda_{\pm} = \pm \sqrt{(\epsilon_{\mathbf{k}} - \mu)^2 + |\Delta_{\mathbf{k}}|^2} \equiv \pm E_k, \tag{4.51}$$

and new spinors $\tilde{\psi}_{\mathbf{k}}^{\dagger} = (\eta_{\mathbf{k}}^{\dagger} \; \gamma_{\mathbf{k}}^{\dagger})$. This is a Bogoliubov transformation. The Hamiltonian is now diagonal

$$\mathcal{H}_{BCS} = \sum_{\mathbf{k}} (\epsilon_{\mathbf{k}} - \mu + \Delta_{\mathbf{k}} b_{\mathbf{k}}^{\dagger}) + \sum_{\mathbf{k}} E_k (\eta_{\mathbf{k}}^{\dagger} \eta_{\mathbf{k}} - \gamma_{\mathbf{k}}^{\dagger} \gamma_{\mathbf{k}}). \tag{4.52}$$

The first sum term, $\sum_{\mathbf{k}} (\epsilon_{\mathbf{k}} - \mu + \Delta_{\mathbf{k}} b_{\mathbf{k}}^{\dagger}) \equiv \mathcal{H}_0$, is the ground state energy of the system, while the second term describe the fermionic excitations. $\Delta_{\mathbf{k}}$ describe a gap, the superconducting gap, in the diagonalized system. $\Delta_{\mathbf{k}}$ is also the order parameter for the superconducting system, and these two names will be used interchangeably. Since mean field theory was applied to the problem, the gap equations(4.47) need to be solved self-consistently. This means that $\Delta_{\mathbf{k}}$ must be chosen so as to minimize the free energy of the system. The relation between the partition function Z and the free energy F is

$$Z = \sum e^{-\beta \mathcal{H}} = e^{-\beta \mathcal{H}_0} \prod_{\mathbf{k}} (1 + e^{-\beta E_{\mathbf{k}}})(1 + e^{\beta E_{\mathbf{k}}}) = e^{-\beta F}, \tag{4.53}$$

which results in the free energy

$$F = \mathcal{H}_0 - \frac{1}{\beta} \sum_{\mathbf{k}} \Big(\ln(1 + e^{-\beta E_{\mathbf{k}}}) + \ln(1 + e^{\beta E_{\mathbf{k}}}) \Big). \tag{4.54}$$

Minimizing F with respect to $\Delta_{\mathbf{k}}$ yields

$$b_{\mathbf{k}}^{\dagger} = \Delta_{\mathbf{k}}^{\dagger} \frac{\tanh(\beta E_{\mathbf{k}}/2)}{2E_{\mathbf{k}}}. \tag{4.55}$$

Since there is only one solution, this is guaranteed to be a minimum as the free energy must be bounded from below. Inserting the solution for $b_{\mathbf{k}}^{\dagger}$ back into the gap equations, results in the self-constistency equations for the gaps

$$\begin{aligned}\Delta_{\mathbf{k}} &= -\sum_{\mathbf{k}'} V_{\mathbf{k},\mathbf{k}'}\Delta_{\mathbf{k}'}\frac{\tanh(\beta E_{\mathbf{k}'}/2)}{2E_{\mathbf{k}'}} \\ &\equiv -\sum_{\mathbf{k}'} V_{\mathbf{k},\mathbf{k}'}\Delta_{\mathbf{k}'}\chi(E_{\mathbf{k}'}),\end{aligned} \tag{4.56}$$

where we have defined

$$\chi(E_{\mathbf{k}}) = \frac{\tanh(\beta E_{\mathbf{k}}/2)}{2E_{\mathbf{k}}}. \tag{4.57}$$

4.3.2 Pairing

The interaction term in the BCS reduced Hamiltonian (4.42) specifies little else than there is a pair of electrons on opposite sides of the fermi surface, with opposite spins. The exact mechanism of $V_{\mathbf{k},\mathbf{k}'}$ is not set, although the original intent in the BCS theory was for it to be a phonon-mediated attractive force between the electrons. As the interaction term stands however, it could be any mechanism dependent on the two momenta, and one can easily generalize to finite-momentum scattering or a spin-dependent mechanism. The BCS theory describes spin-singlet pairing. If we assume $\Delta_{\mathbf{k}} = |\Delta|$, this can easily be seen by applying the fermionic anticommutation relation to the operator pairs in (4.48)

$$c_{-\mathbf{k},\downarrow}c_{\mathbf{k},\uparrow} = -c_{\mathbf{k},\uparrow}c_{-\mathbf{k},\downarrow}. \tag{4.58}$$

This means that the spin-part of the wave function of the Cooper pair is antisymmetric, requiring a symmetric space part, analogous to even angular momentum spherical harmonics, $l = 0, 2, \ldots$. The pairings with $l = 0$ is called s-wave pairing, $l = 2$ d-wave pairing, and so on. These are all singlet states. To make things more general, and to access odd angular momentum states or triplet pairing, one may write[29, 53]

$$V_{\mathbf{k},\mathbf{k}'} = \sum_{\lambda\lambda'} V g_{\mathbf{k}}^{\lambda} g_{\mathbf{k}'}^{\lambda'}, \tag{4.59}$$

i.e. separating the dependency of $V_{\mathbf{k},\mathbf{k}'}$ in $\mathbf{k}$ and $\mathbf{k}'$. Inserting into the self-consistency gap equation (4.56) and summing out $\mathbf{k}'$ and λ' yields

$$\begin{aligned}\Delta_{\mathbf{k}} &= \sum_{\mathbf{k}'}\sum_{\lambda\lambda'} V g_{\mathbf{k}}^{\lambda} g_{\mathbf{k}'}^{\lambda'}\Delta_{\mathbf{k}'}\chi(E_{\mathbf{k}'}) \\ &= \sum_{\lambda} g_{\mathbf{k}}^{\lambda}\sum_{\mathbf{k}',\lambda'} V g_{\mathbf{k}'}^{\lambda'}\Delta_{\mathbf{k}'}\chi(E_{\mathbf{k}'}) \\ &= \sum_{\lambda} g_{\mathbf{k}}^{\lambda}\Delta^{\lambda}(T).\end{aligned} \tag{4.60}$$

The $\mathbf{k}'$- and λ'-dependency disappears, and $\Delta^{\lambda}(T)$ depends only on the thermodynamics of the system. The $\mathbf{k}$-dependency of the $g_{\mathbf{k}}^{\lambda}$ now decides the symmetry properties of $\Delta_{\mathbf{k}}$, and thus the pairing mechanism.

4.3.2.1 Symmetry of the order parameter

At the transition temperature T_c there is a macroscopic phase transition between a normal state and a superconducting state. An essential condition for this is the existence of off-diagonal long-range order[54]. This order is in essence measured by the expectation value $b_{\mathbf{k}} = \langle c_{-\mathbf{k},\downarrow} c_{\mathbf{k},\uparrow} \rangle$, which the order parameter $\Delta_{\mathbf{k}}$ is proportional to. Since the system is going through a phase transition, there is obviously a change in the order parameter, and this has to do with the breaking of symmetries. The symmetry properties of the superconducting gap is of great importance, not only because they describe the spin structure, but also because they illuminate some aspects of high-T_c superconductivity, where BCS-theory fails.

One can choose many different sets of basis functions $g_{\mathbf{k}}$, but one very natural choice is the set of basis functions for the irreducible representations of the symmetry group of the lattice structure one is working with[53, 54]. The superconducting gap function may then be written

$$\Delta_{\mathbf{k}} = \sum_{\lambda=1}^{d_i} \eta_\lambda \xi_\lambda^i(\mathbf{k}), \tag{4.61}$$

where d_i is the dimension of any given irreducible representation Γ_i, and η_λ are complex coefficients invariant under all symmetry operations of the group of the normal state. The group of the superconducting state will be a subgroup of the group of the normal state, i.e. the lattice combined with spin symmetry, gauge symmetry and time-reversal symmetry, if applicable. It is clear that the order parameter can generally be written

$$\Delta_{\mathbf{k}} = |\Delta_{\mathbf{k}}| e^{i\phi}, \tag{4.62}$$

and there is a U(1) gauge symmetry here in the choice of ϕ. Upon entering the superconducting state a singular value of ϕ is chosen by the system, and the transition marks a spontaneously broken U(1) gauge symmetry. This is essentially the whole story for conventional superconductors, while there may be additional symmetries broken, e.g. time-reversal symmetry, in unconventional superconductors. Other sets of basis functions can also be chosen, and in continuum models the choice naturally falls on angular momentum eigenstates[29]. Some symmetry properties of the order parameter also depends on whether the pairing is a triplet, with total spin 1, or singlet, with total spin 0. A singlet pairing may generally be written[55]

$$\Delta^{\text{singlet}}(\mathbf{k}) = g(\mathbf{k}) i\sigma_y = \begin{pmatrix} 0 & g(\mathbf{k}) \\ -g(\mathbf{k}) & 0 \end{pmatrix}. \tag{4.63}$$

Since the total spin is zero, this pairing corresponds to an even wavefunction. The singlet state is thus even under inversion $\Delta^{\text{singlet}}(\mathbf{k}) = \Delta^{\text{singlet}}(-\mathbf{k})$. Similarly, a triplet pairing may generally be written

$$\Delta^{\text{triplet}}(\mathbf{k}) = (d(\mathbf{k}) \cdot \sigma) i\sigma_y = \begin{pmatrix} -d_x(\mathbf{k}) + i d_y(\mathbf{k}) & d_z(\mathbf{k}) \\ d_z(\mathbf{k}) & d_x(\mathbf{k}) + i d_y(\mathbf{k}) \end{pmatrix}. \tag{4.64}$$

The total spin is now 1, and this pairing corresponds to an odd wavefunction, making the triplet pairing odd under inversion $\Delta^{\text{triplet}}(\mathbf{k}) = -\Delta^{\text{triplet}}(-\mathbf{k})$.

4.4 Dirac Materials and Topological Insulators

Dirac materials are systems whose low-energy fermionic excitations satisfy the Dirac equation, linear in momentum

$$E(\mathbf{k}) \sim \mathbf{k}. \tag{4.65}$$

Belonging to Dirac Materials are topological insulators, systems whose non-trivial bulk topology lead to gapless edge states, also satisfying the Dirac equation. Let us look at a simple model for a two-dimensional time-reversal invariant topological insulator[9]. By Kramer's theorem[56] any eigenstate of a time-reversal invariant Hamiltonian are at least twofold degenerate, and thus necessarily require that at time-reversal invariant momenta the energy dispersion display no gaps. On matrix form, the model Hamiltonian reads

$$\mathcal{H} = \sum_{\mathbf{k}} \psi^\dagger_{\mathbf{k}} \begin{pmatrix} \epsilon_{\mathbf{k}} & s_{\mathbf{k}} \\ s^*_{\mathbf{k}} & \epsilon_{\mathbf{k}} \end{pmatrix} \psi_{\mathbf{k}}. \tag{4.66}$$

$\epsilon_{\mathbf{k}}$ is here the one-particle dispersion, satysfying the property $\epsilon^*_{-\mathbf{k}} = \epsilon_{\mathbf{k}}$, while $s_{\mathbf{k}}$ has its origin in spin-orbit coupling. The Nambu spinor is $\psi^\dagger_{\mathbf{k}} = \begin{pmatrix} c^\dagger_{\mathbf{k},\uparrow} & c^\dagger_{\mathbf{k},\downarrow} \end{pmatrix}$. Diagonalizing this problem yields the eigenvalues

$$E(\mathbf{k}) = \epsilon_{\mathbf{k}} \pm |s_{\mathbf{k}}|, \tag{4.67}$$

and the dispersion is gapless where $s_{\mathbf{k}} = 0$. Around these degenerate points $E(\mathbf{k})$ must be linear. In the continuum limit, $\mathbf{k} \to 0$, the one-particle kinetic energy is $\epsilon_{\mathbf{k}} = \frac{\mathbf{k}^2}{2m^*} - \mu$, while a spin-orbit coupling term takes the form $s_{\mathbf{k}} = k_x - ik_y$. $s_{\mathbf{k}} = 0$ for $\mathbf{k} = 0$, and to highest order $E(\mathbf{k}) \sim \mathbf{k}$ around $\mathbf{k} = 0$. The circular cones made up by the linear beahaviour around the degenerate momenta are called Dirac cones, see figure 4.3. What separates this Dirac state from a normal insulating state lies rooted in the topology of the band structure. The topology is classified by the topological invariant, the Chern number. The normal insulator has a trivial Chern number, while the Dirac state, or topological insulator, has a non-zero Chern number. The simplest argument for this lies in the expression of the Berry curvature, equation (3.7). The Chern number is the surface integral of the Berry curvature, and we see from its expression that this integral is non-zero when the curvature has singularities, i.e. when there are degenerate eigenvalues. This is exactly the case when there are Dirac points in the energy dispersion. We also refer to the discussion in chapter 3.

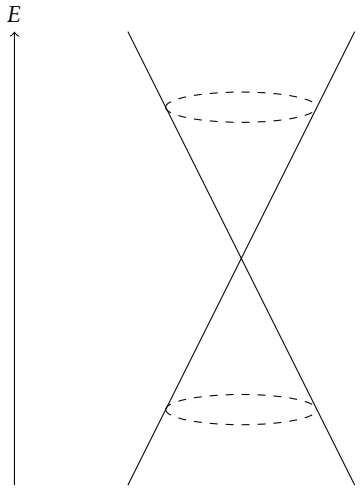

FIGURE 4.3: The spherical cone energy bands, called Dirac cones, touch at the Dirac points.

4.5 Topological Superconductors

Analogous to a topological insulator one can study topological superconductors, where the bulk band gap of the insulator corresponds to the bulk superconducting gap, and the Dirac fermion conducting edge states of the topological insulator are replaced by Majorana fermion edge states[9, 29]. A Majorana fermion is its own anti-(quasi)particle. A topological superconductor is as such viewed as a topological insulator with particle-hole symmetry. The topological invariant for insulators and superconductors is also slightly different, as the invariant for insulators is defined over the entire Brillouin zone, while for a superconductor, pairing is only achieved close to the Fermi surface. One also distinguish time-reversal invariant and breaking topological superconductors. The latter is of great interest in that they relate to non-Abelian statistics, an important feature for immunity to decoherence, ideal for the purposes of quantum computing[31].

The perhaps most studied approach to topological superconductivity is through the chiral p-wave pairing[9]. We start out with the spin-less Bogoliubov-de Gennes Hamiltonian, the form of which we recognize from (4.49),

$$\mathcal{H}_{\text{BdG}} = \sum_{\mathbf{k}} \psi_{\mathbf{k}}^{\dagger} \begin{pmatrix} \epsilon_{\mathbf{k}} - \mu & -\Delta_{\mathbf{k}} \\ -\Delta_{\mathbf{k}}^{\dagger} & -\epsilon_{\mathbf{k}} + \mu \end{pmatrix} \psi_{\mathbf{k}}. \tag{4.68}$$

The spin-less Nambu spinor is $\psi_{\mathbf{k}}^{\dagger} = (c_{\mathbf{k}}^{\dagger} \; c_{-\mathbf{k}})$. Diagonalizing the BdG Hamiltonian results in the eigenvalues

$$E_{\mathbf{k}} = \pm\sqrt{(\epsilon_{\mathbf{k}} - \mu)^2 + |\Delta_{\mathbf{k}}|^2}. \tag{4.69}$$

The Bogoliubov-transformation that has been applied involve the new operators

$$\eta_{\mathbf{k}} = u_{\mathbf{k}} \mathbf{c}_{\mathbf{k}} - v_{\mathbf{k}} \mathbf{c}^{\dagger}_{-\mathbf{k}} \tag{4.70}$$

$$\eta^{\dagger}_{\mathbf{k}} = u^{*}_{\mathbf{k}} \mathbf{c}^{\dagger}_{\mathbf{k}} - v^{*}_{\mathbf{k}} \mathbf{c}_{-\mathbf{k}}. \tag{4.71}$$

In the fermionic case $|u_{\mathbf{k}}|^2 + |v_{\mathbf{k}}|^2 = 1$ to satisfy the anticommutation relations. This diagonalization yield the Bogoliubov-de Gennes (BdG) equations

$$E_{\mathbf{k}} u_{\mathbf{k}} = (\epsilon_{\mathbf{k}} - \mu) u_{\mathbf{k}} - \Delta^{*}_{\mathbf{k}} v_{\mathbf{k}} \tag{4.72}$$

$$E_{\mathbf{k}} v_{\mathbf{k}} = -(\epsilon_{\mathbf{k}} - \mu) v_{\mathbf{k}} - \Delta_{\mathbf{k}} u_{\mathbf{k}}, \tag{4.73}$$

with the following relations

$$\frac{v_{\mathbf{k}}}{u_{\mathbf{k}}} = -\frac{E_{\mathbf{k}} - (\epsilon_{\mathbf{k}} - \mu)}{\Delta^{*}_{\mathbf{k}}} \tag{4.74}$$

$$|u_{\mathbf{k}}|^2 = \frac{1}{2}\left(1 + \frac{(\epsilon_{\mathbf{k}} - \mu)}{E_{\mathbf{k}}}\right) \tag{4.75}$$

$$|v_{\mathbf{k}}|^2 = \frac{1}{2}\left(1 - \frac{(\epsilon_{\mathbf{k}} - \mu)}{E_{\mathbf{k}}}\right). \tag{4.76}$$

An important point to notice about the BdG Hamiltonian is the particle-hole symmetry, arising from the redundant description of operators at both $\mathbf{k}$ and $-\mathbf{k}$. This leads to the simple fact that for any eigenstate with energy $E_{\mathbf{k}}$, there exists an eigenstate with energy $-E_{\mathbf{k}}$. This means that instead of writing the diagonalized Hamiltonian as

$$\mathcal{H}_{\mathrm{BdG}} = \sum_{\mathbf{k}} E_k (\eta^{\dagger}_{+,\mathbf{k}} \eta_{+,\mathbf{k}} - \eta^{\dagger}_{-,\mathbf{k}} \eta_{-,\mathbf{k}}), \tag{4.77}$$

where the negative and positive energy states have been split, all the physics of the problem is contained in

$$\mathcal{H}_{\mathrm{BdG}} = \sum_{\mathbf{k}} E_k \eta^{\dagger}_{+,\mathbf{k}} \eta_{+,\mathbf{k}}, \tag{4.78}$$

due to the particle-hole symmetry. Now, in the continuum limit, the chiral p-wave pairing is

$$\Delta_{\mathbf{k}} = \Delta_0 \cdot (k_x - i k_y), \tag{4.79}$$

while $\epsilon_{\mathbf{k}} = \frac{k^2}{2m} - \mu$. In the low-energy regime, when μ and k are small, we can set $\epsilon_{\mathbf{k}} \approx -\mu$, and to leading order the energy dispersion is

$$E_{\mathbf{k}} \approx \sqrt{|\Delta_0|^2 k^2 + \mu^2}. \tag{4.80}$$

This has the form of a relativistic dispersion relation, with $|\Delta_0|$ taking the role of the speed of light. The time-dependent Schrödinger equation is $i\partial_t \psi_{\mathbf{k}} = E_{\mathbf{k}} \psi_{\mathbf{k}}$, while $k_i = -i\partial_i$, such that the BdG equations (4.73) are now

$$i\partial_t u_{\mathbf{k}} = -\mu u_{\mathbf{k}} + \Delta_0 (i\partial_x + \partial_y) v_{\mathbf{k}} \tag{4.81}$$

$$i\partial_t v_{\mathbf{k}} = \mu v_{\mathbf{k}} + \Delta_0 (i\partial_x - \partial_y) u_{\mathbf{k}}. \tag{4.82}$$

Since they are linear in both spatial- and temporal derivatives, these two equations are a form of the Dirac equation for the spinor $(u,\ v)$[57]. Remarkably, if we take the complex conjugate of the equations, they transform into each other under the condition $(u,\ v) = (v^*,\ u^*)$. This means that the quasiparticles in our diagonalized problem

$$\mathcal{H}_{\text{BdG}} = \sum_{\mathbf{k}} E_k \eta^\dagger_{\mathbf{k}} \eta_{\mathbf{k}}, \tag{4.83}$$

are their own antiparticles, and are as such *Majorana* fermions. Because of the particle-hole symmetry and chiral p-wave pairing we have a singularity in the Berry curvature (3.7), and thus a topologically non-trivial bulk, which by the bulk-edge correspondence lead to these topologically protected Majorana edge states. In addition, a chiral p-wave pairing breaks time-reversal symmetry when the chirality of the spins are the same[21], which is essentially the case in a spinless model, and together with particle-hole symmetry this puts the BdG system in AZ class D (see table 3.1), characterized by a $\mathbb{Z}$ topological invariant in two dimensions.

Chapter 5

Bravais Lattices

This chapter will go into more detail on Bravais lattices, lattices with a single lattice point in the basis. First, the one-particle problem consisting of nearest neighbour hopping and spin-orbit coupling is presented. Next, the two-particle interaction term is investigated, and through mean-field theory a general scheme for superconductivity in these lattices is developed. Finally, the symmetry properties of the system are studied, in order to evaluate the requirements on the superconducting gaps to ensure non-trivial topological behaviour.

5.1 One-Particle Problem

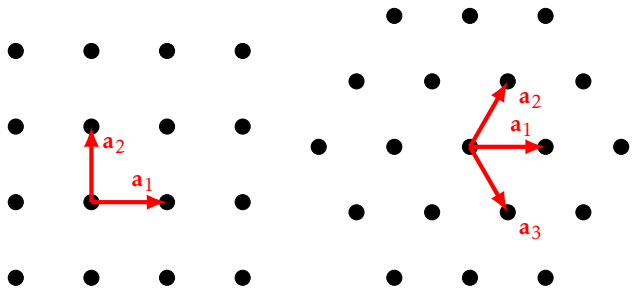

FIGURE 5.1: Left: The square lattice with two of the nearest neighbour vectors $\mathbf{a_1}$ and $\mathbf{a_2}$. Right: The hexagonal lattice with three of the nearest neighbour vectors $\mathbf{a_1}$, $\mathbf{a_2}$ and $\mathbf{a}_3$.

Two-dimensional Bravais lattices are lattices with a single lattice point in the basis. Examples of such lattices are the square and hexagonal lattices, see figure 5.1. One common feature is that each lattice point has an even number of nearest neighbours. These nearest neighbours are characterized by the nearest neighbour vectors, $\mathbf{a}_i$. Notice that for $2n$ neighbours, only n vectors are defned. The reason for this will become clear shortly. The lattice constant, a, is for conveniency set to unity for the remainder of this thesis.

5.1.1 Hopping

The nearest neighbour hopping Hamiltonian $\mathcal{H}_t$ reads

$$\mathcal{H}_t = -t_{NN} \sum_{\mathbf{r}_i, \mathbf{a}_j, \sigma} \left(\mathbf{c}^\dagger_{\mathbf{r}_i,\sigma} \mathbf{c}_{\mathbf{r}_i + \mathbf{a}_j \sigma} + H.c. \right), \tag{5.1}$$

where *H.c.*, the hermitian conjugate of the preceding terms, takes care of the remaining neighbors, because by translational symmetry, hopping from $\mathbf{r}_i + \mathbf{a}_j$ to $\mathbf{r}_i$ is the same as hopping from $\mathbf{r}_i$ to $\mathbf{r}_i - \mathbf{a}_j$. Hopping is a spin-conserving process, which is why creation and annihilation operators here have the same spin index σ. The next step is to Fourier transform to momentum space, resulting in

$$\mathcal{H}_t = -t_{NN} \sum_{\mathbf{k},\mathbf{a}_j,\sigma} \left(\mathbf{c}^\dagger_{\mathbf{k}\sigma} \mathbf{c}_{\mathbf{k}\sigma} e^{-i\mathbf{k}\cdot\mathbf{a}_j} + H.c. \right). \tag{5.2}$$

Summing over σ and using that

$$2\cos(x) = e^{ix} + e^{-ix}, \tag{5.3}$$

leads to

$$\mathcal{H}_t = -2t_{NN} \sum_{\mathbf{k}} \left(\mathbf{c}^\dagger_{\mathbf{k}\uparrow} \mathbf{c}_{\mathbf{k}\uparrow} + \mathbf{c}^\dagger_{\mathbf{k}\downarrow} \mathbf{c}_{\mathbf{k}\downarrow} \right) \sum_j \cos(\mathbf{k}\cdot\mathbf{a}_j). \tag{5.4}$$

This can be written on matrix form

$$\mathcal{H}_t = \sum_{\mathbf{k}} \begin{pmatrix} \mathbf{c}^\dagger_{\mathbf{k}\uparrow} & \mathbf{c}^\dagger_{\mathbf{k}\downarrow} \end{pmatrix} \begin{pmatrix} t_{\mathbf{k}} & 0 \\ 0 & t_{\mathbf{k}} \end{pmatrix} \begin{pmatrix} \mathbf{c}_{\mathbf{k}\uparrow} \\ \mathbf{c}_{\mathbf{k}\downarrow} \end{pmatrix}. \tag{5.5}$$

The hopping amplitude is defined as

$$t_{\mathbf{k}} = -2t_{NN} \sum_j \cos(\mathbf{k}\cdot\mathbf{a}_j). \tag{5.6}$$

With no off-diagonal terms in the Hamilton matrix, the energy dispersion relation is easily found. From $\mathcal{H}|\psi_{\mathbf{k}}\rangle = E(\mathbf{k})|\psi_{\mathbf{k}}\rangle$, solving for the eigenvalues yields

$$E(\mathbf{k}) = t_{\mathbf{k}}. \tag{5.7}$$

This eigenvalue is spin-degenerate, i.e. the same for both $\uparrow$ and $\downarrow$ spins. The energy dispersion for a square lattice along the k_x-axis is plotted in figure 5.2.

5.1.2 Spin-Orbit Coupling

The Rashba spin-orbit coupling term is (4.33)

$$\mathcal{H}_{\text{SOC}} = \lambda_R \sum_{\mathbf{r}_i,\mathbf{a}_j,\alpha,\beta} \left\{ \mathbf{c}^\dagger_{\mathbf{r}_i,\alpha} \Big(-\sigma_x^{\alpha\beta} (i\mathbf{a}_j \cdot \hat{y}) + \sigma_y^{\alpha\beta} (i\mathbf{a}_j \cdot \hat{x}) \Big) \mathbf{c}_{\mathbf{r}_i+\mathbf{a}_j,\beta} + H.c. \right\}. \tag{5.8}$$

Fourier transforming to momentum space yields

$$\begin{aligned} \mathcal{H}_{\text{SOC}} = \lambda_R \sum_{\mathbf{k},\mathbf{a}_j,\alpha,\beta} \Big\{ & \mathbf{c}^\dagger_{\mathbf{k},\alpha} \Big(-\sigma_x^{\alpha\beta} (i\mathbf{a}_j \cdot \hat{y}) + \sigma_y^{\alpha\beta} (i\mathbf{a}_j \cdot \hat{x}) \Big) \mathbf{c}_{\mathbf{k},\beta} e^{i\mathbf{k}\cdot\mathbf{a}_j} \\ & - \mathbf{c}^\dagger_{\mathbf{k},\beta} \Big(-\sigma_x^{\beta\alpha} (i\mathbf{a}_j \cdot \hat{y}) + \sigma_y^{\beta\alpha} (i\mathbf{a}_j \cdot \hat{x}) \Big) \mathbf{c}_{\mathbf{k},\alpha} e^{-i\mathbf{k}\cdot\mathbf{a}_j} \Big\}. \end{aligned} \tag{5.9}$$

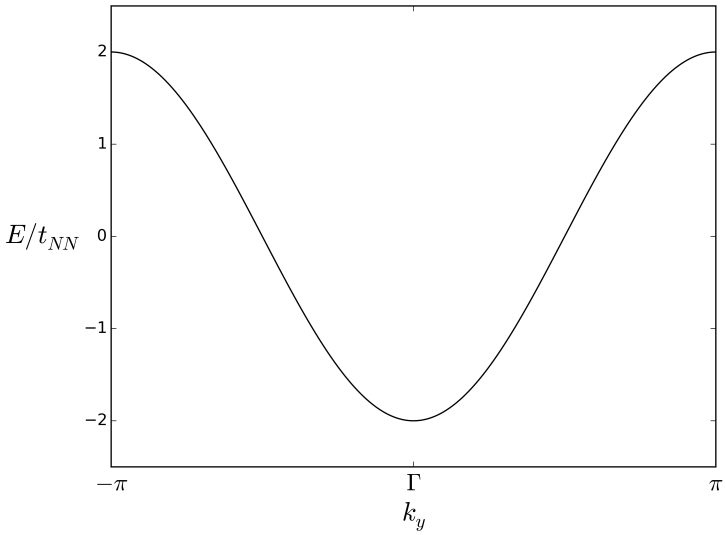

FIGURE 5.2: The energy dispersion with nearest neighbour hopping for a square lattice along the k_y-axis.

Summing over the spin-indices α, β results in

$$\begin{aligned}\mathcal{H}_{\mathrm{SOC}} &= \lambda_R \sum_{\mathbf{k},\mathbf{a}_j} \Big\{ \mathbf{c}^\dagger_{\mathbf{k},\uparrow}\mathbf{c}_{\mathbf{k},\downarrow}(-i\mathbf{a}_j\cdot\hat{y}+\mathbf{a}_j\cdot\hat{x})(e^{i\mathbf{k}\cdot\mathbf{a}_j}-e^{-i\mathbf{k}\cdot\mathbf{a}_j}) \\ &\qquad + \mathbf{c}^\dagger_{\mathbf{k},\downarrow}\mathbf{c}_{\mathbf{k},\uparrow}(-i\mathbf{a}_j\cdot\hat{y}-\mathbf{a}_j\cdot\hat{x})(e^{i\mathbf{k}\cdot\mathbf{a}_j}-e^{-i\mathbf{k}\cdot\mathbf{a}_j}) \Big\} \\ &= 2i\lambda_R \sum_{\mathbf{k},\mathbf{a}_j} \Big\{ \mathbf{c}^\dagger_{\mathbf{k},\uparrow}\mathbf{c}_{\mathbf{k},\downarrow}(-i\mathbf{a}_j\cdot\hat{y}+\mathbf{a}_j\cdot\hat{x})\sin(\mathbf{k}\cdot\mathbf{a}_j) \\ &\qquad + \mathbf{c}^\dagger_{\mathbf{k},\downarrow}\mathbf{c}_{\mathbf{k},\uparrow}(-i\mathbf{a}_j\cdot\hat{y}-\mathbf{a}_j\cdot\hat{x})\sin(\mathbf{k}\cdot\mathbf{a}_j) \Big\}. \end{aligned} \tag{5.10}$$

Noting that the terms $\mathbf{a}_j\cdot\hat{x}-i\mathbf{a}_j\cdot\hat{y}$ and $\mathbf{a}_j\cdot\hat{x}+i\mathbf{a}_j\cdot\hat{y}$ can be written $e^{-i\theta_j}$ and $e^{i\theta_j}$, respectively, with θ_i the polar angle of the nearest neighbour vector $\mathbf{a}_j$, the final expression is

$$\begin{aligned}\mathcal{H}_{\mathrm{SOC}} &= \sum_{\mathbf{k}} \left(\mathbf{c}^\dagger_{\mathbf{k},\uparrow}\mathbf{c}_{\mathbf{k},\downarrow}s_{\mathbf{k}} + \mathbf{c}^\dagger_{\mathbf{k},\downarrow}\mathbf{c}_{\mathbf{k},\uparrow}s^*_{\mathbf{k}} \right) \\ &= \sum_{\mathbf{k}} \begin{pmatrix} \mathbf{c}^\dagger_{\mathbf{k}\uparrow} & \mathbf{c}^\dagger_{\mathbf{k}\downarrow} \end{pmatrix} \begin{pmatrix} 0 & s_{\mathbf{k}} \\ s^*_{\mathbf{k}} & 0 \end{pmatrix} \begin{pmatrix} \mathbf{c}_{\mathbf{k}\uparrow} \\ \mathbf{c}_{\mathbf{k}\downarrow} \end{pmatrix}. \end{aligned} \tag{5.11}$$

The spin-orbit coupling function is defined as

$$s_{\mathbf{k}} = 2i\lambda_R \sum_j e^{-i\theta_j} \sin(\mathbf{k}\cdot\mathbf{a}_j). \tag{5.12}$$

The total Hamiltonian with both hopping and spin-orbit coupling now reads

$$\mathcal{H} = \sum_{\mathbf{k}} \psi^\dagger_{\mathbf{k}} \begin{pmatrix} t_{\mathbf{k}} & s_{\mathbf{k}} \\ s^*_{\mathbf{k}} & t_{\mathbf{k}} \end{pmatrix} \psi_{\mathbf{k}}, \tag{5.13}$$

with $\psi^\dagger_{\mathbf{k}} = \begin{pmatrix} \mathbf{c}^\dagger_{\mathbf{k},\uparrow} & \mathbf{c}^\dagger_{\mathbf{k},\downarrow} \end{pmatrix}$. Diagonalizing this problem yields the energy dispersion

$$\epsilon_{\mathbf{k},\alpha} = t_{\mathbf{k}} \pm |s_{\mathbf{k}}|, \tag{5.14}$$

where the diagonalized band basis $A_{\mathbf{k}} = \begin{pmatrix} \mathbf{a}_{\mathbf{k},1} & \mathbf{a}_{\mathbf{k},2} \end{pmatrix}^T$ and spin basis $\psi_{\mathbf{k}}$ are related by the transformation

$$\psi_{\mathbf{k}} = \mathbf{U} A_{\mathbf{k}} = \begin{pmatrix} -s_{\mathbf{k}}/|s_{\mathbf{k}}| & s_{\mathbf{k}}/|s_{\mathbf{k}}| \\ 1 & 1 \end{pmatrix} A_k. \tag{5.15}$$

The one-particle energy dispersion $\epsilon_{\mathbf{k},\alpha}$ is no longer degenerate, owing to the splitting of the two spin-bands caused by spin-orbit coupling, see figure 5.3. However, there will still be degenerate points wherever $s_{\mathbf{k}}$ is zero. The $\mathbf{k}$-dependency of the energy dispersion close to these points is linear, and consequently these points are Dirac points.

5.2 Interaction Hamiltonian

The BCS-type interaction term is

$$\mathcal{H}_I = \sum_{\mathbf{k},\mathbf{k}'\mathbf{q}} V_{\mathbf{k},\mathbf{k}',\mathbf{q}} \mathbf{c}^\dagger_{\mathbf{k},\uparrow} \mathbf{c}^\dagger_{-\mathbf{k}+\mathbf{q},\downarrow} \mathbf{c}_{-\mathbf{k}'+\mathbf{q},\downarrow} \mathbf{c}_{\mathbf{k}',\uparrow}. \tag{5.16}$$

Inserting for the transformation to the diagonalized band basis (5.15) yields

$$\begin{aligned} \mathcal{H}_I = \sum_{\mathbf{k},\mathbf{k}'\mathbf{q}} V_{\mathbf{k},\mathbf{k}',\mathbf{q}} \Big\{ \Big(-\frac{s^*_{\mathbf{k}}}{|s_{\mathbf{k}}|} \mathbf{a}^\dagger_{\mathbf{k},1} + \frac{s^*_{\mathbf{k}}}{|s_{\mathbf{k}}|} \mathbf{a}^\dagger_{\mathbf{k},2} \Big) \cdot \Big(\mathbf{a}^\dagger_{-\mathbf{k}+\mathbf{q},1} + \mathbf{a}^\dagger_{-\mathbf{k}+\mathbf{q},2} \Big) \\ \cdot \Big(\mathbf{a}_{-\mathbf{k}'+\mathbf{q},1} + \mathbf{a}_{-\mathbf{k}'+\mathbf{q},2} \Big) \cdot \Big(-\frac{s_{\mathbf{k}'}}{|s_{\mathbf{k}'}|} \mathbf{a}_{\mathbf{k}',1} + \frac{s_{\mathbf{k}'}}{|s_{\mathbf{k}'}|} \mathbf{a}_{\mathbf{k}',2} \Big) \Big\}. \end{aligned} \tag{5.17}$$

This can be contracted to

$$\mathcal{H}_I = \sum_{\mathbf{k},\mathbf{k}'\mathbf{q}} \sum_{\alpha\beta\beta'\alpha'} V^{\alpha\beta\beta'\alpha'}_{\mathbf{k},\mathbf{k}',\mathbf{q}} \mathbf{a}^\dagger_{\mathbf{k},\alpha} \mathbf{a}^\dagger_{-\mathbf{k}+\mathbf{q},\beta} \mathbf{a}_{-\mathbf{k}'+\mathbf{q},\beta'} \mathbf{a}_{\mathbf{k}',\alpha'}. \tag{5.18}$$

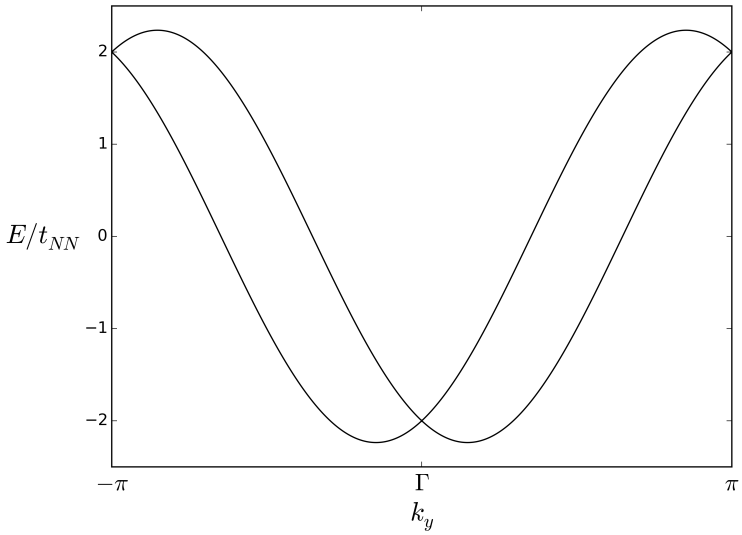

FIGURE 5.3: The energy dispersion with nearest neighbour hopping and spin-orbit coupling ($\lambda_R/t_{NN} = 1$) for a square lattice along the k_x-axis. We see that the spin-orbit coupling lifts the degeneracy, and we get two bands, meeting in a Dirac point at the origin.

$V^{\alpha\beta\beta'\alpha'}_{\mathbf{k},\mathbf{k}',\mathbf{q}}$ is now a tensor consisting of products of the elements in the transformation from the spin basis to the diagonalized band basis, and the original interaction mechanism in the spin basis $V_{\mathbf{k},\mathbf{k}',\mathbf{q}}$. The tensor has the following property

$$V^{\alpha\beta\beta'\alpha'}_{\mathbf{k},\mathbf{k}',\mathbf{q}} = \begin{cases} V_{\mathbf{k},\mathbf{k}',\mathbf{q}} \frac{s^*_{\mathbf{k}} s_{\mathbf{k}'}}{|s_{\mathbf{k}}||s_{\mathbf{k}'}|}, & \text{if } \alpha = \alpha' \\ -V_{\mathbf{k},\mathbf{k}',\mathbf{q}} \frac{s^*_{\mathbf{k}} s_{\mathbf{k}'}}{|s_{\mathbf{k}}||s_{\mathbf{k}'}|}, & \text{if } \alpha \neq \alpha'. \end{cases} \tag{5.19}$$

5.2.1 Intraband $\mathbf{q} = 0$

We will start off by looking at intraband ($\alpha = \alpha' = \beta = \beta'$) $\mathbf{q} = 0$ pairing, the simplest pairing mechanism, see figure 5.4. In the mean field approach, the restricted interaction Hamiltonian is

$$\mathcal{H}_I^{\text{intraband}} = \sum_{\mathbf{k},\mathbf{k}'} \sum_{\alpha} V^{\alpha}_{\mathbf{k},\mathbf{k}'} \Big(b^\dagger_\alpha(\mathbf{k}) \mathbf{a}_{-\mathbf{k}',\alpha} \mathbf{a}_{\mathbf{k}',\alpha} + b_\alpha(\mathbf{k}') \mathbf{a}^\dagger_{\mathbf{k},\alpha} \mathbf{a}^\dagger_{-\mathbf{k},\alpha} - b^\dagger_\alpha(\mathbf{k}) b_\alpha(\mathbf{k}') \Big), \tag{5.20}$$

with

$$b^\dagger_\alpha(\mathbf{k}) = \langle \mathbf{a}^\dagger_{\mathbf{k},\alpha} \mathbf{a}^\dagger_{-\mathbf{k},\alpha} \rangle, \tag{5.21}$$

and

$$V^{\alpha}_{\mathbf{k},\mathbf{k}'} = V_{\mathbf{k},\mathbf{k}'} \frac{s^*_{\mathbf{k}} s_{\mathbf{k}'}}{|s_{\mathbf{k}}||s_{\mathbf{k}'}|}. \tag{5.22}$$

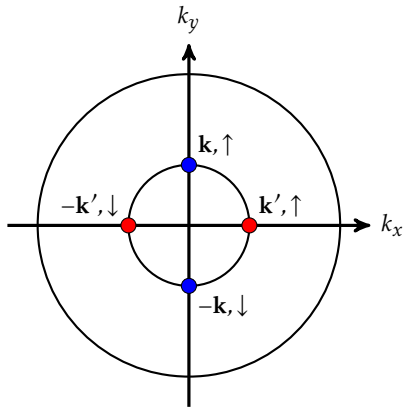

FIGURE 5.4: Intraband $\mathbf{q} = 0$ pairing. The inital (red) and final (blue) pair are in the same band.

Defining the gap functions

$$\Delta_\alpha(\mathbf{k}) = \sum_{\mathbf{k}'} V^\alpha_{\mathbf{k},\mathbf{k}'} b_\alpha(\mathbf{k}'), \tag{5.23}$$

and diagonalizing the mean field approach, following the same procedure as in section 4.3 yields accordingly the energy dispersion

$$E^\pm_{\mathbf{k},\alpha} = \pm\sqrt{(\epsilon_{\mathbf{k},\alpha} - \mu)^2 + |\Delta_\alpha(\mathbf{k})|^2} \tag{5.24}$$

The free energy is

$$F = \mathcal{H}_0 - \frac{1}{\beta}\sum_{\mathbf{k}}\sum_{\alpha}\left(\ln(1 + e^{-\beta E_{\mathbf{k},\alpha}}) + \ln(1 + e^{\beta E_{\mathbf{k},\alpha}})\right). \tag{5.25}$$

$\mathcal{H}_0$ now contains the product $\Delta^\dagger_\alpha(\mathbf{k})b_\alpha(\mathbf{k})$ and minimizing the free energy with respect to $\Delta^\dagger_\alpha(\mathbf{k})$ yields

$$b_\alpha(\mathbf{k}) = \Delta_\alpha(\mathbf{k})\chi(E_{\mathbf{k},\alpha}), \tag{5.26}$$

with $\chi(E_{\mathbf{k},\alpha})$ from (4.57). The gap functions are then

$$\Delta_\alpha(\mathbf{k}) = \sum_{\mathbf{k}'} V^\alpha_{\mathbf{k},\mathbf{k}'}\Delta_\alpha(\mathbf{k}')\chi(E_{\mathbf{k}',\alpha}) \tag{5.27}$$

In this intraband case, the gap functions are independent of each other. In the band basis the Hamiltonian reads

$$\begin{aligned}\mathcal{H}^{\text{intraband}} = \sum_{\mathbf{k},\alpha}\Big\{&|\Delta_\alpha(\mathbf{k})|^2\chi(E_{\mathbf{k},\alpha}) + \frac{\epsilon_{\mathbf{k},\alpha}}{2}(\mathbf{a}^\dagger_{\mathbf{k},\alpha}\mathbf{a}_{\mathbf{k},\alpha} + \mathbf{a}^\dagger_{-\mathbf{k},\alpha}\mathbf{a}_{-\mathbf{k},\alpha}) \\ &+\Delta_\alpha(\mathbf{k})\mathbf{a}^\dagger_{\mathbf{k},\alpha}\mathbf{a}^\dagger_{-\mathbf{k},\alpha} + \Delta^\dagger_\alpha(\mathbf{k})\mathbf{a}_{-\mathbf{k},\alpha}\mathbf{a}_{\mathbf{k},\alpha}\Big\}.\end{aligned} \tag{5.28}$$

Using that $s_{-\mathbf{k}} = -s_{\mathbf{k}}$, the operator products that describe superconductivity are in the spin basis

$$\mathbf{a}_{-\mathbf{k},1}\mathbf{a}_{\mathbf{k},1} = \frac{1}{4}\Big(-\frac{s_{\mathbf{k}}^*}{s_{\mathbf{k}}}\mathbf{c}_{-\mathbf{k},\uparrow}\mathbf{c}_{\mathbf{k},\uparrow} + \frac{|s_{\mathbf{k}}|}{s_{\mathbf{k}}}\mathbf{c}_{-\mathbf{k},\uparrow}\mathbf{c}_{\mathbf{k},\downarrow} - \frac{|s_{\mathbf{k}}|}{s_{\mathbf{k}}}\mathbf{c}_{-\mathbf{k},\downarrow}\mathbf{c}_{\mathbf{k},\uparrow} + \mathbf{c}_{-\mathbf{k},\downarrow}\mathbf{c}_{\mathbf{k},\downarrow}\Big) \tag{5.29}$$

$$\mathbf{a}_{-\mathbf{k},2}\mathbf{a}_{\mathbf{k},2} = \frac{1}{4}\Big(-\frac{s_{\mathbf{k}}^*}{s_{\mathbf{k}}}\mathbf{c}_{-\mathbf{k},\uparrow}\mathbf{c}_{\mathbf{k},\uparrow} - \frac{|s_{\mathbf{k}}|}{s_{\mathbf{k}}}\mathbf{c}_{-\mathbf{k},\uparrow}\mathbf{c}_{\mathbf{k},\downarrow} + \frac{|s_{\mathbf{k}}|}{s_{\mathbf{k}}}\mathbf{c}_{-\mathbf{k},\downarrow}\mathbf{c}_{\mathbf{k},\uparrow} + \mathbf{c}_{-\mathbf{k},\downarrow}\mathbf{c}_{\mathbf{k},\downarrow}\Big), \tag{5.30}$$

and the superconducting terms are

$$\begin{aligned}\mathcal{H}_{SC}^{\text{intraband}} = \frac{1}{4}\sum_{\mathbf{k}}\Big\{&\mathbf{c}_{\mathbf{k},\uparrow}^\dagger\mathbf{c}_{-\mathbf{k},\uparrow}^\dagger\frac{s_{\mathbf{k}}^*}{s_{\mathbf{k}}}(-\Delta_1(\mathbf{k})-\Delta_2(\mathbf{k})) + \mathbf{c}_{\mathbf{k},\downarrow}^\dagger\mathbf{c}_{-\mathbf{k},\downarrow}^\dagger(\Delta_1(\mathbf{k})+\Delta_2(\mathbf{k}))\\ &+\mathbf{c}_{\mathbf{k},\uparrow}^\dagger\mathbf{c}_{-\mathbf{k},\downarrow}^\dagger\frac{|s_{\mathbf{k}}|}{s_{\mathbf{k}}}(\Delta_1(\mathbf{k})-\Delta_2(\mathbf{k})) + \mathbf{c}_{\mathbf{k},\downarrow}^\dagger\mathbf{c}_{-\mathbf{k},\uparrow}^\dagger\frac{|s_{\mathbf{k}}|}{s_{\mathbf{k}}}(-\Delta_1(\mathbf{k})+\Delta_2(\mathbf{k}))\\ &+H.c.\Big\}.\end{aligned} \tag{5.31}$$

The spin structure is that of the two aligned triplet pairing states, and the mixed singlet pairing state. If $\Delta_1(\mathbf{k}) = \Delta_2(\mathbf{k})$ the mixed state disappears. This system could possibly, in addition to superconductivity, support ferromagnetism. Ferromagnetism would shut down the singlet mixed state, and the aligned triplet states are available for ferromagnetic interactions. However, there is also an orbital effect to consider. A magnetic field set up by the aligned magnetic momenta of a ferromagnet would destroy any unitary triplet pairing[58, 59]. What is needed then is a nonunitary triplet pairing, e.g. chiral p-wave, which will be investigated later in this chapter. Assuming a general separation of variables in the pairing mechanism

$$V_{\mathbf{k},\mathbf{k}'} = V g_{\mathbf{k}} g_{\mathbf{k}'}, \tag{5.32}$$

the gap function (5.27), upon summing over $\mathbf{k}'$, reduces to

$$\begin{aligned}\Delta_\alpha(\mathbf{k}) &= \sum_{\mathbf{k}'} V g_{\mathbf{k}} g_{\mathbf{k}'}\frac{s_{\mathbf{k}}^* s_{\mathbf{k}'}}{|s_{\mathbf{k}}||s_{\mathbf{k}'}|}\Delta_\alpha(\mathbf{k}')\chi(E_{\mathbf{k}',\alpha})\\ &= \frac{s_{\mathbf{k}}^*}{|s_{\mathbf{k}}|}g_{\mathbf{k}}\Delta_\alpha^0(T) \qquad (5.33)\\ &\equiv \frac{s_{\mathbf{k}}^*}{|s_{\mathbf{k}}|}\Delta_\alpha'(\mathbf{k}). \qquad (5.34)\end{aligned}$$

The superconducting terms are now

$$\begin{aligned}\mathcal{H}_{SC}^{\text{intraband}} = \frac{1}{4}\sum_{\mathbf{k}}\Big\{&\mathbf{c}_{\mathbf{k},\uparrow}^\dagger\mathbf{c}_{-\mathbf{k},\uparrow}^\dagger\frac{s_{\mathbf{k}}^*|s_{\mathbf{k}}|}{s_{\mathbf{k}}^2}(-\Delta_1'(\mathbf{k})-\Delta_2'(\mathbf{k})) + \mathbf{c}_{\mathbf{k},\downarrow}^\dagger\mathbf{c}_{-\mathbf{k},\downarrow}^\dagger\frac{s_{\mathbf{k}}^*}{|s_{\mathbf{k}}|}(\Delta_1'(\mathbf{k})+\Delta_2'(\mathbf{k}))\\ &+\mathbf{c}_{\mathbf{k},\uparrow}^\dagger\mathbf{c}_{-\mathbf{k},\downarrow}^\dagger\frac{s_{\mathbf{k}}^*}{s_{\mathbf{k}}}(\Delta_1'(\mathbf{k})-\Delta_2'(\mathbf{k})) + \mathbf{c}_{\mathbf{k},\downarrow}^\dagger\mathbf{c}_{-\mathbf{k},\uparrow}^\dagger\frac{s_{\mathbf{k}}^*}{s_{\mathbf{k}}}(-\Delta_1'(\mathbf{k})+\Delta_2'(\mathbf{k}))\\ &+H.c.\Big\}.\end{aligned} \tag{5.35}$$

The only unknown $\mathbf{k}$-dependency of the gap functions is in $g_{\mathbf{k}}$.

5.2.2 Interband $\mathbf{q} = 0$

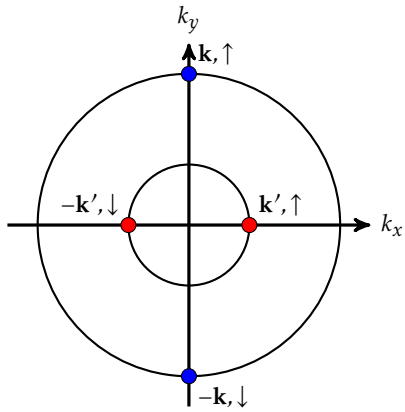

FIGURE 5.5: Interband $\mathbf{q} = 0$ pairing. The inital (red) and final (blue) pair are in different bands.

Another $\mathbf{q} = 0$ contribution is the scattering process where the initial and final pair are in different bands, see figure 5.5. The contribution from this process is

$$\mathcal{H}_I^{\text{interband}} = \sum_{\mathbf{k},\mathbf{k}'} \left\{ V^{1122}_{\mathbf{k},\mathbf{k}'} \mathbf{a}^\dagger_{\mathbf{k},1} \mathbf{a}^\dagger_{-\mathbf{k},1} \mathbf{a}_{-\mathbf{k}',2} \mathbf{a}_{\mathbf{k}',2} + V^{2211}_{\mathbf{k},\mathbf{k}'} \mathbf{a}^\dagger_{\mathbf{k},2} \mathbf{a}^\dagger_{-\mathbf{k},2} \mathbf{a}_{-\mathbf{k}',1} \mathbf{a}_{\mathbf{k}',1} \right\}. \tag{5.36}$$

Applying the mean field theory approach to this yields

$$\begin{aligned} \mathcal{H}_I^{\text{interband}} = \sum_{\mathbf{k},\mathbf{k}'} \Big\{ & V^{1122}_{\mathbf{k},\mathbf{k}'} \Big(b^\dagger_{11}(\mathbf{k}) \mathbf{a}_{-\mathbf{k}',2} \mathbf{a}_{\mathbf{k}',2} + b_{22}(\mathbf{k}') \mathbf{a}^\dagger_{\mathbf{k},1} \mathbf{a}^\dagger_{-\mathbf{k},1} - b^\dagger_{11}(\mathbf{k}) b_{22}(\mathbf{k}') \Big) \\ & + V^{2211}_{\mathbf{k},\mathbf{k}'} \Big(b^\dagger_{22}(\mathbf{k}) \mathbf{a}_{-\mathbf{k}',1} \mathbf{a}_{\mathbf{k}',1} + b_{11}(\mathbf{k}') \mathbf{a}^\dagger_{\mathbf{k},2} \mathbf{a}^\dagger_{-\mathbf{k},2} - b^\dagger_{22}(\mathbf{k}) b_{11}(\mathbf{k}') \Big) \Big\}, \end{aligned} \tag{5.37}$$

with

$$b_{\alpha\beta}(\mathbf{k}) = \langle \mathbf{a}_{-\mathbf{k},\alpha} \mathbf{a}_{\mathbf{k},\beta} \rangle. \tag{5.38}$$

From (5.19) we have that

$$V^{1122}_{\mathbf{k},\mathbf{k}'} = V^{2211}_{\mathbf{k},\mathbf{k}'} = -V_{\mathbf{k},\mathbf{k}'} \frac{s^*_{\mathbf{k}} s_{\mathbf{k}'}}{|s_{\mathbf{k}}||s_{\mathbf{k}'}|}. \tag{5.39}$$

This allows us to define the order parameters

$$\Delta_1(\mathbf{k}) = -\sum_{\mathbf{k}'} V_{\mathbf{k},\mathbf{k}'} \frac{s^*_{\mathbf{k}} s_{\mathbf{k}'}}{|s_{\mathbf{k}}||s_{\mathbf{k}'}|} b_{11}(\mathbf{k}') \tag{5.40}$$

$$\Delta_2(\mathbf{k}) = -\sum_{\mathbf{k}'} V_{\mathbf{k},\mathbf{k}'} \frac{s^*_{\mathbf{k}} s_{\mathbf{k}'}}{|s_{\mathbf{k}}||s_{\mathbf{k}'}|} b_{22}(\mathbf{k}'). \tag{5.41}$$

Reinserting these into the Hamiltonian yields

$$\mathcal{H}_I^{\text{interband}} = \sum_{\mathbf{k}} \Big(\Delta_1^\dagger(\mathbf{k}) \mathbf{a}_{-\mathbf{k},2} \mathbf{a}_{\mathbf{k},2} + \Delta_2(\mathbf{k}) \mathbf{a}_{\mathbf{k},1}^\dagger \mathbf{a}_{-\mathbf{k},1}^\dagger - \Delta_1^\dagger(\mathbf{k}) b_{22}(\mathbf{k}) \\ + \Delta_2^\dagger(\mathbf{k}) \mathbf{a}_{-\mathbf{k},1} \mathbf{a}_{\mathbf{k},1} + \Delta_1(\mathbf{k}) \mathbf{a}_{\mathbf{k},2}^\dagger \mathbf{a}_{-\mathbf{k},2}^\dagger - \Delta_2^\dagger(\mathbf{k}) b_{11}(\mathbf{k}) \Big). \tag{5.42}$$

Diagonalizing the full Hamiltonian now results in the eigenvalues

$$E_{\mathbf{k},\alpha\beta}^{\pm} = \pm \sqrt{(\epsilon_{\mathbf{k},\alpha} - \mu)^2 + |\Delta_\beta(\mathbf{k})|^2}, \tag{5.43}$$

with $\beta \neq \alpha$. The free energy has the same form as in (5.25), with the difference that $\mathcal{H}_0$ contain the terms $\Delta_1^\dagger(\mathbf{k}) b_{22}(\mathbf{k})$ and $\Delta_2^\dagger(\mathbf{k}) b_{11}(\mathbf{k})$. As such, minimizing the free energy with respect to the gaps leads to

$$b_{\beta\beta}(\mathbf{k}) = \Delta_\alpha(\mathbf{k}) \chi(E_{\mathbf{k},\beta\alpha}), \tag{5.44}$$

again with $\beta \neq \alpha$, and the self-consistency equations are

$$\Delta_1(\mathbf{k}) = -\sum_{\mathbf{k}'} V_{\mathbf{k},\mathbf{k}'} \frac{s_{\mathbf{k}}^* s_{\mathbf{k}'}}{|s_{\mathbf{k}}||s_{\mathbf{k}'}|} \Delta_2(\mathbf{k}') \chi(E_{\mathbf{k}',12}) \tag{5.45}$$

$$\Delta_2(\mathbf{k}) = -\sum_{\mathbf{k}'} V_{\mathbf{k},\mathbf{k}'} \frac{s_{\mathbf{k}}^* s_{\mathbf{k}'}}{|s_{\mathbf{k}}||s_{\mathbf{k}'}|} \Delta_1(\mathbf{k}') \chi(E_{\mathbf{k}',21}). \tag{5.46}$$

The gap functions are now coupled to each other. Back in the spin basis the superconducting terms have the following structure, using (5.29) and (5.30)

$$\mathcal{H}_{SC}^{\text{interband}} = \frac{1}{4} \sum_{\mathbf{k}} \Big\{ \mathbf{c}_{\mathbf{k},\uparrow}^\dagger \mathbf{c}_{-\mathbf{k},\uparrow}^\dagger \frac{s_{\mathbf{k}}^*}{s_{\mathbf{k}}} (-\Delta_1(\mathbf{k}) - \Delta_2(\mathbf{k})) + \mathbf{c}_{\mathbf{k},\downarrow}^\dagger \mathbf{c}_{-\mathbf{k},\downarrow}^\dagger (\Delta_1(\mathbf{k}) + \Delta_2(\mathbf{k})) \\ + \mathbf{c}_{\mathbf{k},\uparrow}^\dagger \mathbf{c}_{-\mathbf{k},\downarrow}^\dagger \frac{|s_{\mathbf{k}}|}{s_{\mathbf{k}}} (-\Delta_1(\mathbf{k}) + \Delta_2(\mathbf{k})) + \mathbf{c}_{\mathbf{k},\downarrow}^\dagger \mathbf{c}_{-\mathbf{k},\uparrow}^\dagger \frac{|s_{\mathbf{k}}|}{s_{\mathbf{k}}} (\Delta_1(\mathbf{k}) - \Delta_2(\mathbf{k})) \\ + H.c. \Big\}. \tag{5.47}$$

The same structure as for the simple intraband case is present, with the two aligned triplet states and singlet mixed state. Furthermore, to achieve the mixed triplet state we need to consider the more intricate finite-momentum interband pairings. Assuming again a separation of variables in the pairing mechanism

$$V_{\mathbf{k},\mathbf{k}'} = V g_{\mathbf{k}} g_{\mathbf{k}'}, \tag{5.48}$$

the gap functions (5.45) and (5.46) are now

$$\Delta_\alpha(\mathbf{k}) = -\sum_{\mathbf{k}'} V g_{\mathbf{k}} g_{\mathbf{k}'} \frac{s_{\mathbf{k}}^* s_{\mathbf{k}'}}{|s_{\mathbf{k}}||s_{\mathbf{k}'}|} \Delta_\beta(\mathbf{k}') \chi(E_{\mathbf{k}',\alpha\beta}), \tag{5.49}$$

with $\beta \neq \alpha$. Since these equations are coupled they are different from the gap-functions in the intraband case. We write

$$\Delta_\alpha(\mathbf{k}) = -\frac{s^*_{\mathbf{k}}}{|s_{\mathbf{k}}|}\Delta'_{\alpha\beta}(\mathbf{k}). \tag{5.50}$$

The superconducting terms are now

$$\begin{aligned}\mathcal{H}_{SC}^{\text{interband}} = \frac{1}{4}\sum_{\mathbf{k}}\Big\{&\mathbf{c}^\dagger_{\mathbf{k},\uparrow}\mathbf{c}^\dagger_{-\mathbf{k},\uparrow}\frac{s^*_{\mathbf{k}}|s_{\mathbf{k}}|}{s^2_{\mathbf{k}}}(\Delta'_{12}(\mathbf{k})+\Delta'_{21}(\mathbf{k})) + \mathbf{c}^\dagger_{\mathbf{k},\downarrow}\mathbf{c}^\dagger_{-\mathbf{k},\downarrow}\frac{s^*_{\mathbf{k}}}{|s_{\mathbf{k}}|}(-\Delta'_{12}(\mathbf{k})-\Delta'_{21}(\mathbf{k}))\\ &+\mathbf{c}^\dagger_{\mathbf{k},\uparrow}\mathbf{c}^\dagger_{-\mathbf{k},\downarrow}\frac{s^*_{\mathbf{k}}}{s_{\mathbf{k}}}(-\Delta'_{12}(\mathbf{k})+\Delta'_{21}(\mathbf{k})) + \mathbf{c}^\dagger_{\mathbf{k},\downarrow}\mathbf{c}^\dagger_{-\mathbf{k},\uparrow}\frac{s^*_{\mathbf{k}}}{s_{\mathbf{k}}}(\Delta'_{12}(\mathbf{k})-\Delta'_{21}(\mathbf{k}))\\ &+H.c.\Big\}.\end{aligned} \tag{5.51}$$

These interband superconducting terms have the opposite sign of the intraband terms. Because the new gaps are coupled, this will however not lead to any cancellation in the combined intra- and interband system.

5.2.3 Chiral p-wave pairing

In order to achieve Majorana edge states we saw in section 4.5 that a gap function that goes as $|\Delta_\alpha(\mathbf{k})|^2 \sim k^2$ where $\epsilon_{\mathbf{k},\alpha} = 0$ is needed, all in the notation of the intraband $\mathbf{q} = 0$ case. This ensures a relativistic energy relation $E_{\mathbf{k},\alpha} \approx \pm\sqrt{\mu^2 + |\Delta_\alpha|^2 k^2}$. The origin of such a gap is often taken to be a chiral p-wave pairing, $\Delta(\mathbf{k}) = \Delta_0(k_x - ik_y)$. This is also the continuum limit of the spin-orbit coupling function s_k of the square lattice. Our one-particle dispersion $\epsilon_{\mathbf{k},\alpha}$ has a minimum for $\mathbf{k} = 0$, and by adjusting our on-site energy, $\epsilon_0 \sum_i n_i$, $\mathbf{k} = 0$ can be made to correspond to $\epsilon_{\mathbf{k},\alpha} = 0$. Next we separate the variable dependence of $V^\alpha_{\mathbf{k},\mathbf{k}'}$ as we did in section 4.3

$$V_{\mathbf{k},\mathbf{k}'} = \sum_{\lambda,\lambda'}|V|g^\lambda_{\mathbf{k}}g^{\lambda'}_{\mathbf{k}'}, \tag{5.52}$$

such that after summing over $\mathbf{k}'$ and λ' the gap function may be written

$$\Delta_\alpha(\mathbf{k}) = \sum_\lambda \Delta^0_\alpha g^\lambda_{\mathbf{k}}. \tag{5.53}$$

We keep in mind that $\Delta_\alpha(\mathbf{k}) \propto \frac{s^*_{\mathbf{k}}}{|s_{\mathbf{k}}|}$, from (5.19), contained in $g^\lambda_{\mathbf{k}}$. Since the chiral p-wave pairing has the same form as $s_{\mathbf{k}}$ for the square lattice, we propose choosing a single λ-value, and set $g^\lambda_{\mathbf{k}}$ to be our spin-orbit coupling function $s_{\mathbf{k}}$. Let us check if $s_{\mathbf{k}}$ has the proper chiral p-wave form near $\mathbf{k} = 0$ for lattices other than the square lattice.

- Hexagonal lattice: The hexagonal lattice has nearest neighbour vectors $\mathbf{a_1} = a\hat{x}$, $\mathbf{a_2} = a\left(\frac{1}{2}\hat{x} + \frac{\sqrt{3}}{2}\hat{y}\right)$ and $\mathbf{a_3} = a\left(\frac{1}{2}\hat{x} - \frac{\sqrt{3}}{2}\hat{y}\right)$. The spin-orbit coupling functions

is then

$$\begin{aligned} s_{\mathbf{k}} &= 2i\lambda_R\Big(\sin(\mathbf{k}\cdot\mathbf{a}_1) + e^{-i\frac{\pi}{3}}\sin(\mathbf{k}\cdot\mathbf{a}_2) + e^{i\frac{\pi}{3}}\sin(\mathbf{k}\cdot\mathbf{a}_3)\Big) \\ &\approx 2i\lambda_R\Big(\mathbf{k}\cdot\mathbf{a}_1 + e^{-i\frac{\pi}{3}}\mathbf{k}\cdot\mathbf{a}_2 + e^{i\frac{\pi}{3}}\mathbf{k}\cdot\mathbf{a}_3\Big) \\ &= 2i\lambda_R\Big(k_x + e^{-i\frac{\pi}{3}}(\frac{k_x}{2} + \frac{\sqrt{3}}{2}k_y) + e^{i\frac{\pi}{3}}(\frac{k_x}{2} - \frac{\sqrt{3}}{2}k_y)\Big) \\ &= 2i\lambda_R\Big(\frac{3}{2}k_x - \frac{3}{2}ik_y\Big) \\ &= 3i\lambda_R(k_x - ik_y). \end{aligned} \tag{5.54}$$

As such, the chiral p-wave form is present near $\mathbf{k} = 0$.

- Rhombic lattice: The nearest neighbour vectors of the rhombic lattice may be written $\mathbf{a}_1 = a(\cos\theta\hat{x} + \sin\theta\hat{y}$ and $\mathbf{a}_2 = a(\cos\theta\hat{x} - \sin\theta\hat{y}$. $\theta = 45^o$ corresponds to the square lattice. The spin-orbit coupling function is

$$\begin{aligned} s_{\mathbf{k}} &= 2i\lambda_R\Big(e^{-i\theta}\sin(k_x\cos\theta + k_y\sin\theta) + e^{i\theta}\sin(k_x\cos\theta - k_y\sin\theta)\Big) \\ &\approx 2i\lambda_R\Big(e^{-i\theta}(k_x\cos\theta + k_y\sin\theta) + e^{i\theta}(k_x\cos\theta - k_y\sin\theta)\Big) \\ &= 4i\lambda_R\Big(k_x\cos^2\theta - ik_y\sin^2\theta\Big). \end{aligned} \tag{5.55}$$

For $\theta \neq 45^o$ this function is an anisotropic variant of chiral p-wave.

- Oblique and rectangular lattice: Nearest neighbour vectors are $\mathbf{a}_1 = a_1\hat{x}$ and $\mathbf{a}_2 = a_2(\cos(\theta)\hat{x} + \sin(\theta)\hat{y}$, with $\theta = 90^o$ being the rectangular lattice. The spin-orbit coupling function is

$$\begin{aligned} s_{\mathbf{k}} \approx 2i\lambda_R\Big(&k_x(a_1 + a_2\cos^2\theta - ia_2\cos\theta\sin\theta) \\ &+k_y(a_2\cos\theta\sin\theta - ia_2\sin^2\theta)\Big). \end{aligned} \tag{5.56}$$

A rectangular lattice, $\theta = 90^o$, is needed in order to achieve an anistropic chiral p-wave function.

In summary: $s_{\mathbf{k}}$ can be used as a chiral p-wave pairing function for the hexagonal, rectangular, square, and rhombic lattice. If we take the pairing function $g_{\mathbf{k}}$ to be $s_{\mathbf{k}}$ for these lattices, the energy dispersion will be relativistic, and edge states are Majorana fermions.

It is clear from (5.35) and (5.51) that the gap functions in the spin basis need not be on the chiral p-wave form, since it is the gap-function in the diagonalized basis that go into the energy dispersions (5.24) and (5.43). For the intraband case (5.31) the structure in the spin basis, upon setting $\Delta_\alpha(\mathbf{k}) = \Delta_i^0 s_{\mathbf{k}}$, cancels out some

of the spin-orbit coupling functions, and the resulting structure is

$$\begin{aligned}\mathcal{H}_{SC} = \frac{1}{4}\sum_{\mathbf{k}}\Big\{&\mathbf{c}^{\dagger}_{\mathbf{k},\uparrow}\mathbf{c}^{\dagger}_{-\mathbf{k},\uparrow}s^{*}_{\mathbf{k}}(-\Delta^{0}_{1}-\Delta^{0}_{2})+\mathbf{c}^{\dagger}_{\mathbf{k},\downarrow}\mathbf{c}^{\dagger}_{-\mathbf{k},\downarrow}s_{\mathbf{k}}(\Delta^{0}_{1}+\Delta^{0}_{2})\\&+\mathbf{c}^{\dagger}_{\mathbf{k},\uparrow}\mathbf{c}^{\dagger}_{-\mathbf{k},\downarrow}|s_{\mathbf{k}}|(\Delta^{0}_{1}-\Delta^{0}_{2})+\mathbf{c}^{\dagger}_{\mathbf{k},\downarrow}\mathbf{c}^{\dagger}_{-\mathbf{k},\uparrow}|s_{\mathbf{k}}|(-\Delta^{0}_{1}+\Delta^{0}_{2})\\&+H.c.\Big\}.\end{aligned} \tag{5.57}$$

The superconducting order parameter in the spin basis is of chiral p-wave type for the aligned states, $s^{*}_{\mathbf{k}}$, while for the mixed states it is real-valued. As such, a chiral p-wave form of the gap-function in the diagonalized band basis leads to a chiral p-wave form in the spin basis for the aligned triplet states, and real-valued $\mathbf{k}$-dependency for the mixed state. Rashba spin-orbit coupling causes spin-momentum locking, and in order to describe two-particle interactions we must work in the diagonalized band basis. Consequently, the gap functions are defined in the band basis, and their form in the spin basis will be different.

5.3 Symmetry and Topology

The full Hamiltonian with superconducting terms may now be written

$$\mathcal{H} = \sum_{\mathbf{k}}\psi^{\dagger}_{\mathbf{k}}\begin{pmatrix} t_{\mathbf{k}} & s_{\mathbf{k}} & \Delta_{\uparrow\uparrow}(\mathbf{k}) & \Delta_{\uparrow\downarrow}(\mathbf{k}) \\ s^{*}_{\mathbf{k}} & t_{\mathbf{k}} & \Delta_{\downarrow\uparrow}(\mathbf{k}) & \Delta_{\downarrow\downarrow}(\mathbf{k}) \\ \Delta^{\dagger}_{\uparrow\uparrow}(\mathbf{k}) & \Delta^{\dagger}_{\uparrow\downarrow}(\mathbf{k}) & -t_{\mathbf{k}} & s^{*}_{\mathbf{k}} \\ \Delta^{\dagger}_{\downarrow\uparrow}(\mathbf{k}) & \Delta^{\dagger}_{\downarrow\downarrow}(\mathbf{k}) & s_{\mathbf{k}} & -t_{\mathbf{k}} \end{pmatrix}\psi_{\mathbf{k}}, \tag{5.58}$$

with the Nambu spinor $\psi^{\dagger}_{\mathbf{k}} = (\mathbf{c}^{\dagger}_{\mathbf{k},\uparrow}\ \mathbf{c}^{\dagger}_{\mathbf{k},\downarrow}\ \mathbf{c}_{-\mathbf{k},\uparrow}\ \mathbf{c}_{-\mathbf{k},\downarrow})$. This can be further simplified to

$$\mathcal{H} = \sum_{\mathbf{k}}\psi^{\dagger}_{\mathbf{k}}\begin{pmatrix} \underline{\mathcal{H}_0}(\mathbf{k}) & \underline{\Delta}(\mathbf{k}) \\ \underline{\Delta}^{*}(\mathbf{k}) & -\underline{\mathcal{H}_0}^{*}(-\mathbf{k}) \end{pmatrix}\psi_{\mathbf{k}}, \tag{5.59}$$

where the notation $\underline{A}$ denotes a 2x2 matrix. Let us first look at the symmetries of the one-particle Hamiltonian, $\underline{\mathcal{H}_0}(\mathbf{k})$. The inversion operator, $\hat{P}$ takes $\mathbf{k} \to -\mathbf{k}$. For the one-particle Hamiltonian to have inversion symmetry we require $\hat{P}\underline{\mathcal{H}_0}(\mathbf{k})\hat{P}^{-1} = \underline{\mathcal{H}_0}(-\mathbf{k})$[45]. This is the same as demanding $[\underline{\mathcal{H}_0}(\mathbf{k}), \hat{P}] = 0$. For the one-particle system the following applies

$$\underline{\mathcal{H}_0}(\mathbf{k})\hat{P}\phi_{\mathbf{k}} = \underline{\mathcal{H}_0}(\mathbf{k})\phi_{-\mathbf{k}} = \epsilon_{-\mathbf{k}}\phi_{-\mathbf{k}} \tag{5.60}$$

$$\hat{P}\underline{\mathcal{H}_0}(\mathbf{k})\phi_{\mathbf{k}} = \hat{P}\epsilon_{\mathbf{k}}\phi_{\mathbf{k}} = \epsilon_{-\mathbf{k}}\phi_{-\mathbf{k}}, \tag{5.61}$$

meaning that the one-particle Hamiltonian has inversion symmetry. This can also be easily seen from the one-particle dispersion (5.14), $\epsilon_{-\mathbf{k}} = \epsilon_{\mathbf{k}}$. Next, the time-reversal operator, $\hat{T}$ satisfies $\hat{T}\underline{\mathcal{H}_0}(\mathbf{k})\hat{T}^{-1} = \underline{\mathcal{H}_0}(-\mathbf{k})$[46]. This can be checked

explicitly, by noting that $\hat{T} = i\sigma_y\hat{K}$, where $\hat{K}$ is complex conjugation. The effect of $\hat{K}$ poses the requirement then that $i\sigma_y\underline{\mathcal{H}_0}(\mathbf{k})(-i\sigma_y) = \underline{\mathcal{H}_0}^*(-\mathbf{k})$. This is fulfilled

$$\begin{aligned} i\sigma_y\underline{\mathcal{H}_0}(\mathbf{k})(-i\sigma_y) &= \begin{pmatrix} 0 & 1 \\ -1 & 0 \end{pmatrix}\begin{pmatrix} t_{\mathbf{k}} & s_{\mathbf{k}} \\ s_{\mathbf{k}}^* & t_{\mathbf{k}} \end{pmatrix}\begin{pmatrix} 0 & -1 \\ 1 & 0 \end{pmatrix} \\ &= \begin{pmatrix} t_{\mathbf{k}} & -s_{\mathbf{k}}^* \\ -s_{\mathbf{k}} & t_{\mathbf{k}} \end{pmatrix} \\ &= \underline{\mathcal{H}_0}^*(-\mathbf{k}), \end{aligned} \tag{5.62}$$

because $s_{-\mathbf{k}} = -s_{\mathbf{k}}$ and $t_{\mathbf{k}}$ is real. As such, both inversion and time-reversal symmetry[33] is present for the normal state. From the form of the time-reversal operator, $\hat{T}^2 = -1$, and since there is no particle-hole symmetry in the normal state, the system belongs to AZ class AII, described by a $\mathbb{Z}_2$ topological invariant, see table 3.1. We now turn to the full superconducting Hamiltonian. The time-reversal operator is now[46]

$$\begin{aligned} \hat{T} &= i(\mathcal{I}_{2x2}\otimes\sigma_y)\hat{K} \\ &= \begin{pmatrix} i\sigma_y & 0 \\ 0 & i\sigma_y \end{pmatrix}\hat{K}. \end{aligned} \tag{5.63}$$

We find

$$\hat{T}\mathcal{H}(\mathbf{k})\hat{T}^{-1} = \begin{pmatrix} t_{\mathbf{k}} & -s_{\mathbf{k}}^* & \Delta_{\downarrow\downarrow}(\mathbf{k}) & -\Delta_{\downarrow\uparrow}(\mathbf{k}) \\ -s_{\mathbf{k}} & t_{\mathbf{k}} & -\Delta_{\uparrow\downarrow}(\mathbf{k}) & \Delta_{\uparrow\uparrow}(\mathbf{k}) \\ \Delta_{\downarrow\downarrow}^\dagger(\mathbf{k}) & -\Delta_{\downarrow\uparrow}^\dagger(\mathbf{k}) & -t_{\mathbf{k}} & -s_{\mathbf{k}} \\ -\Delta_{\uparrow\downarrow}^\dagger(\mathbf{k}) & \Delta_{\uparrow\uparrow}^\dagger(\mathbf{k}) & -s_{\mathbf{k}}^* & -t_{\mathbf{k}} \end{pmatrix}. \tag{5.64}$$

The requirement for time-reversal symmetry, $\hat{T}\mathcal{H}(\mathbf{k})\hat{T}^{-1} = \mathcal{H}(-\mathbf{k})^*$, holds if $\Delta_{\sigma\sigma}(\mathbf{k}) = \Delta_{-\sigma,-\sigma}^*(-\mathbf{k})$ and $-\Delta_{\alpha\beta}(\mathbf{k}) = \Delta_{\beta\alpha}^*(-\mathbf{k})$ $(\beta \neq \alpha)$. These are relations connecting the gap-functions when the spins are flipped. For the aligned triplet states we generally have $\Delta_{\uparrow\uparrow}(\mathbf{k}) = -\Delta_{\downarrow\downarrow}^*(\mathbf{k})$, see (4.64). This means that the gap-function for the aligned triplet states must be odd in $\mathbf{k}$ in order to preserve time-reversal symmetry. On the other hand, the requirement for the triplet mixed state is $\Delta_{\downarrow\uparrow}(\mathbf{k}) = -\Delta_{\downarrow\uparrow}^*(-\mathbf{k})$, and that of the singlet mixed state is $\Delta_{\downarrow\uparrow}(\mathbf{k}) = \Delta_{\downarrow\uparrow}^*(-\mathbf{k})$, see (4.63). This means that, in order for time-reversal symmetry to be preserved, the triplet mixed state gap function must be odd in $\mathbf{k}$ and real, and the singlet mixed state gap function must be odd in $\mathbf{k}$ and imaginary *or* even in $\mathbf{k}$ and real. Next we check for particle-hole symmetry. The particle-hole operator $\hat{\Theta}$ is[60]

$$\begin{aligned} \hat{\Theta} &= (\sigma_x\otimes\mathcal{I}_{2x2})\hat{K} \\ &= \begin{pmatrix} 0 & \mathcal{I}_{2x2} \\ \mathcal{I}_{2x2} & 0 \end{pmatrix}\hat{K} \end{aligned} \tag{5.65}$$

and particle-hole symmetry invariance requires $\hat{\Theta}\mathcal{H}(\mathbf{k})\hat{\Theta}^{-1} = -\mathcal{H}^*(-\mathbf{k})$. We find

$$\hat{\Theta}\mathcal{H}(\mathbf{k})\hat{\Theta}^{-1} = \begin{pmatrix} -t_{\mathbf{k}} & s^*_{\mathbf{k}} & \Delta^\dagger_{\uparrow\uparrow}(\mathbf{k}) & \Delta^\dagger_{\uparrow\downarrow}(\mathbf{k}) \\ s_{\mathbf{k}} & -t_{\mathbf{k}} & \Delta^\dagger_{\downarrow\uparrow}(\mathbf{k}) & \Delta^\dagger_{\downarrow\downarrow}(\mathbf{k}) \\ \Delta_{\uparrow\uparrow}(\mathbf{k}) & \Delta_{\uparrow\downarrow}(\mathbf{k}) & t_{\mathbf{k}} & s_{\mathbf{k}} \\ \Delta_{\downarrow\uparrow}(\mathbf{k}) & \Delta_{\downarrow\downarrow}(\mathbf{k}) & s^*_{\mathbf{k}} & t_{\mathbf{k}} \end{pmatrix}. \tag{5.66}$$

Particle-hole symmetry is present if $\Delta_{\sigma\sigma'}(\mathbf{k}) = -\Delta_{\sigma\sigma'}(-\mathbf{k})$, i.e. odd in $\mathbf{k}$. All of this can be summarized as follows, with reference to table 3.1.

- Our one-particle system is both inversion and time-reversal symmetric. With $\hat{T}^2 = -1$ and no particle-hole symmetry, this system is in AZ class AII, classified by a $\mathbb{Z}_2$ topological invariant in two dimension.
- With pairing mechanisms that break time-reversal symmetry, the system belong to class D if particle-hole symmetry is preserved, since $\hat{\Theta}^2 = 1$. This class is characterized by a $\mathbb{Z}$ topological invariant. If particle-hole symmetry is broken, and assuming no chiral symmetry, the system is in class A, also characterized by a $\mathbb{Z}$ topological invariant.
- With pairing mechanisms that preserve both time-reversal and particle-hole symmetry, the system belongs to class DIII, since $\hat{T}^2 = -1$ and $\hat{\Theta}^2 = 1$. This class is characterized by a $\mathbb{Z}_2$ topological invariant. Without particle-hole symmetry, the system remains in class AII.
- Special case: Chiral p-wave pairing. This pairing is odd and imaginary, and consequently preserves particle-hole symmetry. If the spins have the same chirality, time-reversal symmetry is broken[21], which puts the system in class D. With opposite chirality, time-reversal symmetry is conserved. This puts our system in class DIII. It is observed that for time-reversal invariancy a triplet chiral p-wave pairing is only possible with the aligned states, as long as the chirality of the pairs are different, i.e. satisfy $\Delta_{\uparrow\uparrow}(\mathbf{k}) = -\Delta^*_{\downarrow\downarrow}(\mathbf{k})$. For a chiral p-wave pairing in the intraband $\mathbf{q} = 0$ case, (5.57), this is fulfilled.

These results are in accordance with [47]. It is again emphasized that it is the gap function in the diagonalized basis that goes into the energy dispersion, and possibly make it relativistic, and as has been shown, transforming back to the spin basis may lead to a different form of the gap function.

Chapter 6

Bipartite Lattices

This chapter will go into more detail on two-dimensional bipartite lattices, consisting of two sublattices, or equivalently two atoms in the basis. Firstly, the one-particle problem consisting of nearest neighbour hopping and spin-orbit coupling is presented. Next, the two-particle interaction term is investigated, and through mean-field theory a general scheme for superconductivity in these lattices is developed. Finally, the symmetry properties of the system are studied, in order to evaluate the requirements on the superconducting gaps to ensure non-trivial topological behaviour.

6.1 One-Particle Problem

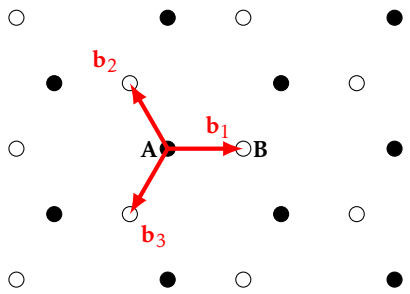

FIGURE 6.1: The honeycomb lattice composed of sublattice A (black sites) and B (white sites), with the three nearest neighbour vectors $\mathbf{b_1}$, $\mathbf{b_2}$ and $\mathbf{b_3}$ to site A.

To illustrate to a better degree we will look at as an example the honeycomb lattice, perhaps the most studied bipartite lattice. The results derived are generalized at the end of this section. The honeycomb lattice exhibits a hexagonal structure, composed of two hexagonal sublattices A and B, see fig. 6.1. The distance between a site A and nearest neighbour site B is a, which is set to unity for simplicity. Basing ourselves on an A site, we have three nearest neighbours on the B-lattice. These nearest neighbours are described by the following neighbour vectors

$$\mathbf{b_1} = \hat{x} \tag{6.1}$$

$$\mathbf{b_2} = -\frac{1}{2}\hat{x} + \frac{\sqrt{3}}{2}\hat{y} \tag{6.2}$$

$$\mathbf{b_3} = -\frac{1}{2}\hat{x} - \frac{\sqrt{3}}{2}\hat{y}. \tag{6.3}$$

The nearest neighbour hopping Hamiltonian is

$$\mathcal{H}_t = -t_{NN}\Big(\sum_i \mathbf{c}^\dagger_{A,\mathbf{r}_i}\mathbf{c}_{B,\mathbf{r}_i+\mathbf{b}_1} + \sum_i \mathbf{c}^\dagger_{A,\mathbf{r}_i}\mathbf{c}_{B,\mathbf{r}_i+\mathbf{b}_2} + \sum_i \mathbf{c}^\dagger_{A,\mathbf{r}_i}\mathbf{c}_{B,\mathbf{r}_i+\mathbf{b}_3} + h.c.\Big). \tag{6.4}$$

Fourier transforming to momentum space by

$$\mathbf{c}^\dagger_{A,\mathbf{r}_i} = \frac{1}{\sqrt{N}}\sum_{\mathbf{k}} \mathbf{c}^\dagger_{A,\mathbf{k}} e^{i\mathbf{k}\cdot\mathbf{r}_i} \tag{6.5}$$

$$\mathbf{c}_{B,\mathbf{r}_i+\mathbf{b}_j} = \frac{1}{\sqrt{N}}\sum_{\mathbf{k}} \mathbf{c}_{B,\mathbf{k}} e^{-i\mathbf{k}\cdot(\mathbf{r}_i+\mathbf{b}_j)}, \tag{6.6}$$

the full nearest neighbour hopping Hamiltonian is written as

$$\mathcal{H}_t = -t_{NN}\sum_{\mathbf{k}} \mathbf{c}^\dagger_{A,\mathbf{k}}\mathbf{c}_{B,\mathbf{k}}\sum_{i=1}^{3} e^{-i\mathbf{k}\cdot\mathbf{b}_i} - t_{NN}\sum_{\mathbf{k}} \mathbf{c}^\dagger_{B,\mathbf{k}}\mathbf{c}_{A,\mathbf{k}}\sum_{i=1}^{3} e^{i\mathbf{k}\cdot\mathbf{b}_i}. \tag{6.7}$$

This can be cast in a more convenient form

$$\mathcal{H}_t = \sum_{\mathbf{k}} (\mathbf{c}^\dagger_{A,\mathbf{k}}\ \mathbf{c}^\dagger_{B,\mathbf{k}}) \begin{pmatrix} 0 & t_{\mathbf{k}} \\ t^*_{\mathbf{k}} & 0 \end{pmatrix} \begin{pmatrix} \mathbf{c}_{A,\mathbf{k}} \\ \mathbf{c}_{B,\mathbf{k}} \end{pmatrix}. \tag{6.8}$$

The matrix entry $t_{\mathbf{k}}$ is given by

$$t_{\mathbf{k}} = -t_{NN}\sum_{i=1}^{3} e^{-i\mathbf{k}\cdot\mathbf{b}_i}. \tag{6.9}$$

This results in the well-known energy dispersion relation for the honeycomb lattice[61]

$$\begin{aligned} E(\mathbf{k}) &= \pm|t_{\mathbf{k}}| \\ &= \pm t_{NN}\sqrt{1 + 4\cos\Big(\frac{3k_x}{2}\Big)\cos\Big(\frac{\sqrt{3}k_y}{2}\Big) + 4\cos^2\Big(\frac{\sqrt{3}k_y}{2}\Big)}. \end{aligned} \tag{6.10}$$

A plot of this energy dispersion along the k_y-axis, out to two of the six K-points, is shown in figure 6.2. The K-points are the corners of the hexagonal reciprocal lattice.

6.1.1 Spin-Orbit Coupling

Next we look at the nearest neighbour spin-orbit coupling between the sublattices. The Rashba spin-orbit coupling Hamiltonian reads

$$\begin{aligned} \mathcal{H}_{\text{SOC}} = \lambda_R \sum_{\mathbf{r}_i,\alpha,\beta} i\Big\{ &\mathbf{c}^\dagger_{A,\mathbf{r}_i,\alpha}\sigma_y^{\alpha\beta}\mathbf{c}_{B,\mathbf{r}_i+\mathbf{b}_1,\beta} + \mathbf{c}^\dagger_{A,\mathbf{r}_i,\alpha}\Big(-\frac{1}{2}\sigma_y^{\alpha\beta} - \frac{\sqrt{3}}{2}\sigma_x^{\alpha\beta}\Big)\mathbf{c}_{B,\mathbf{r}_i+\mathbf{b}_2,\beta} \\ &+ \mathbf{c}^\dagger_{A,\mathbf{r}_i,\alpha}\Big(-\frac{1}{2}\sigma_y^{\alpha\beta} + \frac{\sqrt{3}}{2}\sigma_x^{\alpha\beta}\Big)\mathbf{c}_{B,\mathbf{r}_i+\mathbf{b}_3,\beta} + H.c.\Big\}. \end{aligned} \tag{6.11}$$

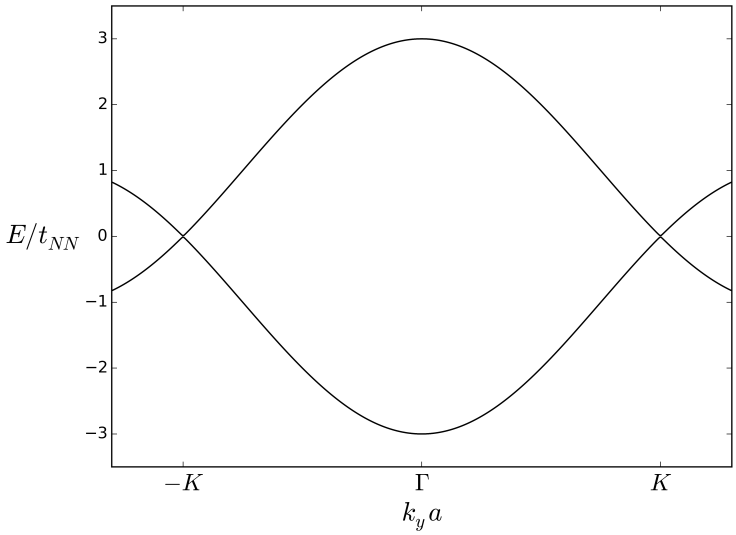

FIGURE 6.2: The energy dispersion with nearest neighbour hopping for the honeycomb lattice along the k_y-axis. Because of the sublattice structure we get two energybands, meeting in Dirac cones at the K-points, the corners of the hexagonal reciprocal lattice.

Going to momentum space results in

$$\mathcal{H}_{\mathrm{SOC}} = \lambda_R \sum_{\mathbf{k},\alpha,\beta} i\Big\{ \mathbf{c}^\dagger_{A,\mathbf{k},\alpha} \sigma_y^{\alpha\beta} \mathbf{c}_{B,\mathbf{k},\beta} e^{i\mathbf{k}\cdot\mathbf{b}_1} + \mathbf{c}^\dagger_{A,\mathbf{k},\alpha} \Big(-\frac{1}{2}\sigma_y^{\alpha\beta} - \frac{\sqrt{3}}{2}\sigma_x^{\alpha\beta} \Big) \mathbf{c}_{B,\mathbf{k},\beta} e^{i\mathbf{k}\cdot\mathbf{b}_2} + \mathbf{c}^\dagger_{A,\mathbf{k},\alpha} \Big(-\frac{1}{2}\sigma_y^{\alpha\beta} + \frac{\sqrt{3}}{2}\sigma_x^{\alpha\beta} \Big) \mathbf{c}_{B,\mathbf{k},\beta} e^{i\mathbf{k}\cdot\mathbf{b}_3} + H.c. \Big\}. \tag{6.12}$$

Summing over the spin indices α, β and writing out the hermitian conjugate leads to

$$\begin{aligned}
\mathcal{H}_{\mathrm{SOC}} = \lambda_R \sum_{\mathbf{k}} i\Big\{ & -i\mathbf{c}^\dagger_{A,\mathbf{k}\uparrow}\mathbf{c}_{B,\mathbf{k}\downarrow} e^{i\mathbf{k}\cdot\mathbf{b}_1} + i\mathbf{c}^\dagger_{A,\mathbf{k}\downarrow}\mathbf{c}_{B,\mathbf{k}\uparrow} e^{i\mathbf{k}\cdot\mathbf{b}_1} + \mathbf{c}^\dagger_{A,\mathbf{k}\uparrow}\Big(\frac{i}{2} - \frac{\sqrt{3}}{2}\Big)\mathbf{c}_{B,\mathbf{k}\downarrow} e^{i\mathbf{k}\cdot\mathbf{b}_2} \\
& + \mathbf{c}^\dagger_{A,\mathbf{k}\downarrow}\Big(-\frac{i}{2} - \frac{\sqrt{3}}{2}\Big)\mathbf{c}_{B,\mathbf{k}\uparrow} e^{i\mathbf{k}\cdot\mathbf{b}_2} + \mathbf{c}^\dagger_{A,\mathbf{k}\uparrow}\Big(\frac{i}{2} + \frac{\sqrt{3}}{2}\Big)\mathbf{c}_{B,\mathbf{k}\downarrow} e^{i\mathbf{k}\cdot\mathbf{b}_3} + \mathbf{c}^\dagger_{A,\mathbf{k}\downarrow}\Big(-\frac{i}{2} + \frac{\sqrt{3}}{2}\Big)\mathbf{c}_{B,\mathbf{k}\uparrow} e^{i\mathbf{k}\cdot\mathbf{b}_3} \\
& + i\mathbf{c}^\dagger_{B,\mathbf{k}\downarrow}\mathbf{c}_{A,\mathbf{k}\uparrow} e^{-i\mathbf{k}\cdot\mathbf{b}_1} - i\mathbf{c}^\dagger_{B,\mathbf{k}\uparrow}\mathbf{c}_{A,\mathbf{k}\downarrow} e^{-i\mathbf{k}\cdot\mathbf{b}_1} + \mathbf{c}^\dagger_{B,\mathbf{k}\downarrow}\Big(-\frac{i}{2} - \frac{\sqrt{3}}{2}\Big)\mathbf{c}_{A,\mathbf{k}\uparrow} e^{-i\mathbf{k}\cdot\mathbf{b}_2} \\
& + \mathbf{c}^\dagger_{B,\mathbf{k}\uparrow}\Big(\frac{i}{2} - \frac{\sqrt{3}}{2}\Big)\mathbf{c}_{A,\mathbf{k}\downarrow} e^{-i\mathbf{k}\cdot\mathbf{b}_2} + \mathbf{c}^\dagger_{B,\mathbf{k}\downarrow}\Big(-\frac{i}{2} + \frac{\sqrt{3}}{2}\Big)\mathbf{c}_{A,\mathbf{k}\uparrow} e^{-i\mathbf{k}\cdot\mathbf{b}_3} + \mathbf{c}^\dagger_{B,\mathbf{k}\uparrow}\Big(\frac{i}{2} + \frac{\sqrt{3}}{2}\Big)\mathbf{c}_{A,\mathbf{k}\downarrow} e^{-i\mathbf{k}\cdot\mathbf{b}_3} \Big\}.
\end{aligned} \tag{6.13}$$

Collecting terms finally yields

$$\begin{aligned}\mathcal{H}_{\text{SOC}} = \lambda_R \sum_{\mathbf{k}} \Big\{ & \mathbf{c}^\dagger_{A,\mathbf{k}\uparrow}\mathbf{c}_{B,\mathbf{k}\downarrow}\Big(e^{i\mathbf{k}\cdot\mathbf{b}_1} + e^{-i\frac{2\pi}{3}}e^{i\mathbf{k}\cdot\mathbf{b}_2} + e^{i\frac{2\pi}{3}}e^{i\mathbf{k}\cdot\mathbf{b}_3}\Big) \\ & + \mathbf{c}^\dagger_{A,\mathbf{k}\downarrow}\mathbf{c}_{B,\mathbf{k}\uparrow}\Big(-e^{i\mathbf{k}\cdot\mathbf{b}_1} + e^{-i\frac{\pi}{3}}e^{i\mathbf{k}\cdot\mathbf{b}_2} + e^{i\frac{\pi}{3}}e^{i\mathbf{k}\cdot\mathbf{b}_3}\Big) \\ & + \mathbf{c}^\dagger_{B,\mathbf{k}\uparrow}\mathbf{c}_{A,\mathbf{k}\downarrow}\Big(-e^{i\mathbf{k}\cdot\mathbf{b}_1} + e^{i\frac{\pi}{3}}e^{-i\mathbf{k}\cdot\mathbf{b}_2} + e^{-i\frac{\pi}{3}}e^{-i\mathbf{k}\cdot\mathbf{b}_3}\Big) \\ & + \mathbf{c}^\dagger_{B,\mathbf{k}\downarrow}\mathbf{c}_{A,\mathbf{k}\uparrow}\Big(e^{-i\mathbf{k}\cdot\mathbf{b}_1} + e^{i\frac{2\pi}{3}}e^{-i\mathbf{k}\cdot\mathbf{b}_2} + e^{-i\frac{2\pi}{3}}e^{-i\mathbf{k}\cdot\mathbf{b}_3}\Big)\Big\}. \end{aligned} \tag{6.14}$$

This can be put on matrix form

$$\mathcal{H}_R = \sum_{\mathbf{k}} \begin{pmatrix} \mathbf{c}^\dagger_{A,\mathbf{k}\uparrow} & \mathbf{c}^\dagger_{A,\mathbf{k}\downarrow} & \mathbf{c}^\dagger_{B,\mathbf{k}\uparrow} & \mathbf{c}^\dagger_{B,\mathbf{k}\downarrow} \end{pmatrix} \begin{pmatrix} 0 & 0 & 0 & s_{\mathbf{k}} \\ 0 & 0 & -s^*_{-\mathbf{k}} & 0 \\ 0 & -s_{-\mathbf{k}} & 0 & 0 \\ s^*_{\mathbf{k}} & 0 & 0 & 0 \end{pmatrix} \begin{pmatrix} \mathbf{c}_{A,\mathbf{k}\uparrow} \\ \mathbf{c}_{A,\mathbf{k}\downarrow} \\ \mathbf{c}_{B,\mathbf{k}\uparrow} \\ \mathbf{c}_{B,\mathbf{k}\downarrow} \end{pmatrix}. \tag{6.15}$$

The spin-orbit coupling function is

$$s_{\mathbf{k}} = \lambda_R \sum_{j=1}^{3} e^{-i\theta_j} e^{i\mathbf{k}\cdot\mathbf{b}_j}, \tag{6.16}$$

with θ_j the polar angle of nearest neighbour vector $\mathbf{b}_j$. The previously derived hopping terms are independent of spin, i.e. they conserve spin, such that with nearest neighbour hopping and Rashba spin-orbit coupling, the full equation reads

$$\mathcal{H} = \sum_{\mathbf{k}} \psi^\dagger_{\mathbf{k}} \begin{pmatrix} 0 & 0 & t_{\mathbf{k}} & s_{\mathbf{k}} \\ 0 & 0 & -s^*_{-\mathbf{k}} & t_{\mathbf{k}} \\ t^*_{\mathbf{k}} & -s_{-\mathbf{k}} & 0 & 0 \\ s^*_{\mathbf{k}} & t^*_{\mathbf{k}} & 0 & 0 \end{pmatrix} \psi_{\mathbf{k}}, \tag{6.17}$$

with $\psi^\dagger_{\mathbf{k}} = \begin{pmatrix} \mathbf{c}^\dagger_{A,\mathbf{k}\uparrow} & \mathbf{c}^\dagger_{A,\mathbf{k}\downarrow} & \mathbf{c}^\dagger_{B,\mathbf{k}\uparrow} & \mathbf{c}^\dagger_{B,\mathbf{k}\downarrow} \end{pmatrix}$. This Hamiltonian equation is general for bipartite lattices if we define

$$t_{\mathbf{k}} = -t_{NN} \sum_j e^{i\mathbf{k}\cdot\mathbf{b}_j} \tag{6.18}$$

$$s_{\mathbf{k}} = \lambda_R \sum_j e^{-i\theta_j} e^{i\mathbf{k}\cdot\mathbf{b}_j}. \tag{6.19}$$

Diagonalizing this problem yields the eigenvalues[a]

$$\epsilon_{1,2,3,4} = \frac{n}{\sqrt{2}} \sqrt{|s_{\mathbf{k}}|^2 + |s_{-\mathbf{k}}|^2 + 2|t_{\mathbf{k}}|^2 + m\chi} \tag{6.20}$$

with $n = \pm 1$ and $m = \pm 1$ and

$$\chi = \sqrt{(|s_{\mathbf{k}}|^2 - |s_{-\mathbf{k}}|^2)^2 + 4(t_{\mathbf{k}} s^*_{\mathbf{k}} - t^*_{\mathbf{k}} s^*_{-\mathbf{k}})(t^*_{\mathbf{k}} s_{\mathbf{k}} - t_{\mathbf{k}} s_{-\mathbf{k}})}. \tag{6.21}$$

[a] The diagonalization was done in *Wolfram Mathematica*. The dispersion is in accordance with [62].

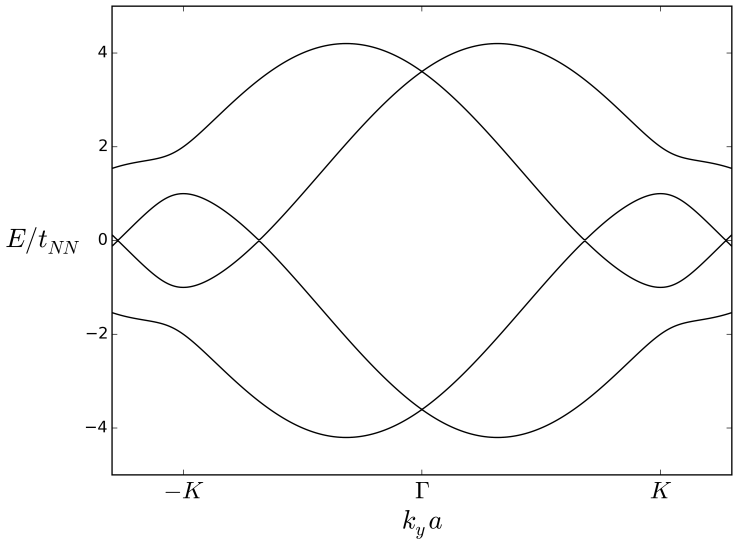

FIGURE 6.3: The energy dispersion with nearest neighbour hopping and spin-orbit coupling ($\lambda_R/t_{NN} = 1$) for the honeycomb lattice along the k_y-axis. Because of the sublattice structure we now get four energybands, and a doubling in Dirac cones.

We note in passing that $\chi(-\mathbf{k}) = \chi(\mathbf{k})$. The energy-dispersion with spin-orbit coupling is shown in figure 6.3, for the value $\lambda_R/t_{NN} = 1$. The spin-orbit coupling lifts the degeneracy, and causes a doubling in the number of Dirac cones, shifted away from the K-points. The transformation from the helicity band basis in which the one-particle Hamiltonian is diagonal looks like

$$\begin{pmatrix} \mathbf{c}_{A,\mathbf{k},\uparrow} \\ \mathbf{c}_{A,\mathbf{k},\downarrow} \\ \mathbf{c}_{B,\mathbf{k},\uparrow} \\ \mathbf{c}_{B,\mathbf{k},\downarrow} \end{pmatrix} = \begin{pmatrix} \eta_{\mathbf{k},+} & \zeta_{\mathbf{k},-} & \xi_{\mathbf{k}} & \rho_{\mathbf{k},+} \\ -\eta_{\mathbf{k},+} & -\zeta_{\mathbf{k},-} & \xi_{\mathbf{k}} & \rho_{\mathbf{k},+} \\ -\eta_{\mathbf{k},-} & \zeta_{\mathbf{k},+} & -\xi_{\mathbf{k}} & -\rho_{\mathbf{k},-} \\ \eta_{\mathbf{k},-} & -\zeta_{\mathbf{k},+} & -\xi_{\mathbf{k}} & -\rho_{\mathbf{k},-} \end{pmatrix} . \begin{pmatrix} \mathbf{a}_{\mathbf{k},1} \\ \mathbf{a}_{\mathbf{k},2} \\ \mathbf{a}_{\mathbf{k},3} \\ \mathbf{a}_{\mathbf{k},4} \end{pmatrix}, \tag{6.22}$$

with

$$\eta_{\mathbf{k},\alpha} = \frac{-2s^*_{-\mathbf{k}} t^{*2}_{\mathbf{k}} - s^*_{\mathbf{k}}(|s_{-\mathbf{k}}|^2 - |s_{\mathbf{k}}|^2 - 2|t_{\mathbf{k}}|^2 + \alpha\chi)}{2\sqrt{2}\chi\sqrt{|s_{\mathbf{k}}|^2 + |s_{-\mathbf{k}}|^2 + 2|t_{\mathbf{k}}|^2 - \alpha\chi}} \tag{6.23}$$

$$\zeta_{\mathbf{k},\alpha} = \frac{-2s_{-\mathbf{k}} s^*_{\mathbf{k}} t_{\mathbf{k}} + t^*_{\mathbf{k}}(|s_{\mathbf{k}}|^2 + |s_{-\mathbf{k}}|^2 + \alpha\chi)}{2\sqrt{2}\chi\sqrt{|s_{\mathbf{k}}|^2 + |s_{-\mathbf{k}}|^2 + 2|t_{\mathbf{k}}|^2 - \alpha\chi}} \tag{6.24}$$

$$\xi_{\mathbf{k}} = \frac{-t_{\mathbf{k}} s^*_{\mathbf{k}} + t^*_{\mathbf{k}} s^*_{-\mathbf{k}}}{2\chi} \tag{6.25}$$

$$\rho_{\mathbf{k},\alpha} = \frac{|s_{-\mathbf{k}}|^2 - |s_{\mathbf{k}}|^2 + \alpha\chi}{4\chi}. \tag{6.26}$$

In other words, the interaction Hamiltonian will consist of products of all four bands. The inverse transformation is

$$\begin{pmatrix} \mathbf{a}_{\mathbf{k},1} \\ \mathbf{a}_{\mathbf{k},2} \\ \mathbf{a}_{\mathbf{k},3} \\ \mathbf{a}_{\mathbf{k},4} \end{pmatrix} = \begin{pmatrix} \rho_{\mathbf{k},+}/\eta_{\mathbf{k},+} & -\rho_{\mathbf{k},+}/\eta_{\mathbf{k},+} & \rho_{\mathbf{k},-}/\eta_{\mathbf{k},-} & -\rho_{\mathbf{k},-}/\eta_{\mathbf{k},-} \\ \xi_{\mathbf{k}}/\eta_{\mathbf{k},+} & -\xi_{\mathbf{k}}/\eta_{\mathbf{k},+} & \xi_{\mathbf{k}}/\eta_{\mathbf{k},-} & -\xi_{\mathbf{k}}/\eta_{\mathbf{k},-} \\ \zeta_{\mathbf{k},-}/\eta_{\mathbf{k},+} & \zeta_{\mathbf{k},-}/\eta_{\mathbf{k},+} & \zeta_{\mathbf{k},+}/\eta_{\mathbf{k},-} & \zeta_{\mathbf{k},+}/\eta_{\mathbf{k},-} \\ 1 & 1 & 1 & 1 \end{pmatrix} \cdot \begin{pmatrix} \mathbf{c}_{A,\mathbf{k},\uparrow} \\ \mathbf{c}_{A,\mathbf{k},\downarrow} \\ \mathbf{c}_{B,\mathbf{k},\uparrow} \\ \mathbf{c}_{B,\mathbf{k},\downarrow} \end{pmatrix}. \tag{6.27}$$

6.2 Interaction Hamiltonian

The general on-site two-particle interaction term on the bipartite lattice reads

$$\mathcal{H}_I = \sum_{\mathbf{k},\mathbf{k}'\mathbf{q}} V_{\mathbf{k},\mathbf{k}',\mathbf{q}} \mathbf{c}^\dagger_{\mathbf{k},\uparrow} \mathbf{c}^\dagger_{-\mathbf{k}+\mathbf{q},\downarrow} \mathbf{c}_{-\mathbf{k}'+\mathbf{q},\downarrow} \mathbf{c}_{\mathbf{k}',\uparrow}, \tag{6.28}$$

for any of the two sublattices. Carrying out the transformation to the diagonal helicity band basis will, in line with the derivation for the single lattice (5.17), generally give

$$\mathcal{H}_I = \sum_{\mathbf{k},\mathbf{k}'\mathbf{q}} \sum_{\alpha\beta\beta'\alpha'} V^{\alpha\beta\beta'\alpha'}_{\mathbf{k},\mathbf{k}',\mathbf{q}} \mathbf{a}^\dagger_{\mathbf{k},\alpha} \mathbf{a}^\dagger_{-\mathbf{k}+\mathbf{q},\beta} \mathbf{a}_{-\mathbf{k}'+\mathbf{q},\beta'} \mathbf{a}_{\mathbf{k}',\alpha'}, \tag{6.29}$$

where $V^{\alpha\beta\beta'\alpha'}_{\mathbf{k},\mathbf{k}',\mathbf{q}}$ is a tensor giving the coefficient to any given combination of the four helicity-band operators as a function of the phases in the transformation from the spin basis to the band basis and the pairing mechanism in the spin basis $V_{\mathbf{k},\mathbf{k}',\mathbf{q}}$, i.e.

$$V^{\alpha\beta\beta'\alpha'}_{\mathbf{k},\mathbf{k}',\mathbf{q}} = V_{\mathbf{k},\mathbf{k}',\mathbf{q}} \mathcal{G}^{\alpha\beta\beta'\alpha'}_{\mathbf{k},\mathbf{k}',\mathbf{q}}, \tag{6.30}$$

with $\mathcal{G}^{\alpha\beta\beta'\alpha'}_{\mathbf{k},\mathbf{k}',\mathbf{q}}$ a product of the phases in the transformation (6.22). (6.29) contain all possible pairing mechanisms in the band basis. The elements in $\mathcal{G}^{\alpha\beta\beta'\alpha'}_{\mathbf{k},\mathbf{k}',\mathbf{q}}$ is dependent on the sublattice nature of the interaction, for instance if only same-lattice interactions contribute

$$\mathbf{c}^\dagger_{A,\mathbf{k},\uparrow} \mathbf{c}^\dagger_{A,-\mathbf{k}+\mathbf{q},\downarrow} \mathbf{c}_{A,-\mathbf{k}'+\mathbf{q},\downarrow} \mathbf{c}_{A,\mathbf{k}',\uparrow} \tag{6.31}$$

or if interlattice interactions are also considered, e.g.

$$\mathbf{c}^\dagger_{A,\mathbf{k},\uparrow} \mathbf{c}^\dagger_{A,-\mathbf{k}+\mathbf{q},\downarrow} \mathbf{c}_{B,-\mathbf{k}'+\mathbf{q},\downarrow} \mathbf{c}_{B,\mathbf{k}',\uparrow}. \tag{6.32}$$

Regardless of the choice, because we have four bands, $\mathcal{G}^{\alpha\beta\beta'\alpha'}_{\mathbf{k},\mathbf{k}',\mathbf{q}}$ will have $4\times4\times4\times4 = 256$ terms that will not be given here. Keep in mind however that phases in $\mathcal{G}^{\alpha\beta\beta'\alpha'}_{\mathbf{k},\mathbf{k}',\mathbf{q}}$ may cancel later transformations back to the spin basis.

6.2.1 Intraband q=0

With intraband $\mathbf{q} = 0$ terms only, the interaction term is

$$\mathcal{H}_I = \sum_{\mathbf{k},\mathbf{k}'} \sum_{\alpha} V^{\alpha}_{\mathbf{k},\mathbf{k}'} \mathbf{a}^{\dagger}_{\mathbf{k},\alpha} \mathbf{a}^{\dagger}_{-\mathbf{k},\alpha} \mathbf{a}_{-\mathbf{k}',\alpha} \mathbf{a}_{\mathbf{k}',\alpha}. \tag{6.33}$$

In the mean field approach this reduces to

$$\mathcal{H}_I = \sum_{\mathbf{k},\mathbf{k}'} \sum_{\alpha} V^{\alpha}_{\mathbf{k},\mathbf{k}'} \Big(b^{\dagger}_{\alpha}(\mathbf{k}) \mathbf{a}_{-\mathbf{k}',\alpha} \mathbf{a}_{\mathbf{k}',\alpha} + b_{\alpha}(\mathbf{k}') \mathbf{a}^{\dagger}_{\mathbf{k},\alpha} \mathbf{a}^{\dagger}_{-\mathbf{k},\alpha} - b^{\dagger}_{\alpha}(\mathbf{k}) b_{\alpha}(\mathbf{k}') \Big), \tag{6.34}$$

with

$$b_{\alpha}(\mathbf{k}) = \langle \mathbf{a}_{\mathbf{k},\alpha} \mathbf{a}_{-\mathbf{k},\alpha} \rangle. \tag{6.35}$$

Going through the standard steps in the BCS-approach, and diagonalizing results in

$$E_{\mathbf{k},\alpha} = \sqrt{(\epsilon_{\mathbf{k},\alpha} - \mu)^2 + |\Delta_{\alpha}(\mathbf{k})|^2} \tag{6.36}$$

$$\Delta_{\alpha}(\mathbf{k}) = -\sum_{\mathbf{k}'} V^{\alpha}_{\mathbf{k},\mathbf{k}'} \Delta_{\alpha}(\mathbf{k}') \frac{\tanh(\beta E_{\mathbf{k}',\alpha}/2)}{2E_{\mathbf{k}',\alpha}} \tag{6.37}$$

$$\mathcal{H}_I = -\sum_{\mathbf{k},\mathbf{k}'} \sum_{\alpha} \Big(\Delta^{\dagger}_{\alpha}(\mathbf{k}) \mathbf{a}_{-\mathbf{k},\alpha} \mathbf{a}_{\mathbf{k},\alpha} + \Delta_{\alpha}(\mathbf{k}) \mathbf{a}^{\dagger}_{\mathbf{k},\alpha} \mathbf{a}^{\dagger}_{-\mathbf{k},\alpha} - \Delta^{\dagger}_{\alpha}(\mathbf{k}) b_{\alpha}(\mathbf{k}') \Big). \tag{6.38}$$

We would now like to transform back to the spin-basis to evaluate the form of the superconductivity, i.e. if it is singlet, triplet or both. Transforming the $\Delta_{\alpha}(\mathbf{k})$-terms back to the spin-basis using (6.22) yields

$$\begin{aligned}
\mathcal{H}_I = \sum_{\mathbf{k},\alpha} \Big\{ & \Delta_{\alpha}(\mathbf{k}) (\phi^{\alpha,*}_{A,\mathbf{k},\uparrow} \mathbf{c}^{\dagger}_{A,\mathbf{k},\uparrow} + \phi^{\alpha,*}_{A,\mathbf{k},\downarrow} \mathbf{c}^{\dagger}_{A,\mathbf{k},\downarrow} + \phi^{\alpha,*}_{B,\mathbf{k},\uparrow} \mathbf{c}^{\dagger}_{B,\mathbf{k},\uparrow} + \phi^{\alpha,*}_{B,\mathbf{k},\downarrow} \mathbf{c}^{\dagger}_{B,\mathbf{k},\downarrow}) \\
& \cdot (\phi^{\alpha,*}_{A,-\mathbf{k},\uparrow} \mathbf{c}^{\dagger}_{A,-\mathbf{k},\uparrow} + \phi^{\alpha,*}_{A,-\mathbf{k},\downarrow} \mathbf{c}^{\dagger}_{A,-\mathbf{k},\downarrow} + \phi^{\alpha,*}_{B,-\mathbf{k},\uparrow} \mathbf{c}^{\dagger}_{B,-\mathbf{k},\uparrow} + \phi^{\alpha,*}_{B,-\mathbf{k},\downarrow} \mathbf{c}^{\dagger}_{B,-\mathbf{k},\downarrow}) \\
& + \Delta^{\dagger}_{\alpha}(\mathbf{k}) (\phi^{\alpha}_{A,-\mathbf{k},\uparrow} \mathbf{c}_{A,-\mathbf{k},\uparrow} + \phi^{\alpha}_{A,-\mathbf{k},\downarrow} \mathbf{c}_{A,-\mathbf{k},\downarrow} + \phi^{\alpha}_{B,-\mathbf{k},\uparrow} \mathbf{c}_{B,-\mathbf{k},\uparrow} + \phi^{\alpha}_{B,\mathbf{k},\downarrow} \mathbf{c}_{B,-\mathbf{k},\downarrow}) \\
& \cdot (\phi^{\alpha}_{A,\mathbf{k},\uparrow} \mathbf{c}_{A,\mathbf{k},\uparrow} + \phi^{\alpha}_{A,\mathbf{k},\downarrow} \mathbf{c}_{A,\mathbf{k},\downarrow} + \phi^{\alpha}_{B,\mathbf{k},\uparrow} \mathbf{c}_{B,\mathbf{k},\uparrow} + \phi^{\alpha}_{B,-\mathbf{k},\downarrow} \mathbf{c}_{B,\mathbf{k},\downarrow}) \Big\}.
\end{aligned} \tag{6.39}$$

The ϕ-amplitudes are here defined as the phase in the transformation (6.27) for the given operator. Summing over $\alpha = 1, 2, 3, 4$ yields

$$\begin{aligned}
\mathcal{H}_I = \sum_{\mathbf{k}} \Big\{ & \Delta_{A,A,\uparrow,\uparrow} \mathbf{c}^{\dagger}_{A,\mathbf{k},\uparrow} \mathbf{c}^{\dagger}_{A,-\mathbf{k},\uparrow} + \Delta_{A,A,\downarrow,\downarrow} \mathbf{c}^{\dagger}_{A,\mathbf{k},\downarrow} \mathbf{c}^{\dagger}_{A,-\mathbf{k},\downarrow} + \Delta_{A,A,\uparrow,\downarrow} \mathbf{c}^{\dagger}_{A,\mathbf{k},\uparrow} \mathbf{c}^{\dagger}_{A,-\mathbf{k},\downarrow} \\
& + \Delta_{A,A,\downarrow,\uparrow} \mathbf{c}^{\dagger}_{A,\mathbf{k},\downarrow} \mathbf{c}^{\dagger}_{A,-\mathbf{k},\uparrow} + \Delta_{B,B,\uparrow,\uparrow} \mathbf{c}^{\dagger}_{B,\mathbf{k},\uparrow} \mathbf{c}^{\dagger}_{B,-\mathbf{k},\uparrow} + \Delta_{B,B,\downarrow,\downarrow} \mathbf{c}^{\dagger}_{B,\mathbf{k},\downarrow} \mathbf{c}^{\dagger}_{B,-\mathbf{k},\downarrow} \\
& + \Delta_{B,B,\uparrow,\downarrow} \mathbf{c}^{\dagger}_{B,\mathbf{k},\uparrow} \mathbf{c}^{\dagger}_{B,-\mathbf{k},\downarrow} + \Delta_{B,B,\downarrow,\uparrow} \mathbf{c}^{\dagger}_{B,\mathbf{k},\downarrow} \mathbf{c}^{\dagger}_{B,-\mathbf{k},\uparrow} + \Delta_{A,B,\uparrow,\uparrow} \mathbf{c}^{\dagger}_{A,\mathbf{k},\uparrow} \mathbf{c}^{\dagger}_{B,-\mathbf{k},\uparrow} \\
& + \Delta_{A,B,\downarrow,\downarrow} \mathbf{c}^{\dagger}_{A,\mathbf{k},\downarrow} \mathbf{c}^{\dagger}_{B,-\mathbf{k},\downarrow} + \Delta_{A,B,\uparrow,\downarrow} \mathbf{c}^{\dagger}_{A,\mathbf{k},\uparrow} \mathbf{c}^{\dagger}_{B,-\mathbf{k},\downarrow} + \Delta_{A,B,\downarrow,\uparrow} \mathbf{c}^{\dagger}_{A,\mathbf{k},\downarrow} \mathbf{c}^{\dagger}_{B,-\mathbf{k},\uparrow} \\
& + \Delta_{B,A,\uparrow,\uparrow} \mathbf{c}^{\dagger}_{B,\mathbf{k},\uparrow} \mathbf{c}^{\dagger}_{A,-\mathbf{k},\uparrow} + \Delta_{B,A,\downarrow,\downarrow} \mathbf{c}^{\dagger}_{B,\mathbf{k},\downarrow} \mathbf{c}^{\dagger}_{A,-\mathbf{k},\downarrow} + \Delta_{B,A,\uparrow,\downarrow} \mathbf{c}^{\dagger}_{B,\mathbf{k},\uparrow} \mathbf{c}^{\dagger}_{A,-\mathbf{k},\downarrow} \\
& + \Delta_{B,A,\downarrow,\uparrow} \mathbf{c}^{\dagger}_{B,\mathbf{k},\downarrow} \mathbf{c}^{\dagger}_{A,-\mathbf{k},\uparrow} + H.c \Big\}.
\end{aligned} \tag{6.40}$$

The gaps in the spin-basis are

$$\begin{aligned}
\Delta_{A,A,\uparrow,\uparrow} = \Delta_{A,A,\downarrow,\downarrow} &= \Delta_1(\mathbf{k})\frac{\rho^*_{-\mathbf{k},+}\rho^*_{\mathbf{k},+}}{\eta^*_{-\mathbf{k},+}\eta^*_{\mathbf{k},+}} + \Delta_2(\mathbf{k})\frac{\xi^*_{-\mathbf{k}}\xi^*_{\mathbf{k}}}{\eta^*_{-\mathbf{k},+}\eta^*_{\mathbf{k},+}} + \Delta_3(\mathbf{k})\frac{\zeta^*_{-\mathbf{k},-}\zeta^*_{\mathbf{k},-}}{\eta^*_{-\mathbf{k},+}\eta^*_{\mathbf{k},+}} + \Delta_4(\mathbf{k}) \\
\Delta_{A,A,\uparrow,\downarrow} = \Delta_{A,A,\downarrow,\uparrow} &= -\Delta_1(\mathbf{k})\frac{\rho^*_{-\mathbf{k},+}\rho^*_{\mathbf{k},+}}{\eta^*_{-\mathbf{k},+}\eta^*_{\mathbf{k},+}} - \Delta_2(\mathbf{k})\frac{\xi^*_{-\mathbf{k}}\xi^*_{\mathbf{k}}}{\eta^*_{-\mathbf{k},+}\eta^*_{\mathbf{k},+}} + \Delta_3(\mathbf{k})\frac{\zeta^*_{-\mathbf{k},-}\zeta^*_{\mathbf{k},-}}{\eta^*_{-\mathbf{k},+}\eta^*_{\mathbf{k},+}} + \Delta_4(\mathbf{k}) \\
\Delta_{B,B,\uparrow,\uparrow} = \Delta_{B,B,\downarrow,\downarrow} &= \Delta_1(\mathbf{k})\frac{\rho^*_{-\mathbf{k},-}\rho^*_{\mathbf{k},-}}{\eta^*_{-\mathbf{k},-}\eta^*_{\mathbf{k},-}} + \Delta_2(\mathbf{k})\frac{\xi^*_{-\mathbf{k}}\xi^*_{\mathbf{k}}}{\eta^*_{-\mathbf{k},-}\eta^*_{\mathbf{k},-}} + \Delta_3(\mathbf{k})\frac{\zeta^*_{-\mathbf{k},+}\zeta^*_{\mathbf{k},+}}{\eta^*_{-\mathbf{k},-}\eta^*_{\mathbf{k},-}} + \Delta_4(\mathbf{k}) \\
\Delta_{B,B,\uparrow,\downarrow} = \Delta_{B,B,\downarrow,\uparrow} &= -\Delta_1(\mathbf{k})\frac{\rho^*_{-\mathbf{k},-}\rho^*_{\mathbf{k},-}}{\eta^*_{-\mathbf{k},-}\eta^*_{\mathbf{k},-}} - \Delta_2(\mathbf{k})\frac{\xi^*_{-\mathbf{k}}\xi^*_{\mathbf{k}}}{\eta^*_{-\mathbf{k},-}\eta^*_{\mathbf{k},-}} + \Delta_3(\mathbf{k})\frac{\zeta^*_{-\mathbf{k},+}\zeta^*_{\mathbf{k},+}}{\eta^*_{-\mathbf{k},-}\eta^*_{\mathbf{k},-}} + \Delta_4(\mathbf{k}) \\
\Delta_{A,B,\uparrow,\uparrow} = \Delta_{A,B,\downarrow,\downarrow} &= \Delta_1(\mathbf{k})\frac{\rho^*_{-\mathbf{k},+}\rho^*_{\mathbf{k},-}}{\eta^*_{-\mathbf{k},+}\eta^*_{\mathbf{k},-}} + \Delta_2(\mathbf{k})\frac{\xi^*_{-\mathbf{k}}\xi^*_{\mathbf{k}}}{\eta^*_{-\mathbf{k},+}\eta^*_{\mathbf{k},-}} + \Delta_3(\mathbf{k})\frac{\zeta^*_{-\mathbf{k},-}\zeta^*_{\mathbf{k},+}}{\eta^*_{-\mathbf{k},+}\eta^*_{\mathbf{k},-}} + \Delta_4(\mathbf{k}) \\
\Delta_{A,B,\uparrow,\downarrow} = \Delta_{A,B,\downarrow,\uparrow} &= -\Delta_1(\mathbf{k})\frac{\rho^*_{-\mathbf{k},+}\rho^*_{\mathbf{k},-}}{\eta^*_{-\mathbf{k},+}\eta^*_{\mathbf{k},-}} - \Delta_2(\mathbf{k})\frac{\xi^*_{-\mathbf{k}}\xi^*_{\mathbf{k}}}{\eta^*_{-\mathbf{k},+}\eta^*_{\mathbf{k},-}} + \Delta_3(\mathbf{k})\frac{\zeta^*_{-\mathbf{k},-}\zeta^*_{\mathbf{k},+}}{\eta^*_{-\mathbf{k},+}\eta^*_{\mathbf{k},-}} + \Delta_4(\mathbf{k}) \\
\Delta_{B,A,\uparrow,\uparrow} = \Delta_{B,A,\downarrow,\downarrow} &= \Delta_1(\mathbf{k})\frac{\rho^*_{-\mathbf{k},-}\rho^*_{\mathbf{k},+}}{\eta^*_{-\mathbf{k},-}\eta^*_{\mathbf{k},+}} + \Delta_2(\mathbf{k})\frac{\xi^*_{-\mathbf{k}}\xi^*_{\mathbf{k}}}{\eta^*_{-\mathbf{k},-}\eta^*_{\mathbf{k},+}} + \Delta_3(\mathbf{k})\frac{\zeta^*_{-\mathbf{k},+}\zeta^*_{\mathbf{k},-}}{\eta^*_{-\mathbf{k},-}\eta^*_{\mathbf{k},+}} + \Delta_4(\mathbf{k}) \\
\Delta_{B,A,\uparrow,\downarrow} = \Delta_{B,A,\downarrow,\uparrow} &= -\Delta_1(\mathbf{k})\frac{\rho^*_{-\mathbf{k},-}\rho^*_{\mathbf{k},+}}{\eta^*_{-\mathbf{k},-}\eta^*_{\mathbf{k},+}} - \Delta_2(\mathbf{k})\frac{\xi^*_{-\mathbf{k}}\xi^*_{\mathbf{k}}}{\eta^*_{-\mathbf{k},-}\eta^*_{\mathbf{k},+}} + \Delta_3(\mathbf{k})\frac{\zeta^*_{-\mathbf{k},+}\zeta^*_{\mathbf{k},-}}{\eta^*_{-\mathbf{k},-}\eta^*_{\mathbf{k},+}} + \Delta_4(\mathbf{k}).
\end{aligned} \tag{6.41}$$

$\Delta_{i,j,\sigma,\sigma'} = \Delta_{i,j,\sigma',\sigma}$ for all sublattice combinations indicate a triplet nature, and both the mixed and the aligned states are present. From the inverse transformation (6.27) it is seen that mixing of bands 1,2 and 3,4 is needed for a singlet character, i.e. interband pairing. The phases in $\Delta_{i,j,\sigma,\sigma'}$ might cancel against phases in $\Delta_\alpha(\mathbf{k})$ stemming from $\mathcal{G}^{\alpha\beta\beta'\alpha'}_{\mathbf{k},\mathbf{k}',\mathbf{q}}$ in (6.30). Assuming an even $\mathbf{k}$-dependence of the $\Delta_\alpha(\mathbf{k})$, the following properties are noticed for the mixed sublattice combinations by looking at (6.23)-(6.26),

$$\Delta_{A,B,\uparrow,\uparrow}(\mathbf{k}) = \Delta_{A,B,\downarrow,\downarrow}(\mathbf{k}) = \Delta_{B,A,\uparrow,\uparrow}(-\mathbf{k}) = \Delta_{B,A,\downarrow,\downarrow}(-\mathbf{k}) \tag{6.42}$$

$$\Delta_{A,B,\uparrow,\downarrow}(\mathbf{k}) = \Delta_{A,B,\downarrow,\uparrow}(\mathbf{k}) = \Delta_{B,A,\uparrow,\downarrow}(-\mathbf{k}) = \Delta_{B,A,\downarrow,\uparrow}(-\mathbf{k}). \tag{6.43}$$

This is reminiscent of a singlet character between mixed sublattice operators. If the $\mathbf{k}$-dependence of the $\Delta_\alpha(\mathbf{k})$ is odd, a triplet character between mixed sublattice operators is present

$$\Delta_{A,B,\uparrow,\uparrow}(\mathbf{k}) = \Delta_{A,B,\downarrow,\downarrow}(\mathbf{k}) = -\Delta_{B,A,\uparrow,\uparrow}(-\mathbf{k}) = -\Delta_{B,A,\downarrow,\downarrow}(-\mathbf{k}) \tag{6.44}$$

$$\Delta_{A,B,\uparrow,\downarrow}(\mathbf{k}) = \Delta_{A,B,\downarrow,\uparrow}(\mathbf{k}) = -\Delta_{B,A,\uparrow,\downarrow}(-\mathbf{k}) = -\Delta_{B,A,\downarrow,\uparrow}(-\mathbf{k}). \tag{6.45}$$

6.2.2 Interband $\mathbf{q} = 0$

Once again, the pairing where the initial and final pairs are in different bands could be considered. Instead of going through the rather tedious exercise of writing out

phases and gap equations, we can draw on the results in the case of Bravais lattices and the structure of the transformation (6.27). First of all, the superconducting interaction Hamiltonian will be

$$\mathcal{H}_{SC}^{\text{interband}} = \sum_{\mathbf{k}} \sum_{\alpha} \left(\Delta_{\alpha}^{\dagger}(\mathbf{k}) \mathbf{a}_{-\mathbf{k},\alpha} \mathbf{a}_{\mathbf{k},\alpha} + \Delta_{\alpha}(\mathbf{k}) \mathbf{a}_{\mathbf{k},\alpha}^{\dagger} \mathbf{a}_{-\mathbf{k},\alpha}^{\dagger} - \Delta_{\alpha}^{\dagger} b_{\alpha}(\mathbf{k}) \right), \tag{6.46}$$

with $b_{\alpha}(\mathbf{k}) = \langle \mathbf{a}_{\mathbf{k},\alpha} \mathbf{a}_{-\mathbf{k},\alpha} \rangle$, and the coupled gap equations

$$\Delta_{\alpha}(\mathbf{k}) = \sum_{\mathbf{k}'} \sum_{\beta \neq \alpha} V_{\mathbf{k},\mathbf{k}'} \mathcal{G}_{\mathbf{k},\mathbf{k}'}^{\alpha\alpha\beta\beta} \Delta_{\beta}(\mathbf{k}') \chi(E_{\mathbf{k}',\beta}), \tag{6.47}$$

with the energy dispersion

$$E_{\mathbf{k},\alpha}^{\pm} = \pm \sqrt{(\epsilon_{\mathbf{k},\alpha} - \mu)^2 + |\Delta_{\alpha}(\mathbf{k})|^2}. \tag{6.48}$$

The spin structure of all this will be the exact same as in the intraband case, only with these new coupled $\Delta_{\alpha}(\mathbf{k})$ replacing the ones in (6.41). The exact band-dependence of $\mathcal{G}_{\mathbf{k},\mathbf{k}'}^{\alpha\alpha\beta\beta}$ will determine if there is any cancellation of phase functions.

6.2.3 Chiral p-wave pairing

The Bravais lattice model allowed writing the chiral p-wave pairing by the spin-orbit coupling function $s_{\mathbf{k}}$ in a straight-forward fashion. This is not the case in the bipartite lattice, due to the non-trivial dependency of the one-particle dispersion (6.20) on the hopping and spin-orbit coupling function. No easy-to-find combination of the spin-orbit coupling functions behave as chiral p-wave around the momenta where the one-particle dispersion is equal to zero. Therefore, the choice rather falls on expanding the gap function in the basis functions of the irreducible representations of the symmetry group[54]

$$\Delta(\mathbf{k}) = \sum_{\lambda=1}^{d_i} \eta_{\lambda} \xi_{\lambda}^{i}(\mathbf{k}). \tag{6.49}$$

The gap function may always be put together to have a chiral p-wave form, by adjusting the complex coefficients η_{λ} to suit the basis functions $\xi_{\lambda}^{i}(\mathbf{k})$. Basis functions for common lattice symmetry groups can be found in the literature[63]. The structure of the gaps in the spin basis have the form

$$\Delta_{i,j,\sigma,\sigma'}(\mathbf{k}) = \sum_{\alpha} \Delta_{\alpha}(\mathbf{k}) \phi_{i,j,\sigma,\sigma'}^{\alpha}(\mathbf{k}), \tag{6.50}$$

With the ϕ-amplitudes given by the inverse transformation. Assuming that $\Delta_{\alpha}(\mathbf{k})$ (6.47) can be expanded as to have a chiral p-wave form close to momenta where the one-particle dispersion is zero, the gap function may be written

$$\Delta_{\alpha}(\mathbf{k}) = \Delta_{\alpha}^{0} g_{\mathbf{k}}. \tag{6.51}$$

$g_{\mathbf{k}}$ will now be a product of $\mathbf{k}$-dependent functions arising from $\mathcal{G}^{\alpha\alpha\beta\beta}_{\mathbf{k},\mathbf{k}'}$ and $V_{\mathbf{k},\mathbf{k}'}$, which together forms a function that behaves as chiral p-wave around zeroes in $\epsilon_{\mathbf{k},\alpha}$. From (6.50) it is clear that the spin structure of the gaps need not exhibit the chiral p-wave behaviour, because of the $\mathbf{k}$-dependency of the ϕ-amplitudes. As such, the same conclusion can be drawn as for the Bravais lattice case. The spin-momentum locking caused på spin-orbit coupling forces the two-particle interactions to be defined in the diagonalized band basis, and the structure in the spin-basis will be different.

6.3 Symmetry and Topology

Let us analyze the symmetries of the one-particle bipartite Hamiltonian. It is known that the system with hopping only has both parity and time-reversal symmetry, particularly in the honeycomb case[21]. Let us check the effect of spin-orbit coupling. The parity operator is[45]

$$\hat{P} = \sigma_x \otimes \mathbb{I}_{2x2} = \begin{pmatrix} 0 & 0 & 1 & 0 \\ 0 & 0 & 0 & 1 \\ 1 & 0 & 0 & 0 \\ 0 & 1 & 0 & 0 \end{pmatrix}. \tag{6.52}$$

Inversion symmetry demands $\hat{P}\underline{\underline{\mathcal{H}_0}}(\mathbf{k})\hat{P}^{-1} = \underline{\underline{\mathcal{H}_0}}(-\mathbf{k})$. The notation $\underline{\underline{A}}$ denotes a 4x4 matrix. With $\underline{\underline{\mathcal{H}_0}}(\mathbf{k})$ from (6.17) the result is

$$\hat{P}\underline{\underline{\mathcal{H}_0}}(\mathbf{k})\hat{P}^{-1} = \begin{pmatrix} 0 & 0 & t^*_{\mathbf{k}} & -s_{-\mathbf{k}} \\ 0 & 0 & s^*_{\mathbf{k}} & t^*_{\mathbf{k}} \\ t_{\mathbf{k}} & s_{\mathbf{k}} & 0 & 0 \\ -s^*_{-\mathbf{k}} & t_{\mathbf{k}} & 0 & 0 \end{pmatrix}. \tag{6.53}$$

Since $t_{-\mathbf{k}} = t^*_{\mathbf{k}}$, inversion symmetry is present if $s_{\mathbf{k}} = 0$, i.e. spin-orbit coupling breaks inversion symmetry. Let us next check time-reversal symmetry with spin-orbit coupling. The time-reversal operators is

$$\hat{T} = i(\mathbb{I}_{2x2} \otimes \sigma_y)\hat{K} = \begin{pmatrix} 0 & 1 & 0 & 0 \\ -1 & 0 & 0 & 0 \\ 0 & 0 & 0 & 1 \\ 0 & 0 & -1 & 0 \end{pmatrix}\hat{K}, \tag{6.54}$$

where complex conjugation, $\hat{K}$, demands $\hat{T}\underline{\underline{\mathcal{H}_0}}(\mathbf{k})\hat{T}^{-1} = \underline{\mathcal{H}_0}(-\mathbf{k})^*$. Applying this relation to the one-particle Hamiltonian yields

$$\begin{aligned} \hat{T}\underline{\underline{\mathcal{H}_0}}(\mathbf{k})\hat{T}^{-1} &= \begin{pmatrix} 0 & 0 & t_{\mathbf{k}} & s^*_{-\mathbf{k}} \\ 0 & 0 & -s_{\mathbf{k}} & t_{\mathbf{k}} \\ t^*_{\mathbf{k}} & -s^*_{\mathbf{k}} & 0 & 0 \\ s_{-\mathbf{k}} & t^*_{\mathbf{k}} & 0 & 0 \end{pmatrix} \\ &= \underline{\underline{\mathcal{H}_0}}(-\mathbf{k})^*. \end{aligned} \tag{6.55}$$

As such, time-reversal is preserved with the addition of spin-orbit coupling. With no particle-hole symmetry in the one-particle Hamiltonian, and $\hat{T}^2 = -1$ we are in AZ class AII, characterized by a $\mathbb{Z}_2$ topological invariant. Let us next look at the full superconducting Hamiltonian for the bipartite lattice

$$\mathcal{H}(\mathbf{k}) = \begin{pmatrix} 0 & 0 & t_{\mathbf{k}} & s_{\mathbf{k}} & \Delta_{A,A,\uparrow,\uparrow} & \Delta_{A,A,\uparrow,\downarrow} & \Delta_{A,B,\uparrow,\uparrow} & \Delta_{A,B,\uparrow,\downarrow} \\ 0 & 0 & -s^*_{-\mathbf{k}} & t_{\mathbf{k}} & \Delta_{A,A,\downarrow,\uparrow} & \Delta_{A,A,\downarrow,\downarrow} & \Delta_{A,B,\downarrow,\uparrow} & \Delta_{A,B,\downarrow,\downarrow} \\ t^*_{\mathbf{k}} & -s_{-\mathbf{k}} & 0 & 0 & \Delta_{B,A,\uparrow,\uparrow} & \Delta_{B,A,\uparrow,\downarrow} & \Delta_{B,B,\uparrow,\uparrow} & \Delta_{B,B,\uparrow,\downarrow} \\ s^*_{\mathbf{k}} & t^*_{\mathbf{k}} & 0 & 0 & \Delta_{B,A,\downarrow,\uparrow} & \Delta_{B,A,\downarrow,\downarrow} & \Delta_{B,B,\downarrow,\uparrow} & \Delta_{B,B,\downarrow,\downarrow} \\ \Delta^\dagger_{A,A,\uparrow,\uparrow} & \Delta^\dagger_{A,A,\uparrow,\downarrow} & \Delta^\dagger_{A,B,\uparrow,\uparrow} & \Delta^\dagger_{A,B,\uparrow,\downarrow} & 0 & 0 & -t_{\mathbf{k}} & -s^*_{-\mathbf{k}} \\ \Delta^\dagger_{A,A,\downarrow,\uparrow} & \Delta^\dagger_{A,A,\downarrow,\downarrow} & \Delta^\dagger_{A,B,\downarrow,\uparrow} & \Delta^\dagger_{A,B,\downarrow,\downarrow} & 0 & 0 & s_{\mathbf{k}} & -t_{\mathbf{k}} \\ \Delta^\dagger_{B,A,\uparrow,\uparrow} & \Delta^\dagger_{B,A,\uparrow,\downarrow} & \Delta^\dagger_{B,B,\uparrow,\uparrow} & \Delta^\dagger_{B,B,\uparrow,\downarrow} & -t^*_{\mathbf{k}} & s^*_{\mathbf{k}} & 0 & 0 \\ \Delta^\dagger_{B,A,\downarrow,\uparrow} & \Delta^\dagger_{B,A,\downarrow,\downarrow} & \Delta^\dagger_{B,B,\downarrow,\uparrow} & \Delta^\dagger_{B,B,\downarrow,\downarrow} & -s_{-\mathbf{k}} & -t^*_{\mathbf{k}} & 0 & 0 \end{pmatrix}, \tag{6.56}$$

The Nambu spinor is now $\psi^\dagger_{\mathbf{k}} = \left(\mathbf{c}^\dagger_{A,\mathbf{k},\uparrow}\ \mathbf{c}^\dagger_{A,\mathbf{k},\downarrow}\ \mathbf{c}^\dagger_{B,\mathbf{k},\uparrow}\ \mathbf{c}^\dagger_{B,\mathbf{k},\downarrow}\ \mathbf{c}_{A,-\mathbf{k},\uparrow}\ \mathbf{c}_{A,-\mathbf{k},\downarrow}\ \mathbf{c}_{B,-\mathbf{k},\uparrow}\ \mathbf{c}_{B,-\mathbf{k},\downarrow}\right)$. This can be compactified to

$$\mathcal{H}(\mathbf{k}) = \begin{pmatrix} \underline{\underline{\mathcal{H}_0}}(\mathbf{k}) & \underline{\underline{\Delta}}(\mathbf{k}) \\ \underline{\underline{\Delta}}^*(-\mathbf{k}) & -\underline{\underline{\mathcal{H}_0}}^*(-\mathbf{k}) \end{pmatrix}. \tag{6.57}$$

Analogous to the 4x4 Bravais lattice case, we take the time-reversal and particle-hole symmetry operators to be

$$\hat{T} = i(\mathcal{I}_{4x4} \otimes \sigma_y)\hat{K} \tag{6.58}$$

$$\hat{\Theta} = (\sigma_x \otimes \mathcal{I}_{4x4})\hat{K}. \tag{6.59}$$

This form on the operators ensures time-reversal and particle-hole symmetry of the one-particle part of the full Hamiltonian, $\underline{\underline{\mathcal{H}_0}}(\mathbf{k})$. Applying the time-reversal symmetry operator on (6.56) results in

$$\hat{T}\mathcal{H}(\mathbf{k})\hat{T}^{-1} = \begin{pmatrix} 0 & 0 & t_{\mathbf{k}} & s^*_{-\mathbf{k}} & \Delta_{A,A,\downarrow,\downarrow} & -\Delta_{A,A,\downarrow,\uparrow} & \Delta_{A,B,\downarrow,\downarrow} & -\Delta_{A,B,\downarrow,\uparrow} \\ 0 & 0 & -s_{\mathbf{k}} & t_{\mathbf{k}} & -\Delta_{A,A,\uparrow,\downarrow} & \Delta_{A,A,\uparrow,\uparrow} & -\Delta_{A,B,\uparrow,\downarrow} & \Delta_{A,B,\uparrow,\uparrow} \\ t^*_{\mathbf{k}} & -s^*_{\mathbf{k}} & 0 & 0 & \Delta_{B,A,\downarrow,\downarrow} & -\Delta_{B,A,\downarrow,\uparrow} & \Delta_{B,B,\downarrow,\downarrow} & -\Delta_{B,B,\downarrow,\uparrow} \\ s_{-\mathbf{k}} & t^*_{\mathbf{k}} & 0 & 0 & -\Delta_{B,A,\uparrow,\downarrow} & \Delta_{B,A,\uparrow,\uparrow} & -\Delta_{B,B,\uparrow,\downarrow} & \Delta_{B,B,\uparrow,\uparrow} \\ \Delta^\dagger_{A,A,\downarrow,\downarrow} & -\Delta^\dagger_{A,A,\downarrow,\uparrow} & \Delta^\dagger_{A,B,\downarrow,\downarrow} & -\Delta^\dagger_{A,B,\downarrow,\uparrow} & 0 & 0 & -t_{\mathbf{k}} & -s_{\mathbf{k}} \\ -\Delta^\dagger_{A,A,\uparrow,\downarrow} & \Delta^\dagger_{A,A,\uparrow,\uparrow} & -\Delta^\dagger_{A,B,\uparrow,\downarrow} & \Delta^\dagger_{A,B,\uparrow,\uparrow} & 0 & 0 & s^*_{-\mathbf{k}} & -t_{\mathbf{k}} \\ \Delta^\dagger_{B,A,\downarrow,\downarrow} & -\Delta^\dagger_{B,A,\downarrow,\uparrow} & \Delta^\dagger_{B,B,\downarrow,\downarrow} & -\Delta^\dagger_{B,B,\downarrow,\uparrow} & -t^*_{\mathbf{k}} & s_{-\mathbf{k}} & 0 & 0 \\ -\Delta^\dagger_{B,A,\uparrow,\downarrow} & \Delta^\dagger_{B,A,\uparrow,\uparrow} & -\Delta^\dagger_{B,B,\uparrow,\downarrow} & \Delta^\dagger_{B,B,\uparrow,\uparrow} & -s_{\mathbf{k}} & -t^*_{\mathbf{k}} & 0 & 0 \end{pmatrix}, \tag{6.60}$$

The constraints on the gap functions in order to satisfy time-reversal symmetry are for the aligned states, $\Delta_{i,j,\sigma,\sigma}(\mathbf{k}) = \Delta^*_{i,j,-\sigma,-\sigma}(-\mathbf{k})$, and for the mixed states

$-\Delta_{i,j,\alpha,\beta}(\mathbf{k}) = \Delta^*_{i,j,\beta,\alpha}(-\mathbf{k})$ ($\beta \neq \alpha$). Clearly, the constraints are the same as for the Bravais lattice case. Under the particle-hole symmetry operator the Hamiltonian transforms as

$$\hat{\Theta}\mathcal{H}(\mathbf{k})\hat{\Theta}^{-1} = \begin{pmatrix} 0 & 0 & -t_{\mathbf{k}} & -s^*_{-\mathbf{k}} & \Delta^\dagger_{A,A,\uparrow,\uparrow} & \Delta^\dagger_{A,A,\uparrow,\downarrow} & \Delta^\dagger_{A,B,\uparrow,\uparrow} & \Delta^\dagger_{A,B,\uparrow,\downarrow} \\ 0 & 0 & s_{\mathbf{k}} & -t_{\mathbf{k}} & \Delta^\dagger_{A,A,\downarrow,\uparrow} & \Delta^\dagger_{A,A,\downarrow,\downarrow} & \Delta^\dagger_{A,B,\downarrow,\uparrow} & \Delta^\dagger_{A,B,\downarrow,\downarrow} \\ -t^*_{\mathbf{k}} & -s^*_{\mathbf{k}} & 0 & 0 & \Delta^\dagger_{B,A,\uparrow,\uparrow} & \Delta^\dagger_{B,A,\uparrow,\downarrow} & \Delta^\dagger_{B,B,\uparrow,\uparrow} & \Delta^\dagger_{B,B,\uparrow,\downarrow} \\ s_{-\mathbf{k}} & -t^*_{\mathbf{k}} & 0 & 0 & \Delta^\dagger_{B,A,\downarrow,\uparrow} & \Delta^\dagger_{B,A,\downarrow,\downarrow} & \Delta^\dagger_{B,B,\downarrow,\uparrow} & \Delta^\dagger_{B,B,\downarrow,\downarrow} \\ \Delta_{A,A,\uparrow,\uparrow} & \Delta_{A,A,\uparrow,\downarrow} & \Delta_{A,B,\uparrow,\uparrow} & \Delta_{A,B,\uparrow,\downarrow} & 0 & 0 & t_{\mathbf{k}} & s_{\mathbf{k}} \\ \Delta_{A,A,\downarrow,\uparrow} & \Delta_{A,A,\downarrow,\downarrow} & \Delta_{A,B,\downarrow,\uparrow} & \Delta_{A,B,\downarrow,\downarrow} & 0 & 0 & -s^*_{-\mathbf{k}} & t_{\mathbf{k}} \\ \Delta_{B,A,\uparrow,\uparrow} & \Delta_{B,A,\uparrow,\downarrow} & \Delta^\dagger_{B,B,\uparrow,\uparrow} & \Delta_{B,B,\uparrow,\downarrow} & t^*_{\mathbf{k}} & -s_{-\mathbf{k}} & 0 & 0 \\ \Delta_{B,A,\downarrow,\uparrow} & \Delta_{B,A,\downarrow,\downarrow} & \Delta_{B,B,\downarrow,\uparrow} & \Delta_{B,B,\downarrow,\downarrow} & s^*_{\mathbf{k}} & t^*_{\mathbf{k}} & 0 & 0 \end{pmatrix}, \tag{6.61}$$

Again, the same requirements on the gaps are found for particle-hole symmetry as in the Bravais lattice case, namely $\Delta_{i,j,\sigma,\sigma'}(\mathbf{k}) = -\Delta_{i,j,\sigma,\sigma'}(-\mathbf{k})$. This translates to an odd $\mathbf{k}$-dependence of the gap functions.

In conclusion: The same time-reversal and particle-hole symmetry properties of the one-particle Hamiltonian is found as in the Bravais lattice case. As opposed to the Bravais lattice case, spin-orbit coupling breaks inversion symmetry. Parity, however, does not directly affect the topological classification. In addition, the same requirements on the gaps arise from these two symmetries when the superconducting terms are considered.

Chapter 7

Conclusion

This thesis has presented and derived the diagonalization of the one-particle problem consisting of nearest neighbour hopping and Rashba spin-orbit coupling in Bravais and bipartite lattices. A general interaction Hamiltonian has been studied in these systems through mean-field theory, resulting in superconducting terms. In the diagonalized basis, inter- and intraband pairings have been studied under the condition that there is no momentum transfer in the scattering process. This has allowed for a study of the spin-structure for these pairing mechanisms. The main focus has been on a chiral p-wave pairing, which is shown to lead to a relativistic energy dispersion, and Majorana fermion edge states. For many of the Bravais lattices, the spin-orbit coupling function may be used as the chiral p-wave pairing function. For the bipartite lattices the chiral p-wave pairing function is constructed from basis functions of the irreducible representations of the symmetry group. An important result of this thesis is that it is the superconducting gap in the diagonalized basis that need to be on a chiral p-wave form in order to ensure this. This is because of spin-momentum locking caused by the Rashba spin-orbit coupling. The form of the superconducting gap in the spin basis does not necessarily have to be on a chiral p-wave form. Next, important symmetry properties of the Hamiltonian matrices, both with and without superconducting terms have been derived, and from these, a topological classification is put forth. Symmetry restrictions has led to requirements on the pairing functions in order to achieve non-trivial topological phases, thus ensuring the existence of gapless edge states.

Possible future work includes, but is not limited to, expanding from one orbital to several, and to look at three-dimensional lattice models. One could also add magnetism to the systems, and investigate how it affects the spin structure of the pairings. A more immediate task is considering in more detail the finite-momentum interband scatterings, and the resulting gap functions and spin structure.

Appendix A

Example Code

What follows is a simplified script written in `Python`, exemplifying the methods used to plot energybands. Two methods are pesented; solving the Hamiltonian numerically, and a simple expressional implementation based on the results of this thesis. Both, of course, produce the same results. This script is for the honeycomb lattice, and comments and descriptions follow throughout. Functions for saving a figure, labeling axes, adding text to plots, or other non-essential functionalities are omitted.

```
1  import numpy as np
2  import matplotlib.pyplot as plt
3  import scipy
4
5  #Number of discrete points in momentum space
6  Nx=1000
7  Ny=1000
8
9  #Energy parameters
10 tNN=1 #Nearest neighbor hopping energy
11 lambdaR=1 #Nearest neighbor spin-orbit coupling energy
12
13 #Nearest neighbor vector components, assuming a=1
14 b1x=1
15 b1y=0
16 b2x=-0.5
17 b2y=0.5*np.sqrt(3)
18 b3x=-0.5
19 b3y=-0.5*np.sqrt(3)
20
21 #Momentum space
22 kx=np.linspace(-np.pi,np.pi,Nx)
23 ky=np.linspace(-np.pi,np.pi,Ny)
24 KX, KY = np.meshgrid(kx,ky)
25
26
27 #Initialize energy eigenvalue arrays
28 Eval1=np.zeros((Nx,Ny))
29 Eval2=np.zeros((Nx,Ny))
30 Eval3=np.zeros((Nx,Ny))
```

```
31 Eval4=np.zeros((Nx,Ny))
32
33 #Function that takes in tNN, lambdaR and calculates energy
       eigenvalues from the Hamiltonian matrix.
34 def energy_honeycomb(tNN,sNN):
35     #Loop over discretized k-space and calculate
       eigenvalues and eigenvectors of our system
36     for m in range(0,Ny):
37         for n in range(0,Nx):
38             #Matrix elements of the Hamiltonian
39             t=-tNN*(np.exp(1j*(kx[n]*b1x+ky[m]*b1y))+np.
       exp(1j*(kx[n]*b2x+ky[m]*b2y))+np.exp(1j*(kx[n]*b3x+ky[
       m]*b3y)))
40
41             s_plus=lambdaR*(np.exp(1j*(kx[n]*b1x+ky[m]*b1y
       ))+np.exp(1j*np.pi/3)*np.exp(1j*(kx[n]*b2x+ky[m]*b2y))
       +np.exp(-1j*np.pi/3)*np.exp(1j*(kx[n]*b3x+ky[m]*b3y)))
42
43             s_minus=lambdaR*(-np.exp(1j*(kx[n]*b1x+ky[m]*
       b1y))+np.exp(1j*2*np.pi/3)*np.exp(1j*(kx[n]*b2x+ky[m]*
       b2y))+np.exp(-1j*2*np.pi/3)*np.exp(1j*(kx[n]*b3x+ky[m
       ]*b3y)))
44
45             #Hamiltonian matrix
46             H=np.array([[0,0,t,s_plus],[0,0,-np.conjugate(
       s_minus),t],[np.conjugate(t),-s_minus,0,0],[np.
       conjugate(s_plus),np.conjugate(t),0,0]])
47
48             #Solve for the eigenvalues of the Hamiltonian
       matrix
49             Evals=scipy.linalg.eigh(H, eigvals_only=True)
50
51             Eval1[n,m]=Evals[0]
52             Eval2[n,m]=Evals[1]
53             Eval3[n,m]=Evals[2]
54             Eval4[n,m]=Evals[3]
55     return Eval1,Eval2,Eval3,Eval4
56
57 #Alternative function that simply calculates the energy
       eigenvalues from the calculated expressions
58 def energy_honeycomb_exp(tNN,lambdaR):
59     #Loop over discretized k-space and calculate
       eigenvalues and eigenvectors of our system
60     for m in range(0,Ny):
61         for n in range(0,Nx):
```

```
62              #Matrix elements of the Hamiltonian
63              t=-tNN*(np.exp(1j*(kx[n]*b1x+ky[m]*b1y))+np.
    exp(1j*(kx[n]*b2x+ky[m]*b2y))+np.exp(1j*(kx[n]*b3x+ky[
    m]*b3y)));
64              s_plus=lambdaR*(np.exp(1j*(kx[n]*b1x+ky[m]*b1y
    ))+np.exp(1j*np.pi/3)*np.exp(1j*(kx[n]*b2x+ky[m]*b2y))
    +np.exp(-1j*np.pi/3)*np.exp(1j*(kx[n]*b3x+ky[m]*b3y)))
65              s_minus=lambdaR*(-np.exp(1j*(kx[n]*b1x+ky[m]*
    b1y))+np.exp(1j*2*np.pi/3)*np.exp(1j*(kx[n]*b2x+ky[m]*
    b2y))+np.exp(-1j*2*np.pi/3)*np.exp(1j*(kx[n]*b3x+ky[m
    ]*b3y)))
66
67              chi=np.sqrt((s_plus*np.conjugate(s_plus)-
    s_minus*np.conjugate(s_minus))**2+4*(t*np.conjugate(
    s_plus)-np.conjugate(t)*np.conjugate(s_minus))*(np.
    conjugate(t)*s_plus-t*s_minus))
68
69
70              Eval1[n,m]=np.sqrt(2*tp*np.conjugate(t)+s_plus
    *np.conjugate(s_plus)+s_minus*np.conjugate(s_minus)+
    chi)*1/np.sqrt(2)
71              Eval2[n,m]=np.sqrt(2*tp*np.conjugate(t)+s_plus
    *np.conjugate(s_plus)+s_minus*np.conjugate(s_minus)-
    chi)*1/np.sqrt(2)
72              Eval3[n,m]=-np.sqrt(2*tp*np.conjugate(t)+
    s_plus*np.conjugate(s_plus)+s_minus*np.conjugate(
    s_minus)+chi)*1/np.sqrt(2)
73              Eval4[n,m]=-np.sqrt(2*tp*np.conjugate(t)+
    s_plus*np.conjugate(s_plus)+s_minus*np.conjugate(
    s_minus)-chi)*1/np.sqrt(2)
74      return Eval1,Eval2,Eval3,Eval4
75
76  #Call on the energy eigenvalue function (change to
    energy_honeycomb_exp(tNN,lambdaR) for expressional
    version)
77  Eval1,Eval2,Eval3,Eval4=energy_honeycomb(tNN,lambdaR)
78
79  #Block for plotting a 3D surface plot of the energy
    eigenvalues of all four bands
80  plt.figure()
81  ax = plt.gca(projection='3d')
82  surf = ax.plot_surface(KX, KY, Eval1)
83  surf = ax.plot_surface(KX, KY, Eval2)
84  surf = ax.plot_surface(KX, KY, Eval3)
85  surf = ax.plot_surface(KX, KY, Eval4)
```

```
86 plt.colorbar(surf, shrink=0.5, aspect=5)
87
88 #Block for plotting the energy dispersion along the k_y-
       axis
89 plt.figure()
90 E1_band=[];
91 E2_band=[];
92 E3_band=[];
93 E4_band=[];
94 for j in range(0,Ny):
95     E1_band.append(Eval1[Nx/2,j]);
96     E2_band.append(Eval2[Nx/2,j]);
97     E3_band.append(Eval3[Nx/2,j]);
98     E4_band.append(Eval4[Nx/2,j]);
99 plt.plot(ky,E1_band,'k',ky,E2_band,'k',ky,E3_band,'k',ky,
       E3_band,'k')
```

Bibliography

[1] H. K. Onnes. "The resistance of pure mercury at helium temperatures". In: *Commun. Phys. Lab. Univ. Leiden* 12 (1911), p. 120.

[2] W. Meissner and R. Ochsenfeld. "Ein neuer Effekt bei Eintritt der Supraleitfahigkeit". In: *Naturwissenschaften* 21.44 (), pp. 787–788. ISSN: 1432-1904. DOI: 10.1007/BF01504252.

[3] F. London and H. London. "The Electromagnetic Equations of the Supraconductor". In: *Proceedings of the Royal Society of London A: Mathematical, Physical and Engineering Sciences* 149.866 (1935), pp. 71–88. ISSN: 0080-4630. DOI: 10.1098/rspa.1935.0048. eprint: http://rspa.royalsocietypublishing.org/content/149/866/71.full.pdf.

[4] V. L. Ginzburg and L. D. Landau. "On the theory of superconductivity". In: *Zhurnal Eksperimentalnoi i Teoreticheskoi Fiziki* 20 (1950), p. 1064.

[5] J. Bardeen, L. N. Cooper, and J. R. Schrieffer. "Theory of Superconductivity". In: *Phys. Rev.* 108 (5 1957), pp. 1175–1204. DOI: 10.1103/PhysRev.108.1175.

[6] F. Steglich, J. Aarts, C. D. Bredl, W. Lieke, D. Meschede, W. Franz, and H. Schäfer. "Superconductivity in the Presence of Strong Pauli Paramagnetism: $CeCu_2Si_2$". In: *Physical Review Letters* 43 (Dec. 1979), pp. 1892–1896. DOI: 10.1103/PhysRevLett.43.1892.

[7] J. G. Bednorz and K. A. Müller. "Possible high T_c superconductivity in the Ba-La-Cu-O system". In: *Zeitschrift fur Physik B Condensed Matter* 64 (June 1986), pp. 189–193. DOI: 10.1007/BF01303701.

[8] S. Badoux, W. Tabis, F. Laliberté, G. Grissonnanche, B. Vignolle, D. Vignolles, J. Béard, D. A. Bonn, W. N. Hardy, R. Liang, N. Doiron-Leyraud, L. Taillefer, and C. Proust. "Change of carrier density at the pseudogap critical point of a cuprate superconductor". In: *Nature* 531.7593 (Mar. 2016), pp. 210–214.

[9] X.-L. Qi and S.-C. Zhang. "Topological insulators and superconductors". In: *Rev. Mod. Phys.* 83 (4 2011), pp. 1057–1110. DOI: 10.1103/RevModPhys.83.1057.

[10] M. Konig, S. Wiedmann, C. Brune, A. Roth, H. Buhmann, L. W. Molenkamp, X.-L. Qi, and S.-C. Zhang. "Quantum Spin Hall Insulator State in HgTe Quantum Wells". In: *Science* 318.5851 (2007), pp. 766–770. DOI: 10.1126/science.1148047.

[11] Y. Xia, D. Qian, D. Hsieh, L. Wray, A. Pal, H. Lin, A. Bansil, D. Grauer, Y. S. Hor, R. J. Cava, and M. Z. Hasan. "Observation of a large-gap topological-insulator class with a single Dirac cone on the surface". In: *Nat Phys* 5.6 (June 2009), pp. 398–402.

[12] J. Moore. "Topological insulators: The next generation". In: *Nat Phys* 5.6 (June 2009), pp. 378–380.

[13] L. Fu and C. L. Kane. "Superconducting Proximity Effect and Majorana Fermions at the Surface of a Topological Insulator". In: *Phys. Rev. Lett.* 100 (9 2008), p. 096407. DOI: 10.1103/PhysRevLett.100.096407.

[14] H. Zhang, C.-X. Liu, X.-L. Qi, X. Dai, Z. Fang, and S.-C. Zhang. "Topological insulators in Bi2Se3, Bi2Te3 and Sb2Te3 with a single Dirac cone on the surface". In: *Nat Phys* 5.6 (June 2009), pp. 438–442.

[15] P. Sengupta, T. Kubis, Y. Tan, and G. Klimeck. "Proximity induced ferromagnetism, superconductivity, and finite-size effects on the surface states of topological insulator nanostructures". In: *Journal of Applied Physics* 117.4, 044304 (2015). DOI: http://dx.doi.org/10.1063/1.4906842.

[16] J. Linder, Y. Tanaka, T. Yokoyama, A. Sudbø, and N. Nagaosa. "Interplay between superconductivity and ferromagnetism on a topological insulator". In: *Phys. Rev. B* 81 (18 2010), p. 184525. DOI: 10.1103/PhysRevB.81.184525.

[17] J. D. Sau, R. M. Lutchyn, S. Tewari, and S. Das Sarma. "Generic New Platform for Topological Quantum Computation Using Semiconductor Heterostructures". In: *Phys. Rev. Lett.* 104 (4 2010), p. 040502. DOI: 10.1103/PhysRevLett.104.040502.

[18] P. R. Wallace. "The Band Theory of Graphite". In: *Phys. Rev.* 71 (9 1947), pp. 622–634. DOI: 10.1103/PhysRev.71.622.

[19] K. S. Novoselov, A. K. Geim, S. V. Morozov, D. Jiang, Y. Zhang, S. V. Dubonos, I. V. Grigorieva, and A. A. Firsov. "Electric Field Effect in Atomically Thin Carbon Films". In: *Science* 306.5696 (2004), pp. 666–669. DOI: 10.1126/science.1102896. eprint: http://www.sciencemag.org/content/306/5696/666.full.pdf.

[20] D. P. DiVincenzo and E. J. Mele. "Self-consistent effective-mass theory for intralayer screening in graphite intercalation compounds". In: *Phys. Rev. B* 29 (4 1984), pp. 1685–1694. DOI: 10.1103/PhysRevB.29.1685.

[21] B. A. Bernevig and T. L. Hughes. *Topological Insulators and Topological Superconductors*. 1st Edition. Princeton University Press, 2013. ISBN: 9780691151755.

[22] O. A. Pankratov, S. V. Pakhomov, and B. A. Volkov.
"Supersymmetry in heterojunctions: Band-inverting contact on the basis of $Pb_{1-x}Sn_xTe$ and $Hg_{1-x}Cd_xTe$".
In: *Solid State Communications* 61 (Jan. 1987), pp. 93–96.
DOI: 10.1016/0038-1098(87)90934-3.

[23] M. Z. Hasan and C. L. Kane. "*Colloquium* : Topological insulators".
In: *Rev. Mod. Phys.* 82 (4 2010), pp. 3045–3067.
DOI: 10.1103/RevModPhys.82.3045.

[24] T. O. Wehling, A. M. Black-Schaffer, and A. V. Balatsky. "Dirac materials".
In: *Advances in Physics* 63 (Jan. 2014), pp. 1–76.
DOI: 10.1080/00018732.2014.927109.
arXiv: 1405.5774 [cond-mat.mtrl-sci].

[25] C. L. Kane and E. J. Mele.
"Z_2 Topological Order and the Quantum Spin Hall Effect".
In: *Phys. Rev. Lett.* 95 (14 2005), p. 146802.
DOI: 10.1103/PhysRevLett.95.146802.

[26] X.-L. Qi, T. L. Hughes, and S.-C. Zhang.
"Topological field theory of time-reversal invariant insulators".
In: *Phys. Rev. B* 78 (19 2008), p. 195424.
DOI: 10.1103/PhysRevB.78.195424.

[27] G. E. Volovik. *The Universe in a Helium Droplet*. 1st Edition.
Clarendon Press/Oxford Science Publications, 2003. ISBN: 9780198507826.

[28] L. Fu and C. L. Kane. "Superconducting Proximity Effect and Majorana Fermions at the Surface of a Topological Insulator".
In: *Phys. Rev. Lett.* 100 (9 2008), p. 096407.
DOI: 10.1103/PhysRevLett.100.096407.

[29] T. Mizushima, Y. Tsutsumi, T. Kawakami, M. Sato, M. Ichioka, and K. Machida. "Symmetry-Protected Topological Superfluids and Superconductors "From the Basics to 3He"".
In: *Journal of the Physical Society of Japan* 85.2 (2016), p. 022001.
DOI: 10.7566/JPSJ.85.022001.
eprint: http://dx.doi.org/10.7566/JPSJ.85.022001.

[30] E. Majorana. "Teoria simmetrica dell'elettrone e del positrone".
In: *Il Nuovo Cimento* 14.4 (1937), pp. 171–184. ISSN: 1827-6121.
DOI: 10.1007/BF02961314.

[31] C. Nayak, S. H. Simon, A. Stern, M. Freedman, and S. Das Sarma.
"Non-Abelian anyons and topological quantum computation".
In: *Rev. Mod. Phys.* 80 (3 2008), pp. 1083–1159.
DOI: 10.1103/RevModPhys.80.1083.

[32] A. Banerjee, C. A. Bridges, J. Q. Yan, A. A. Aczel, L. Li, M. B. Stone, G. E. Granroth, M. D. Lumsden, Y. Yiu, J. Knolle, S. Bhattacharjee, D. L. Kovrizhin, R. Moessner, D. A. Tennant, D. G. Mandrus, and S. E. Nagler.
"Proximate Kitaev quantum spin liquid behaviour in a honeycomb magnet".
In: *Nat Mater* advance online publication (Apr. 2016), pp. –.

[33] A. Manchon, H. C. Koo, J. Nitta, S. M. Frolov, and R. A. Duine.
"New perspectives for Rashba spin-orbit coupling".
In: *Nat Mater* 14.9 (Sept. 2015), pp. 871–882.

[34] D. J. Griffiths. *Introduction to Quantum Mechanics*. 2nd Edition.
Pearson Prentice Hall, 2004. ISBN: 9780131118928.

[35] H. Bruus and K. Flensberg.
Many-Body Quantum Theory in Condensed Matter Physics: An Introduction.
1st Edition. Oxford University Press, 2004. ISBN: 9780198566335.

[36] M. V. Berry. "Quantal Phase Factors Accompanying Adiabatic Changes".
In: *Proceedings of the Royal Society of London A: Mathematical, Physical and Engineering Sciences* 392.1802 (1984), pp. 45–57. ISSN: 0080-4630.
DOI: 10.1098/rspa.1984.0023.

[37] C. E. Robert A. Adams. *Calculus: A Complete Course*. 8th Edition.
Pearson, 2014. ISBN: 9780321880215.

[38] M Gradhand, D. V. Fedorov, F Pientka, P Zahn, I Mertig, and B. L. Györffy.
"First-principle calculations of the Berry curvature of Bloch states for charge and spin transport of electrons".
In: *Journal of Physics: Condensed Matter* 24.21 (2012), p. 213202.

[39] K. M. D. Hals, A. K. Nguyen, X. Waintal, and A. Brataas.
"Effective Magnetic Monopoles and Universal Conductance Fluctuations".
In: *Physical Review Letters* 105.20, 207204 (Nov. 2010), p. 207204.
DOI: 10.1103/PhysRevLett.105.207204.
arXiv: 1008.0269 [cond-mat.mes-hall].

[40] M. Kohmoto.
"Topological invariant and the quantization of the Hall conductance".
In: *Annals of Physics* 160 (Apr. 1985), pp. 343–354.
DOI: 10.1016/0003-4916(85)90148-4.

[41] K. v. Klitzing, G. Dorda, and M. Pepper.
"New Method for High-Accuracy Determination of the Fine-Structure Constant Based on Quantized Hall Resistance".
In: *Phys. Rev. Lett.* 45 (6 1980), pp. 494–497.
DOI: 10.1103/PhysRevLett.45.494.

[42] D. J. Thouless, M. Kohmoto, M. P. Nightingale, and M. den Nijs.
"Quantized Hall Conductance in a Two-Dimensional Periodic Potential".
In: *Phys. Rev. Lett.* 49 (6 1982), pp. 405–408.
DOI: 10.1103/PhysRevLett.49.405.

[43] B. I. Halperin.
"Quantized Hall conductance, current-carrying edge states, and the existence of extended states in a two-dimensional disordered potential".
In: *Phys. Rev. B* 25 (4 1982), pp. 2185–2190.
DOI: 10.1103/PhysRevB.25.2185.

[44] Y. Hatsugai.
"Chern number and edge states in the integer quantum Hall effect".
In: *Phys. Rev. Lett.* 71 (22 1993), pp. 3697–3700.
DOI: 10.1103/PhysRevLett.71.3697.

[45] L. Fu and C. L. Kane. "Topological insulators with inversion symmetry".
In: *Phys. Rev. B* 76 (4 2007), p. 045302. DOI: 10.1103/PhysRevB.76.045302.

[46] M. Sato. "Topological properties of spin-triplet superconductors and Fermi surface topology in the normal state".
In: *Phys. Rev. B* 79 (21 2009), p. 214526.
DOI: 10.1103/PhysRevB.79.214526.

[47] A. P. Schnyder, S. Ryu, A. Furusaki, and A. W. W. Ludwig. "Classification of topological insulators and superconductors in three spatial dimensions".
In: *Phys. Rev. B* 78 (19 2008), p. 195125.
DOI: 10.1103/PhysRevB.78.195125.

[48] A. Altland and M. R. Zirnbauer. "Nonstandard symmetry classes in mesoscopic normal-superconducting hybrid structures".
In: *Phys. Rev. B* 55 (2 1997), pp. 1142–1161.
DOI: 10.1103/PhysRevB.55.1142.

[49] P. A. M. Dirac. "The Quantum Theory of the Electron".
In: *Proceedings of the Royal Society of London A: Mathematical, Physical and Engineering Sciences* 117.778 (1928), pp. 610–624. ISSN: 0950-1207.
DOI: 10.1098/rspa.1928.0023.

[50] O. Krupin. *Dichroism and Rashba effect at magnetic crystal surfaces of rare-earth metals (Inaugural Dissertation)*. Freie Universitet Berlin, 2004.
eprint: http://www.diss.fu-berlin.de/2004/249/.

[51] D. J. Griffiths. *Introduction to Electrodynamics*. 4th Edition.
Pearson Prentice Hall, 2012. ISBN: 978-0321856562.

[52] Y. A. Bychkov and E. I. Rashba. "Oscillatory effects and the magnetic susceptibility of carriers in inversion layers".
In: *Journal of Physics C: Solid State Physics* 17.33 (1984), p. 6039.

[53] K. Fossheim and A. Sudbø. *Superconductivity: Physics and Applications*.
1st Edition. John Wiley and Sons, Ltd, 2004. ISBN: 9780470844526.

[54] K.-H. Benneman and J. B. Ketterson.
Superconductivity Vol I: Conventional and Unconventional Superconductors.
1st Edition. Springer-Verlag Berlin Heidelberg, 2008. ISBN: 9783540732532.

[55] K. Hashimoto. *Non-Universal Superconducting Gap Structure in Iron-Pnictides Revealed by Magnetic Penetration Depth Measurements*. 1st Edition. Springer Japan, 2013. ISBN: 978-4-431-54293-3.

[56] H. A. Kramers. "General theory of paramagnetic rotation in crystals". In: *Proc. Amsterdam Acad.* 33 (1930), p. 959.

[57] N. Read and D. Green. "Paired states of fermions in two dimensions with breaking of parity and time-reversal symmetries and the fractional quantum Hall effect". In: *Phys. Rev. B* 61 (15 2000), pp. 10267–10297. DOI: 10.1103/PhysRevB.61.10267.

[58] A. H. Nevidomskyy. "Coexistence of Ferromagnetism and Superconductivity Close to a Quantum Phase Transition: The Heisenberg- to Ising-type Crossover". In: *Phys. Rev. Lett.* 94 (9 2005), p. 097003. DOI: 10.1103/PhysRevLett.94.097003.

[59] K. Machida and T. Ohmi. "Phenomenological Theory of Ferromagnetic Superconductivity". In: *Phys. Rev. Lett.* 86 (5 2001), pp. 850–853. DOI: 10.1103/PhysRevLett.86.850.

[60] J. Linder, Y. Tanaka, T. Yokoyama, A. Sudbø, and N. Nagaosa. "Unconventional Superconductivity on a Topological Insulator". In: *Phys. Rev. Lett.* 104 (6 2010), p. 067001. DOI: 10.1103/PhysRevLett.104.067001.

[61] A. H. Castro Neto, F. Guinea, N. M. R. Peres, K. S. Novoselov, and A. K. Geim. "The electronic properties of graphene". In: *Rev. Mod. Phys.* 81 (1 2009), pp. 109–162. DOI: 10.1103/RevModPhys.81.109.

[62] T.-W. Chen, C.-L. Hsiao, and C.-D. Hu. "Out-of-plane spin polarization of edge currents in Chern insulator with Rashba spin-orbit interaction". In: *ArXiv e-prints* (May 2016). arXiv: 1605.00850 [cond-mat.mes-hall].

[63] M. Sigrist and K. Ueda. "Phenomenological theory of unconventional superconductivity". In: *Rev. Mod. Phys.* 63 (2 1991), pp. 239–311. DOI: 10.1103/RevModPhys.63.239.